UNIVERSIDADE DA BEIRA INTERIOR
Ciências

Development of intelligent vehicles for co-delivery of anti-tumoral drugs to breast cancer cells

João Filipe Gonçalves Marques

Dissertação para a obtenção de grau de Mestre em
Bioquímica

Orientador: Professor Doutor Ilídio Joaquim Sobreira Correia
Coorientador: Mestre Vítor Manuel Abreu Gaspar

Covilhã, junho de 2013

UNIVERSIDADE DA BEIRA INTERIOR
Ciências

Desenvolvimento de veículos inteligentes para co-entrega de drogas anti-tumorais nas células do cancro da mama

João Filipe Gonçalves Marques

Dissertação para a obtenção de grau de Mestre em
Bioquímica

Orientador: Professor Doutor Ilídio Joaquim Sobreira Correia
Coorientador: Mestre Vítor Manuel Abreu Gaspar

Covilhã, junho de 2013

“Cum mente et malleo”
Claude-Henri Gorceix

Aknowlegments

First, I would like to thank to Professor Ilídio Correia for the possibility of developing my master thesis in his group, making every day easier because of its ability to join the group, resulting in an optimum work environment.

I thank to Master Vítor Gaspar, my co-supervisor, for his relentless support, guidance and advices, unlimited knowledge, and for being a friend. The constant discussion of ideas and issues made me grow up, and without him I would never be able to develop this work.

I would like to thank Master David Märkl and Professor Eugénia Gallardo, for providing UPLC column as well as for all the support in my work, without their help I would not have achieved my aims.

Moreover, I would like to thank to Elisabete Costa, for the endless support, help, and mainly for her friendship, being my partner every day and night, during this year.

I thank all my family, specially my father, mother, sister and brother-in-law for their unlimited support, patience, love, support, affection and most of all, for never stop believing in me.

Finally, and foremost, a very special thanks to my girlfriend, Agustina, for all her love, advices and support during my thesis development. An unending acknowledge for her patience in my busy lab days and her limitless affection and care.

Abstract

Presently breast cancer arises as one of the most prevalent malignancy in women worldwide, contributing for high rates of mortality and morbidity in several million patients. Currently there is still no available cure for this disease and to further aggravate this scenario the existing treatments such as chemotherapy, are generally ineffective due to poor tumor bioavailability. Moreover, the commonly used anti-tumoral compounds also lead to the development of drug resistant malignant cells after repeated administration, a fact that originates the development of more aggressive cells that possess the capacity to metastasize and spread to healthy organs. These facts evidence the urgent need for the development of novel therapeutic approaches that improve the therapeutic outcome and patient survival. The recent developments in the field of Nanotechnology, particularly regarding the capacity to manipulate matter at the nanoscale, has brought forth the opportunity to devise novel drug delivery systems to tackle some of these issues. From this stand point, the research work presented in this thesis describes the development of a novel drug delivery system based on micellar carriers, with a core-shell structure, that are capable to simultaneously deliver multiple drugs to breast cancer cells. These nanocarriers are comprised by a hydrophilic and a hydrophobic polymer organized in a block-by-block structure that was synthesized through macromolecular chemistry. The manipulation of the various reaction conditions yielded block co-polymers with different hydrophobic chains, which influenced the available space in the nanocarrier core. The nanocarriers were formulated by co-polymer self-assembly into nanosized micelles that demonstrated the capacity to encapsulate with high efficiency, an anti-tumoral drug, Crizotinib and a potent inhibitor of the cell transporters responsible for drug resistance, Sildenafil. The drug release profile of the micellar carriers revealed a spatiotemporally controlled release that was faster for Sildenafil than Crizotinib. Moreover, the drug loaded micelles demonstrated to be highly biocompatible and accomplished uptake into adherent breast adenocarcinoma cells. This relevant finding let to the intracellular localization of both the anti-tumoral drug and the drug resistance inhibitor, and thus, improved the bioavailability of the bioactive therapeutics. Subsequently, the study of the therapeutic performance of the co-delivery systems illustrated that the simultaneous delivery of both drugs improved the anti-tumoral capacity of Crizotinib evidencing the existence of a highly synergistic effect. Strikingly, the micellar systems achieved the same anti-tumoral effect of the free drugs, using 2-fold less drug concentration. Besides indicating that the release profile maintains drug concentrations in the therapeutic window, these crucial results highlight the effect of dual drug conjugation and the use of Crizotinib as an anti-tumoral compound for breast cancer therapy and Sildenafil as a multidrug resistance inhibitor. Overall, the unique approach developed in this thesis possesses tremendous potential for a future clinical application in breast cancer patients that acquired resistance to standard therapies.

Keywords:

Anti-tumoral effect, Block co-polymers, Breast cancer, Co-delivery, Micelles.

Resumo alargado

Atualmente, o cancro de mama surge como uma das neoplasias com maior prevalência no sexo feminino em todo o mundo, contribuindo para altas taxas de mortalidade e morbilidade em vários milhões de pacientes. Atualmente, ainda não se encontra disponível uma cura para esta doença e para agravar ainda mais este cenário, os tratamentos existentes geralmente baseados na quimioterapia, são extremamente ineficazes devido à baixa biodisponibilidade do fármaco no local do tumor. Além destas limitações, estes tratamentos também provocam graves efeitos secundários que afetam órgãos vitais como o fígado, coração ou rins. Este facto contribui para uma progressão desta neoplasia de forma mais acelerada e é responsável por um prognóstico bastante limitado em termos do tempo de vida das pacientes.

Não obstante, devido à necessidade de manter a concentração terapêutica dos fármacos no organismo são efetuadas múltiplas administrações em regimes que usualmente se prolongam durante meses, para promover um aumento da probabilidade de localização dos fármacos nas células alvo. Esta abordagem terapêutica é crucial para a redução da massa tumoral, no entanto, foi recentemente descoberto que este tratamento origina a formação de células tumorais mamárias com mutações que lhes permitem adquirir um fenótipo muito mais agressivo e resistente ao fármaco anti-tumoral administrado. Esta resistência é muitas vezes atribuída ao aumento da expressão de proteínas membranares que têm a capacidade de expelir os ingredientes farmacêuticos ativos para o meio extracelular, eliminando-os assim do seu local alvo. Além do desenvolvimento de resistência, é despoletada também nas células tumorais a capacidade de metastização, permitindo o alastrar da doença para os órgãos saudáveis. Estes factos evidenciam a necessidade urgente do desenvolvimento de novas abordagens terapêuticas com vista a melhorar o prognóstico clínico e a qualidade de vida do paciente.

Neste contexto, os desenvolvimentos recentes no campo da Nanotecnologia, particularmente em relação à capacidade de manipular a matéria à escala nanométrica, têm trazido a oportunidade de conceber novos sistemas de entrega de drogas para resolver alguns destes problemas. Diversos nanoveículos, com base polimérica e/ou lipídica, têm sido desenvolvidos durante as últimas décadas, tendo sido alguns deles já aprovados e usados no tratamento de doentes em unidades hospitalares. No entanto, apesar dos grandes avanços obtidos no design e produção de nano-veículos para aplicação na terapia do cancro da mama num âmbito clínico, a sua maioria apenas consegue melhorar a biodisponibilidade e biodistribuição do fármaco anti-tumoral nas células alvo. De facto, até à data, apesar da panóplia de nanotransportadores disponíveis para terapia do cancro da mama muito poucos exploram a entrega de vários fármacos ou moléculas bioativas em simultâneo, como forma de combater os problemas associados à multirresistência adquirida pelas células neoplásicas.

Com o conhecimento destas limitações atuais, e tendo como objetivo principal melhorar cada vez mais a terapia contra o cancro da mama, o trabalho de investigação apresentado nesta

tese descreve o desenvolvimento de um novo sistema de entrega de drogas baseado em nano-veículos micelares, com uma estrutura "núcleo-concha" que lhes permite transportar e entregar simultaneamente múltiplas drogas a células de cancro da mama. Estas micelas, são formadas por dois polímeros rearranjados numa estrutura em bloco. Cada um dos blocos é constituído por um polímero hidrofílico e outro polímero hidrofóbico, um facto que imprime características anfifilicas aos nanotransportadores produzidos com estes biomateriais. Esta estrutura única foi sintetizada por intermédio de reações químicas macromoleculares. A manipulação das diversas condições da reação originou a síntese de co-polímeros com diferentes cadeias hidrofóbicas, um factor crucial visto que este influencia o espaço disponível no núcleo da micela, assim como a sua estabilidade e capacidade de encapsulação de moléculas bioativas. Os materiais sintetizados foram caracterizados física e químicamente por intermédio de técnicas referidas nas diretivas internacionais como adequadas para caraterizar nanomateriais para aplicações biomédicas. As micelas foram posteriormente formuladas pelos co-polímeros sintetizados recorrendo a um método de formação espontânea que origina micelas nanoméricas com uma morfologia esférica, como revelado por microscopia eletrónica de varrimento.

O Crizotinib, um conhecido fármaco anti-tumoral neste momento em ensaios clínicos de fase IV e o Sildenafil, um potente inibidor dos transportadores celulares responsáveis pela resistência aos fármacos, foram escolhidos posteriormente para serem incluídos dentro das nano-micelas poliméricas. Após a otimização do processo de encapsulação foi obtida uma elevada eficácia de inclusão destes dois fármacos no interior dos transportadores micelares. O perfil de liberação destes fármacos dos transportadores micelares revelou ser controlado, sendo mais rápido para o Sildenafil do que para o Crizotinib. Além disso, as micelas produzidas demonstraram ser altamente biocompatíveis quando administradas a células humanas saudáveis. A sua internalização nas células cancerígenas da mama revelou ser muito elevada, um resultado extremamente vital pois, evidencia, a entrega intracelular de ambos os fármacos, o anti-tumoral e o inibidor da resistência celular, levando a um aumento da sua biodisponibilidade.

Consequentemente, o estudo do desempenho terapêutico destes nanotransportadores demonstrou que a co-entrega de ambos os fármacos potenciou a atividade anti-tumoral do Crizotinib, evidenciando a obtenção de um efeito sinérgico. Surpreendentemente, os sistemas micelares obtiveram um efeito anti-tumoral similar ao obtido com os fármacos na sua formulação farmacêutica livre, administrando no entanto concentrações de fármaco duas vezes menores. Estes resultados ilustram a importância do sistema desenvolvido na terapia do cancro da mama. Além deste facto, uma vez que o perfil de libertação mantém as concentrações dos fármacos dentro da janela terapêutica, estes resultados realçam o efeito da conjugação das duas drogas e a utilização do Crizotinib como um composto anti-tumoral para a terapia do cancro da mama.

Em geral, a abordagem exclusiva desenvolvida nesta tese demonstra um enorme potencial para aplicação futura em pacientes com cancro da mama, que apresentem resistência às terapias convencionais.

Palavras-chave

Cancro da mama, Co-entrega, Co-polímeros em bloco, Efeito anti-tumoral, Micelas

List of Publications

Articles in peer reviewed international journals:

Costa, C.E., Gaspar. V.M., Marques, J.G., Coutinho, P., Correia, I.J. (2013). Evaluation of Nanoparticle Uptake in Co-culture Cancer Models, PloS one. Article in press.

Gaspar V. M., Marques J. G., Sousa F., Louro R. O., Queiroz J. A. and Correia I. J. (2013). Biofunctionalized nanoparticles with pH-responsive and cell penetrating blocks for gene Delivery, Nanotechnology (24) 275101.

Poster communications:

Gaspar, V.M., Marques, J.M., Sousa, F., Louro, R.O., Queiroz, J.A., Correia, I.J., Characterization of Chitosan Nanoparticles Uptake and Intracellular Trafficking in Cancer Cells, 11th International Conference of the European Chitin Society, 5-8 May 2013, Porto, Portugal.

Elisabete C. Costa, Vítor M. Gaspar, João F.G. Marques, Paula Coutinho, Ilídio J. Correia, Mimicking Breast Cancer Microenvironment with *In Vitro* Co-culture Models, Instituto Politécnico da Guarda (IPG), 3rd of May 2013, Guarda, Portugal.

Poster awards:

Costa, C. E., Gaspar. V. M., Marques, J.G., Coutinho, P., Correia, I. J., Mimicking Breast Cancer Microenvironment with In Vitro Co-culture Models, Instituto Politécnico da Guarda (IPG), 3rd of May 2013, Guarda, Portugal.

Oral Presentations:

Gaspar, V.M., Marques, J.M., Sousa, F., Louro, R.O., Queiroz, J.A., Correia, I.J., Characterization of Nanomedicines Uptake and Intracellular Trafficking in Cancer Cells, VI Symposium on Technology and Health, Instituto Politécnico da Guarda (IPG), 3rd of May 2013, Guarda, Portugal.

Index

Figure Index

Table Index

List of abbreviations

ΔH	Heat Enthalpy
ABC	ATP-Binding Cassettes
AKT	Protein Kinase B
ANOVA	One-way Aanalysis of Variance
BCRP	Breast Cancer Resisting Protein
bFGF	Basic Fibroblast Growth Factor
$CDCl_3$	Deuterated Chloroform
cGMP	Cyclic Guanosine Monophosphate
CLSM	Confocal Laser Scanning Microscopy
CMC	Critical Micellar Concentration
DDS	Drug Delivery Systems
DIC	Differential Interference Contrast
DLS	Dynamic Light Scattering
DMEM	Dulbecco's Modified Eagle's Medium
DNA	Deoxyribonucleic Acid
DSC	Differential Scanning Calorimetry
EDTA	Ethylenediamine Tetraacetic Acid
EMA	European Medicines Agency
EO	Poly(ethylene glycol) Monomer
EPR	Enhanced Permeability and Retention
ER	Oestrogen Receptor
FBS	Fetal Bovine Serum
FDA	Food and Drug Administration
FPLC	Fast Protein Liquid Chromatography
FTIR	Fourier Transform Infrared Spectroscopy
GPC	Gel Permeation Chromatography
HER2	Human Epidermal Growth Factor Receptor 2
hFIB	Human Fibroblasts
HGF	Hepatocyte Growth Factor
HPLC	High Performance Liquid Chromatography
IC50	Half Maximum Inhibitory Concentration
LA	Lactic Acid
MCF-7	Michigan Cancer Foundation-7
MDR	Multi-Drug Resistance
MetOH	Methanol
Mn	Number Average Molecular Weight
MPS	Mononuclear Phagocytic System
MRT	Mean Residence Time
MTD	Maximum Tolerated Dose
MTS	3-(4,5-dimethylthiazol-2-yl)-5-(3-carboxymethoxyphenyl)-2-(4-sulfophenyl)-2H-tetrazolium)
Mw	Molecular Weight
NA	Not Applicable
NMR	Nuclear Magnetic Resonance
PBS	Phosphate Buffer Saline
PCL	Poly (ε−Caprolactone)

PDE5	Phosphodiesterase 5
PDI	Polydispersity Index
PEG	Poly(ethylene glycol)
PEG-PCL	Poly(ethylene glycol)-block-Poly(ε−caprolactone)
PEG-PLA	Poly(ethylene glycol)-Poly(lactic acid)
PEOz	Poly(oxazoline)
PFS	Patient Free Survival
PHEMA	Poly (2-hydroxyethyl methacrylate)
PL	Synthesized Poly(ethylene glycol)-Poly(lactic acid)
PLA	Poly (lactic acid)
PTA	Phosphotungstic Acid
PLGA	Poly (D,L-lactide-co-glycolide)
P-gp	P-glycoprotein
RBC	Red Blood Cell
RITC	Rhodamine B Isothiocyanate
ROI	Region of Interest
ROP	Ring Opening Polymerization
RT	Room Temperature
SEM	Scanning Electron Microscopy
siRNA	Small Interfering RNA
$Sn(Oct)_2$	Stannous Octoate
TEA	Triethylamine
Tm	Melting Temperature
UPLC	Ultra Performance Liquid Chromatography
USA	United Stated of America
VEGF	Vascular Endothelial Growth Factor
XRD	X-ray Powder Diffraction

Chapter 1

Introduction

1. Cancer

1.1. Malignant Phenotype and Cancer Cell Hallmarks

Cancer is a disease that is mainly characterized by an uncontrolled cell proliferation that ultimately leads to the formation of a tumor mass. Generally, healthy cells accurately control their growth by carefully delivering signalling agents to nearby cells and guaranteeing tissue homeostasis [1]. When homeostasis is affected, for example, by the accumulation of genetic mutations, cells begin to acquire a malignant phenotype (Figure 1) [2]. Age, growth signal molecules, hormones, genetic background, ionizing radiation, pollution and unhealthy working environments are the major risk factors for the development of cancer [3, 4]. These factors normally induce genetic mutations in normal cells, that often result in metabolically and physicochemical dysfunctional cells [5]. These genetic abnormalities present in tumor cells are generally correlated with the activation oncogenes (c-MET) and silencing of tumor suppressor genes (p53) [2]. This fact results in the deregulation of major signalling pathways that promote cell survival and proliferation [1]. Usually, cancer cells overexpress proteins responsible for cell cycle progression and underexpress proteins involved in growth suppression [1].

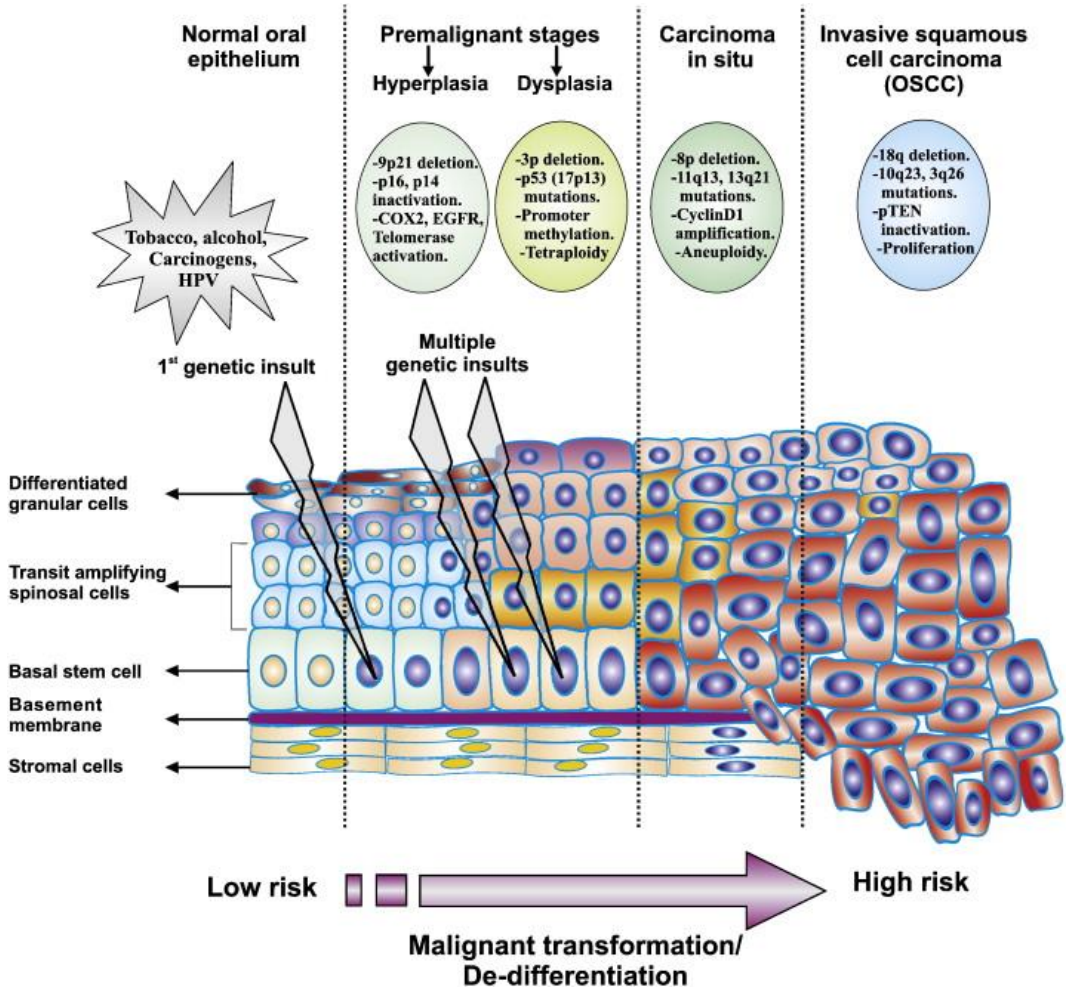

Figure 1 – Schematic representation of the tumorigenesis process (Adapted from [6]).

After acquiring the malignant phenotype, cancer cells commonly exhibit major characteristics, the so termed "Hallmarks of cancer" (Figure 2). This set of unique features ultimately differentiates malignant cells from their healthy counterparts [1].

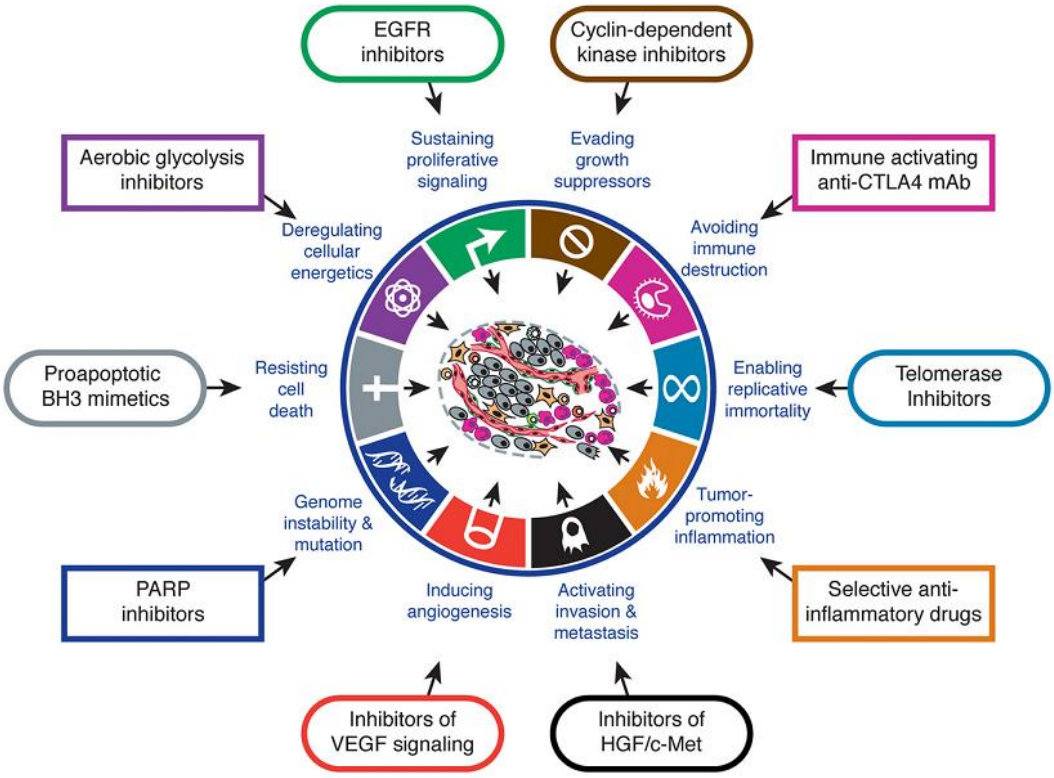

Figure 2 - Cancer hallmarks and their possible therapeutic pathways to overcome cancer. A multi-combinational drug therapy could be an interesting approach to fight some of hallmarks described. (Adapted from [1]).

One of the most relevant hallmarks that tumor cells possess is their capacity to sustain proliferative signalling. To successfully promote sustained proliferation, cancer cells need to bypass growth suppressor supervision mechanisms, that are commonly mediated by p53 and retinoblastoma-associated proteins (Rb) [1]. Remarkably, it is currently known that approximately 50% of all cancer cells have a mutation in the p53 gene, a fact that completely eliminates its pro-apoptotic activity [1, 7]. Yet another strategy that cancer cells acquire in order to resist to cell death is the increase of expression of anti-apoptotic proteins from the Bcl family, such as Bcl-2 and Bcl-xL [1]. Moreover, the immortalized (i.e., limitless replicative potential of cancer cells), is also a hallmark that greatly impairs patient survival rates [1]. To achieve this unique characteristic cancer cells recruit telomere stabilizing proteins, such as reverse transcriptase telomerase, that maintain telomere size across all the cell division cycles [8]. Telomeres are the main actors in the unlimited proliferation and cell immortality process. They regulate the cell replication capacity by shortening at each division till restrict completely cell division, a fact that hence does not occur in most cancer cells [9]. Another important hallmark of cancer cells is their highly activated metabolic rates that constantly

need an uptake of nutrients in order to remain metabolically overactive [1]. To sustain the need for large amounts of nutrients, tumor cells trigger the development of new blood vessels from nearby vasculature by constantly expressing angiogenesis inducers, like vascular endothelial growth factor (VEGF) and basic fibroblast growth factor (bFGF) [10-13]. This relentless expression of VEGF induces the formation of aberrant vasculature characterized by a leaky profile due to the existence of large fenestrations (600-800nm) in the endothelial walls [14, 15]. The high abundance of rich vascular networks together with the lack of expression of cell adhesion molecules such as E-cadherin, leads to cell extravasation. These cells consequently invade and colonize other organs and tissues throughout the body, a process known as metastization [16]. These unique characteristics are common to all types of cancer and contribute for a poor patient's clinical prognostic and disease progression.

1.2. Breast Cancer and its heterogeneity

Focusing particularly on breast cancer, this is actually the most diagnosed malignancy in women, in what concerns to solid tumors [17, 18]. This disease affected about 1.5 million of women worldwide in 2010 [17, 18] and 464.000 new cases have arisen in 2012, in the European Union, representing the third most deadliest cause among women [19]. When this disease is diagnosed at a very early stage of development, it has an excellent long-term prognosis in terms of patient free survival (PFS) rate [20]. However, in late stages of disease (stage III and IV) that often involve metastization, especially to adjacent lymph nodes, the survival rate decreases dramatically [20]. In this scenario even after mastectomy, 40% of women still develop metastasis in auxiliary lymph nodes [20]. Surprisingly, this type of tumor represents a particularly heterogeneous group with defined biological features and responses to therapy [21]. Actually, nowadays breast cancers are divided accordingly to their gene-expression subtypes into: i.) luminal (related with estrogen and progesterone receptors) ii.) human epidermal growth factor receptor 2 (HER2) and iii.) basal-like, which typically do not express HER2hormone receptors, having generally a triple negative phenotype [21-23]. HER2 are characteristic of different breast cancer subtypes. Cancers that do not have ERBB2, progesterone (PR) or estrogen (ER) receptors, are called triple negative breast cancer cells [24]. These type of cells present a constitutively enhanced Protein Kinase B (AKT) activity due to a mutation in MAGI3–AKT3 gene [21]. Currently available chemotherapies for cancer treatment are still largely limited by deleterious side effects that contribute for a limited therapeutic outcome. These side-effects are often associated with the lack of tumor cell specificity, with the consequent drug partitioning in other tissues and organs, such as the liver and lungs [20]. Such bottlenecks significantly reduce the bioavailability of chemotherapeutics at the target tumor site and are responsible for the administration of anti-tumoral drugs to patients for an extended period of time, at lower dosages (commonly between each 21 days across 6 to 8 sessions of chemotherapy [25]. Moreover, the rapid

systemic clearance of drugs and the difficult vascular access to lymph nodes of patients with breast cancer, contribute for the ineffectiveness of the treatments [26]. This therapeutic regime is also commonly associated with the development of drug resistant breast cancer cells.

1.3. Multidrug Resistant Cancer Cells

One of the main causes of chemotherapy failure in the improvement of PFS is the acquired drug resistance of cancer cells, after a few rounds of chemotherapy, a phenomenon that is termed multi-drug resistance (MDR) [27, 28]. MDR can result from non-cellular and cellular based mechanisms [28-30]. Furthermore, barrier mechanisms, that are not directly related to cells, such as poorly vascularized tumor regions that are protected against chemotherapy drugs also contribute to the MDR phenotype [29-31]. High interstitial pressure and the lack of microvasculature are additional barriers that affect drug extravasation into tumor tissues [32]. To overcome these issues the administration multiple chemotherapy drugs, can arise as a very promising approach [32]. In fact, since the acquired MDR by cancer cells is related to an over-expression of enzymes with specific drug metabolization or efflux capacity, the additional administration of chemical compounds that can shut-down their activity can contribute to MDR reversal [28-30]. Among the different resistance mechanisms, drug efflux pumps are currently the most extensively studied [30]. The resistance mediated by these efflux pumps can be attributed to an overwhelming decrease in drug uptake, since drug efflux to the extracellular medium is constantly promoted by P-glycoprotein (P-gp) and other ATP-binding cassettes (ABC) proteins that are over-expressed in these type of cells [30]. ABC's are a particularly relevant superfamily of transmenbrane proteins that have the capacity to transport various kinds of substrates, such as hydrophobic drugs (Doxorubicin, Cisplatin, Paclitaxel) [30, 33]. Some types of cancer cells over-express particular types of ABC's, such as ABCB1 (P-gp), ABCC1, and ABCG2 (also termed Breast Cancer Resisting Protein, BCRP), that are involved in the regulation of the intra cellular concentration of chemotherapy agents [27, 34]. It is described that these ABC transporters are highly expressed in inner regions of the tumors, due to the existence of hypoxic microenvironments [35]. In addition, MDR can also result from coordinated detoxification processes mediated by cytochrome P450 and deoxyribonucleic acid (DNA) repair mechanisms [36] reducing the effect of some drugs that have DNA damaging as a target (Cisplatin, Doxorubicin), however to a less extent than that dependent on ABC transporters [28]. Since the majority of efflux activity is ATP dependent, researchers have recently begun to explore more powerful P-gp inhibitors to overcome this critical hurdle [30].

1.4. Anti-tumoral drugs used for breast cancer therapy

The vast majority of drugs currently used for cancer therapy are severely limited by their low specificity to target tissues and cells, a fact that is responsible for deleterious side-effects [37]. A part from this, also drug physicochemical characteristics contribute for a rather ineffective biological activity. The latter is a consequence of the poor water solubility of anti-tumoral pharmaceuticals [38]. Due to this characteristic, chemotherapeutics have a narrow mean residence time (MRT) in blood circulation and a higher administered dosage is required to produce a therapeutic effect, dangerously increasing the associated toxic side-effects [38]. A particularly potent drug used for the treatment of breast cancer is Tamoxifen [39]. This drug is an antagonist of breast cancer cells oestrogen receptor (ER) and is currently used also against several other types of cancer [40]. Despite this, the effective doses that reach the tumor site limits its effectiveness [40, 41]. Other anthracycline-based therapeutics, such as Doxorubicin, Trastuzumab, Daunorubicin and Mitoxantrone are effectively used as chemotherapy agents for breast cancer [42]. However, their high cardiotoxic effects restrains their widespread use in a clinical context [40]. In addition, it has been extensively reported in the literature that after the administration of these drugs, breast cancer cells acquire an aggressive MDR phenotype, making different therapeutics ineffective [39].

Recently an interesting approach based on the use of multiple drugs has been proposed to overcome these issues [43, 44]. This unique strategy relies on the establishment of a synergistic effect by attacking various intracellular targets, with diverse drugs during the various stages of treatment, thereby improving treatment effectiveness [43]. Unique conjugation of compounds (Doxorubicin and Sildenafil [44]) has shown to reverse drug resistance to a certain extent, increasing the refractory period of the development of novel cancers [45, 46]. Nevertheless, regardless of this potential, the differences in the pharmacokinetic/pharmacodynamic profiles of each administered drug, the low stability and permeability still limits their *in vivo* application [45].

1.5. Exploring novel combinatorial drug therapies to overcome MDR and improve anti-cancer therapy

Currently, the investigation of novel drug combinations that target key hallmarks in cancer cells may unlock the possibility to discover extremely valuable synergies. Such investigation of new combinations using recently approved drugs is particularly valuable since, in the last decade, several improvements have been made in the drug development pipeline, especially in drugs aimed to be used in cancer therapy.

Taking this into account, Crizotinib (PF-2341066), an anti-tumoral drug that has been recently approved by the United States Food and Drug Administration (FDA) for non-small lung cancer arises as an interesting bioactive molecule to be used also in breast cancer therapy [47].

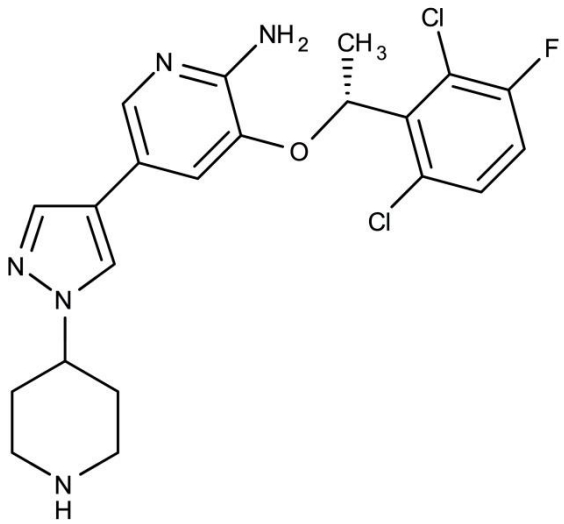

Figure 3 – Molecular structure of Crizotinib (PF-2341066).

In fact, regarding the specific antitumoral activity of Crizotinib in breast cancer cells, it has been reported that this particular drug has a half maximum inhibitory concentration (IC50) of 3.34 ± 0.52 μM in Michigan Cancer Foundation-7 (MCF-7) cell line, illustrating its possible use in the treatment of this malignancy [48]. Crizotinib mechanism of action is based on its capacity to be an ATP-competitive molecule (inhibiting ATP-dependent efflux pumps), and a potent inhibitor of c-MET phosphorylation [49, 50]. c-MET is a receptor that is overexpressed in most cancers, including breast cancer cells [51, 52]. When over-expressed c-MET receptors are activated by hepatocyte growth factor (HGF) binding, a massive cellular proliferation and invasion are stimulated and these are deeply related with tumor progression and growth [53]. Complementary studies have shown that Crizotinib has the ability to induce apoptosis via Caspase-3, as well as reduce micro vessel density [49]. Furthermore, it is described that this drug also specifically inhibits the ABCB1 efflux transporter, both *in vitro* and *in vivo* [33]. The anti-angiogenic effects, some MDR reversal capacity and the direct inhibition of tumor growth render it as a potent drug with very suitable characteristics for cancer therapy if it achieves high levels of bioavailability at target cells [33, 49]. However, since Crizotinib, as other chemotherapy drugs, is rather limited in the inhibition of several other ABC transporters, it is valuable to explore its conjugation with other drugs that have a broad spectrum of ABC inhibition [54].

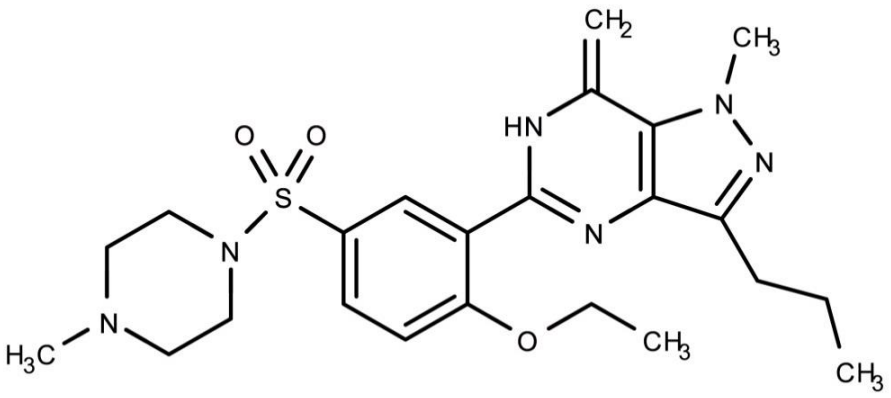

Figure 4 – Molecular structure of Sildenafil (PF-4540124).

Sildenafil, also known commercially as Viagra®, is a potent antagonist of ABC efflux pumps, since it inhibits the action of ABCG1, ABCC4, ABCC5 and ABCG2 that are present in breast cancer cells (Figure 5) [27]. This drug is also a phosphodiesterase 5 (PDE5) inhibitor that has been widely used to treat male erectile dysfunction and pulmonary hypertension [27, 55]. Recently, its application for anti-cancer therapy has been evaluated, and the obtained results [27, 55-57], suggested that this drug has the capacity to potentiate the effect of standard chemotherapeutics, by blocking the above mentioned ABC proteins [34, 55, 56, 58, 59]. The inhibition of these ABC transporters, that are involved in the efflux of chemotherapy drugs to the extracellular medium, results in drug accumulation inside the cell cytoplasm, thus potentiating the therapeutic effects. Besides, it is described that PDE 5 expression is enhanced in diverse human carcinomas such as metastatic breast cancer, giving Sildenafil an excellent potential to be used synergistically with other potent chemotherapy drugs [60].
Interestingly, Sildenafil has also shown to protect the heart from toxic effects of chemotherapeutic drugs, such as Doxorubicin [34, 56]. The cardio protective effect is assigned to the enhanced expression of nitric oxide synthase, a enzyme that is involved in the activation of protein kinase C and G, and up-regulation of Bcl-2/Bax [56, 58, 61, 62].

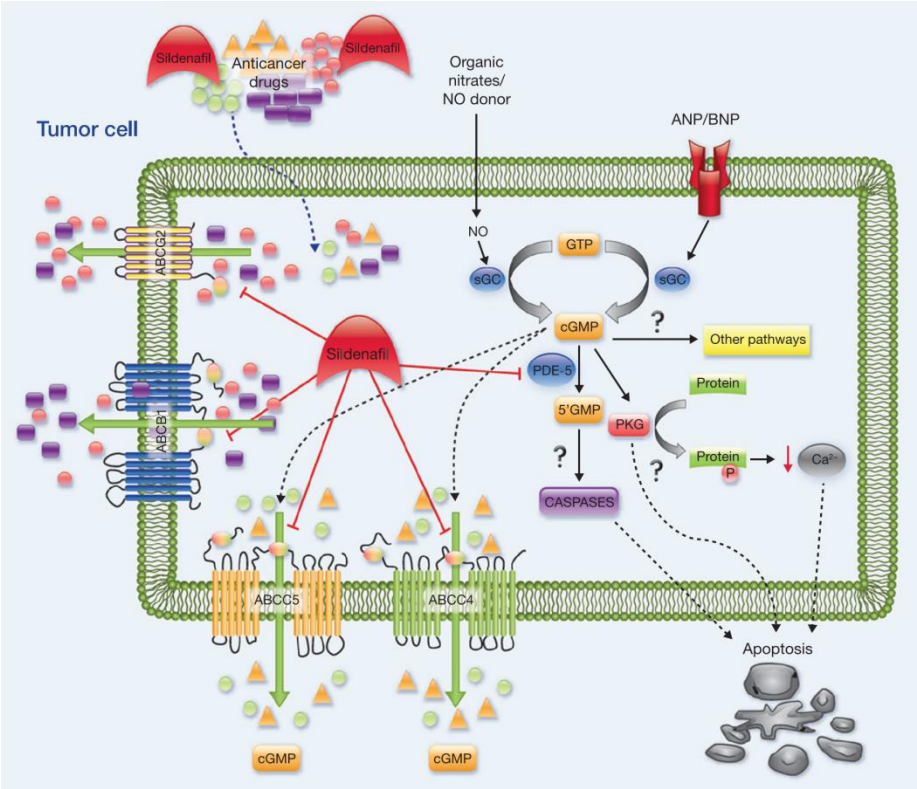

Figure 5 – Proposed mechanism of action for Sildenafil synergic activity in conjugation with other chemotherapy drugs by blocking drug efflux from MDR transporters (ABC's) and increasing intracellular cyclic guanosine monophosphate (cGMP) levels (Adapted from [27]).

2. Nanotechnology-based carriers for cancer drug delivery

In the last couple of decades the technological breakthrough of manipulating matter at the nanoscale, has encouraged an emerging and compelling interconnection between Nanotechnology, Pharmacy and Medicine, that will surely remain for many years to come [63]. This close affiliation has opened up the opportunity to devise novel and effective therapeutic approaches based on miniaturized nanoscale delivery systems to treat a multitude of impairing diseases, such as cancer [64]. Nanomedicine focused on cancer therapeutics is a particularly interdisciplinary field, that gathers knowledge from Biology, Chemistry, Engineering, Physics and Medicine in order to tackle the complexity associated with cancer cells through the development of drug delivery systems (DDS), that can increase drug bioavailability in diseased tissues and also minimize deleterious side effects in healthy cells [65]. Nano-sized devices, commonly with size ranges within 1 to 100 nm [66], or 1 to 1000 nm [67], provide a unique molecular interaction with biological systems and particularly with single cells [15, 40, 68, 69]. In fact, the sub-cellular size of nanoparticles is a unique characteristic that renders them as an ideal platform to concentrate highly potent anti-

tumoral drugs inside malignant cells, since they are readily internalized by various cell uptake pathways [70]. This concept was initially described in the late 60's, when liposomes where proposed as carriers for proteins and drugs, in order to enhance their delivery to a broad spectrum of pathologies (Figure 6) [71]. Since then, a wide variety of nanomaterials has been used for the manufacture of ever more evolved and efficient DDS's [15, 45].

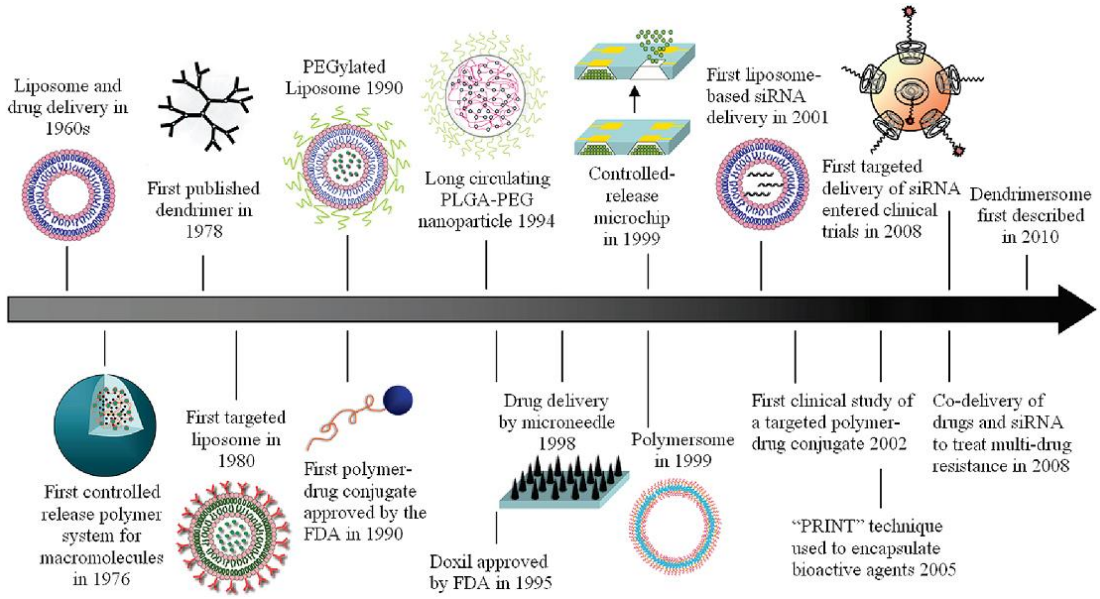

Figure 6 – Evolution of drug delivery systems along time (Adapted from [45]).

The use of nanoparticulated carriers changes the pharmacological properties of anti-tumoral compounds, to an extent that dramatically increases their overall therapeutic effect and prolongs PFS rates [72]. In fact, the inclusion of chemotherapeutics in DDS, utterly modulates their pharmacokinetic/pharmacodynamic profiles, especially their serum half-life and bioavailability at the target site (Figure 7) [72]. More importantly, their loading in DDS significantly reduces their toxicity, unlocking the potential to administrate pharmaceutic compounds with remarkable anti-tumoral activity [15, 45], using these nanotransporters. Furthermore, they can also contribute to reduce the frequency of administration to achieve an increased therapeutic effect, in comparison to systemic free-drug administration [15, 45].

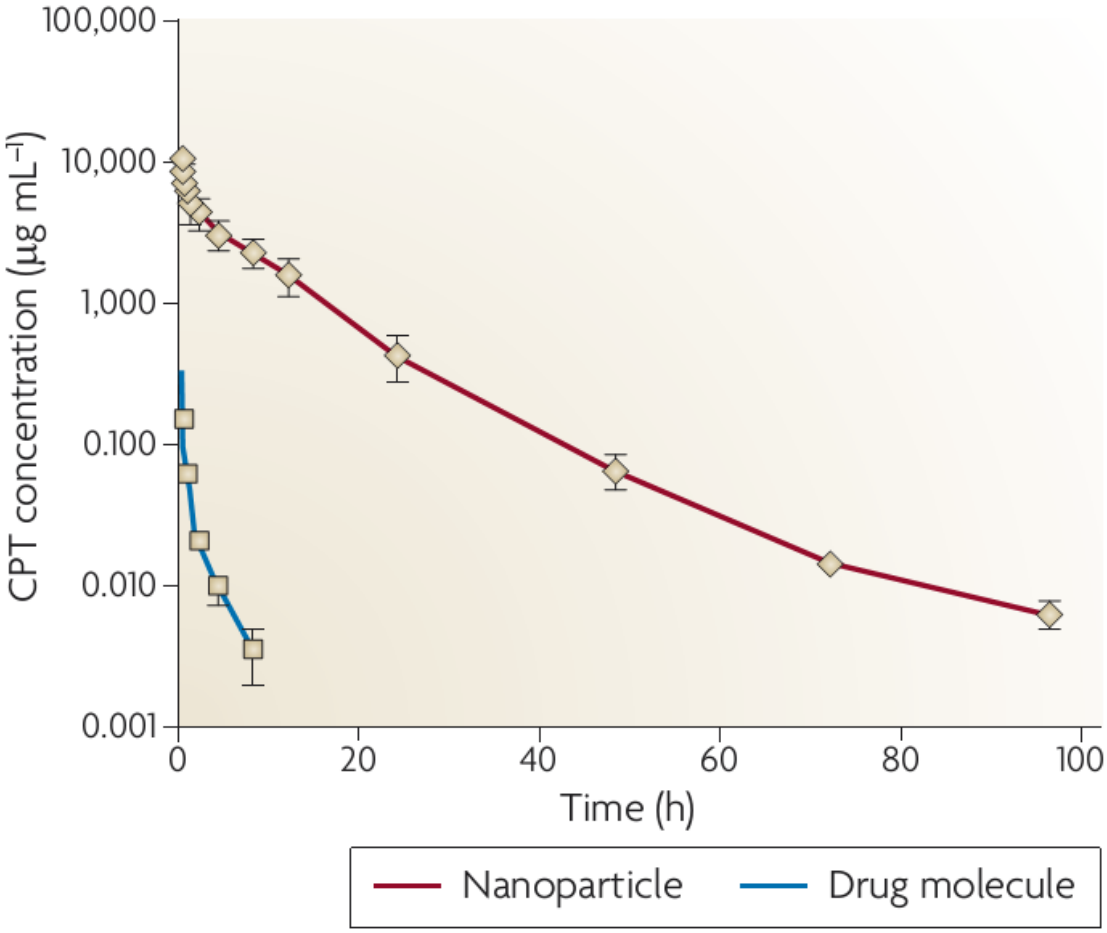

Figure 7 - Enhancement of drug concentration and bioavailability through nanoparticle conjugation. (Adapted from [73]).

Nanocarriers designed for cancer therapy may be administered through various routes such as: i.) nasal airways, ii.) oral-bucal, iii.) intra-dermic and intramuscular, iv.) intra-ocular and v.) systemic injection through the blood stream [74]. The administration modality affects the overall biodistribution of the nanocarrier-drug conjugate and should be carefully chosen according to each cancer type and location [72]. Regardless of the administration route, once the nanocarriers interact with biological fluids their physicochemical properties change to such an extent that influences nanocarrier-cell interactions, and consequently internalization in target cells [74]. Opsonization process is one of the major barriers that DDS need to overcome [75]. Opsonization and consequent phagocytosis is mediated by the Mononuclear Phagocytic System (MPS). This system is comprised by immune system cells such as phagocytic cells, that are especially present in the spleen and liver. Depending on nanoparticle surface and size, opsonins, proteins present in serum, rapidly bind to nanoparticles enabling macrophages to remove these nanovehicles from blood circulation, affecting their function [75, 76]. It has been previously reported by Letchford and co-workers that nanoparticles with less than 200 nm present a decreased elimination by MPS, and accordingly longer blood circulation times [67]. This size-dependent interaction with the immune system determines the extent of nanoparticle susceptibility to phagocytosis [77]. Once nanocarriers successfully

evade MPS, they can fulfil their accumulation in tumor tissues. The accumulation of DDS in diseased tissues after intravenous administration is a critical parameter, since it dictates drug delivery efficiency into target cells. Presently, two major strategies can be employed to promote this accumulation in the tumor microenvironment, the so-termed active and passive targeting [78]. The latter will be particularly focused in this work.

2.1. Passive Targeting – The Enhanced permeability and Retention Effect

Passive targeting takes advantage of the biological characteristics of the tumor microenvironment itself, namely by exploiting the existence of a highly vascularized network of leaky blood vessels that surround tumor tissues [79, 80]. The lack of lymphatic drainage also contributes for molecule retention in tumors [81]. This phenomenon is generally termed as the enhanced permeability and retention (EPR) effect and is characteristic of solid tumors (Figure 8) [82]. EPR is a probabilistic effect that depends on an extended serum half-life of molecules, such as nanoparticulated carriers, and on their capacity to extravasate through the fenestrations on the endothelial wall of blood vessels to the tumor periphery [83].

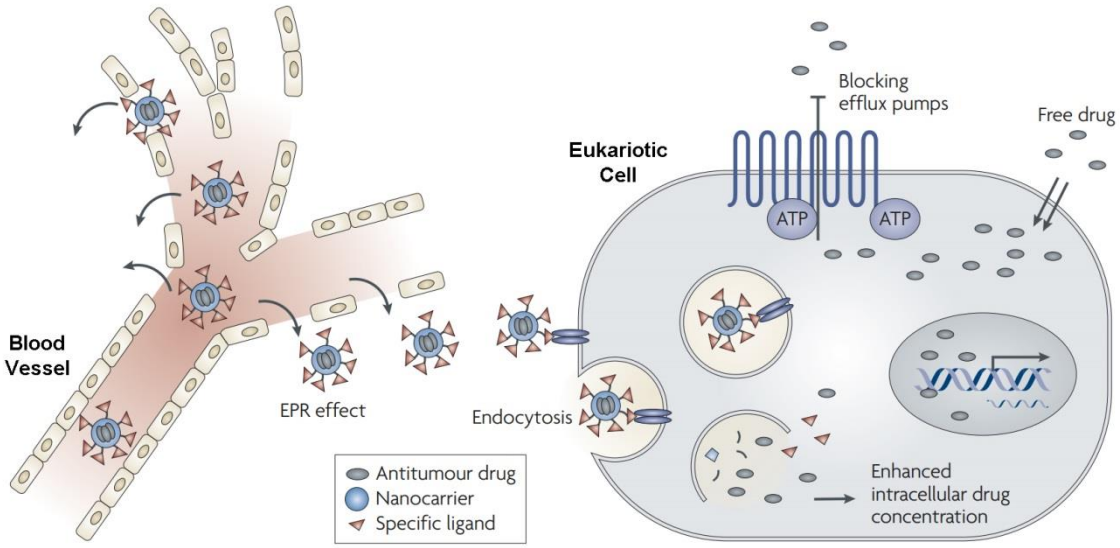

Figure 8 - Presentation of nanoparticle EPR effect and enhanced intracellular drug concentration due to efflux pump inhibition. Nanoparticles extravasate through the leaky vasculature due to the fenestrations in the endothelial wall surrounding the tumor microenvironment (Adapted from [68]).

These fenestrations are formed due to the uncontrolled angiogenesis. Such process causes high vascular density originating large gaps [68]. It is clear that free chemotherapy drugs distribute throughout the entire body will be partitioned through the various organs (e.g. the liver, kidney or lungs), but due to the EPR effect they can also be accumulated in diseased tissues, although to a far less extent than that of their initial concentration. This EPR effect

has provided the basis for the formulation of nanodevices suitable for anti-cancer therapy [81, 82]. Studies with animal models conclude that neutral to slightly negatively charged drug-loaded nanoparticles, with sizes below 150 nm, have the ability to accumulate into tumor tissues by the EPR effect [84]. This tumor accumulation potentiates the anti-tumoral effect, since it increases the bioavailability of chemotherapeutics at the tumor site [15]. However, despite this potential, the EPR effect still presents some limitations, especially due to the pathophysiological heterogeneity of each tumor and the high, interstitial pressure [85]. However, the increased blood flow and reduced blood pressure caused by the tumor vasculature, enhances nanoparticle extravasation into tumors [86, 87].

3. Organic and Inorganic biomaterials used for self-assembly drug delivery systems

Among the different types of nanoparticles produced, they can be classified according to their composition into two major groups: inorganic and organic [40]. Inorganic DDS are characterized by their stability, good loading capacity and controlled release of drugs. However, some inorganic nanoparticles can have cytotoxic effects such as those associated with the accumulation of iron, silver and gold in the human body. Nevertheless, these are versatile systems that can also be employed in theranostic applications, due to their bioimaging capacity [88, 89].

Organic DDS are particularly advantageous for the formulation of anti-cancer therapeutics for breast cancer therapy, due to their high biocompatibility, biodegradability, high loading capacity and versatile chemical composition that allows their modification with bioactive macromolecules [90, 91]. Among organic DDS, amphiphilic nanoparticles present advantages over the other organic nanoparticles due to their self-assembly behaviour [92]. This particular class comprises: i.) liposomes; ii.) dendrimers; iii.) protein nanoparticles and iii.) polymeric DDS, namely micelles, polymersomes and nanocapsules among others, some of which are present in Figure 9.

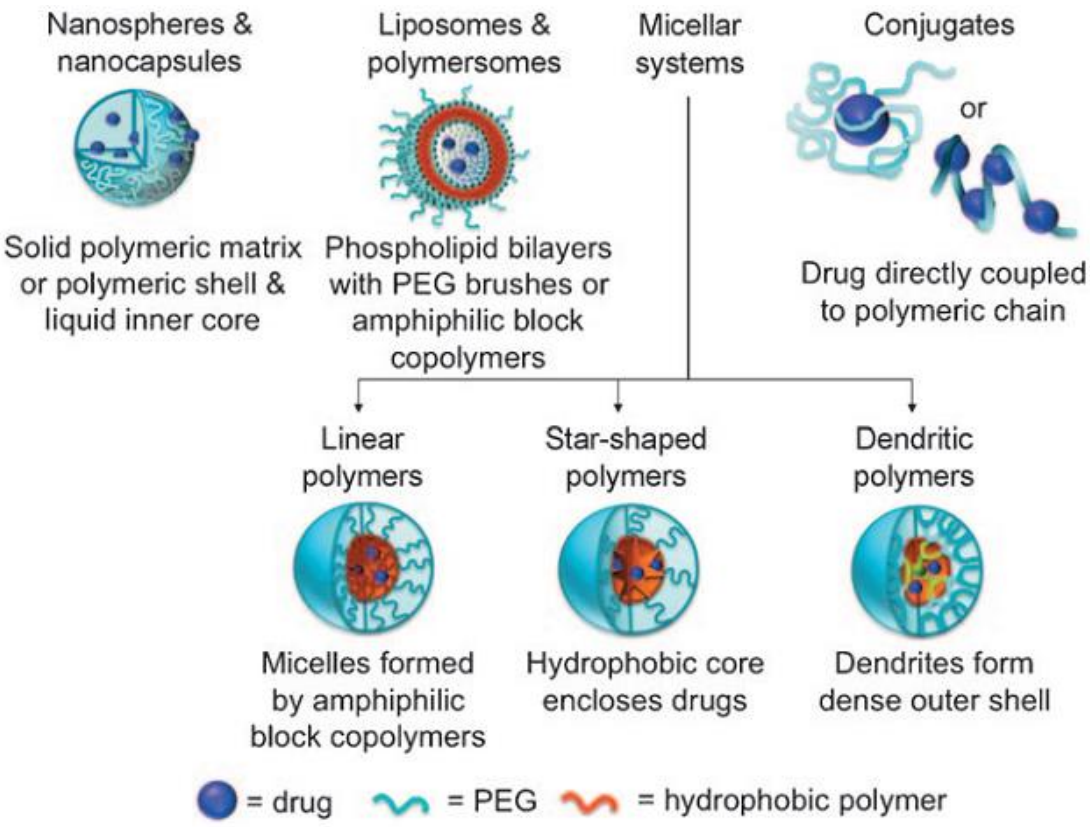

Figure 9 – Representation of the drug-delivery systems currently available. (Adapted from [93]).

Lipid-based nanoparticles, also termed liposomes, where one of the first delivery vehicles used in medicine [15]. Liposomes are generally comprised of natural or synthetic lipids, having diverse architectures (multilamelar, core shell, rod like or star shaped), which can accommodate both hydrophilic and hydrophobic molecules [15, 94, 95] like liposome based nanoparticle designed for delivery Tamoxifen to breast cancer cells [96]. However, the use of liposomes as DDS for cancer therapy has several issues that hinder their widespread application in the clinic. Liposomes present a very rapid blood clearance, which is further accelerated after multiple administrations of liposomal formulations coated with hydrophilic polymers that are aimed to increase their blood circulation time. This phenomenon has been only recently described [97]. Opsonisation of liposomes and consequent capture by MPS [68, 94] and their cytotoxicity to healthy cells are the main disadvantages of this class of DDS. Nevertheless, some polymer-modified liposomes that take advantage of the EPR effect and prove to be non-toxic, have been developed for cancer therapy [38, 98]. Doxil®, is a FDA approved and commercially available pegylated-liposomal formulation, that carries Doxorubicin for cancer therapy [99, 100]. Polymeric nanocarriers provide several advantages over liposomes such as better overall drug/carrier stability [101] and sustained drug controlled release [102]. Polymers used in drug delivery can be synthetic or natural [103]. The synthetic polymers have some advantages over the natural. They can provide a

spatiotemporally controlled drug delivery of bioactive pharmaceutics for longer periods than some natural polymers, such as chitosan or alginate that suffer from extensive swelling [103]. Among the different DDS that can be formulated with polymeric materials, micelle carriers are one of the most versatile vehicles for being applied in cancer therapy. They can be used for increasing the solubility of poor water soluble chemotherapeutic drugs, by approximately one thousand fold, a fact that renders them ideal candidates for cancer treatment [104]. Micelles are commonly formulated by two blocks of polymers, hydrophobic and hydrophilic, that are generally grafted together by chemical linkages [67]. The so termed block co-polymers are generally formed by a hydrophilic shell and a hydrophobic core, thus having an amphiphilic character (Figure 10). The hydrophobic core is used to encapsulate hydrophobic molecules, such as chemotherapy drugs. Micelle formation occurs spontaneously in water solutions, if the concentration of the amphiphilic polymer increases to a point in which the hydrophobic chains establish favourable hydrophobic interactions, among each other. This is an interesting phenomena that ultimately results in the formation of the so termed core-shell structure [67]. The minimum concentration required for a micelle self-assembly is called Critical Micellar Concentration (CMC) [67]. Micelles formed with amphiphilic co-polymers are advantageous due to the lower CMC, than those formed with the use of surfactants [67]. In this unique core-shell architecture the drug is protected from biological degradation and its deleterious side effects are significantly reduced [38]. Polymeric micelles can also be easily modified by imprinting targeting moieties on their surface, in order to increase their tissue specificity [105, 106]. Furthermore, the drug loading efficiency and the release profile can be largely improved by simply manipulating the size of hydrophobic or hydrophilic polymer backbones [38, 107]. Poly (ethylene glycol) (PEG) is one of the most used hydrophilic polymers (generally between 1 and 15 kDa) for the formation of the outer shell [38]. However, in the last decade other hydrophilic polymers have also been used to assemble polymeric micelles such as poly (2-hydroxyethyl methacrylate) (PHEMA) and poly (oxazoline) (PEOz) [108, 109]. Nowadays, several formulations of polymeric micelles are currently available for cancer therapy. These include SP1049C® a Pluronic-based micelle for Doxorubicin delivery [101], Genexol-PM® a Poly (ethylene glycol)-Poly (lactic acid) (PEG-PLA) micelle loaded with paclitaxel, among others (Table 1) [101].

Table 1 - Comparison of micelles approved or enrolled in clinical trials by FDA. NA (not applicable) (Adapted from [68]).

Name	Formulation	Diameter (nm)	t½ (h)	Clearance (mL/min/kg)	Comments
Doxorubicin	0.9% NaCl	NA	0.8	14.4	Small-molecule drug
SP1049C	Pluronic micelle + Doxorubicin	22–27	2.4	12.6	Micelle nanoparticle
NK911	PEG–Asp micelle + Doxorubicin	40	2.8	6.7	Micelle nanoparticle
Doxil	PEG–liposome + Doxorubicin	80–90	84.0	0.02	PEGylated liposome nanoparticle with long circulation
Cremophor EL	Polyethoxylated Castor Oil Taxol (Paclitaxel)	NA	21.8 (20.5)	3.9 (9.2)	Small-molecule drug
Genexol-PM	PEG–PLA micelle + Paclitaxel	20–50	11.0	4.8	Micelle nanoparticle
Abraxane	Albumin + Paclitaxel	120	21.6	6.5	Albumin nanoparticle before injection; status *in vivo* unknown
XYOTAX	PG + Paclitaxel	Unknown	70–120	0.07–0.12	Polymer nanoparticle
Camptosar (prodrug of SN-38)	0.9% NaCl	NA	11.7	5.8	Small-molecule prodrug
LE-SN-38	Liposome + SN-38	Unknown	7–58	3.5–13.6	Liposome nanoparticle
Topotecan (camptothecin analogue)	0.9% NaCl	NA	3.0	13.5	Small-molecule drug
CT-2106	PG + Camptothecin	Unknown	65–99	0.44	Polymer nanoparticle
IT-101	Cyclodextrin-containing polymer + Camptothecin	30–40	38	0.03	Polymer nanoparticle with extended circulation times

In a recent study, a combination of two block co-polymers (poly(HEMA-co-histidine)-g-PLA and PEG-PLA) was used to specifically target HeLa cells and deliver Doxorubicin [110]. A modified poly (ethylene glycol)-block-poly (ε−caprolactone) (PEG-PCL) micelle, carrying paclitaxel, showed to be effective against MCF-7 cells and breast cancer stem cells [111].

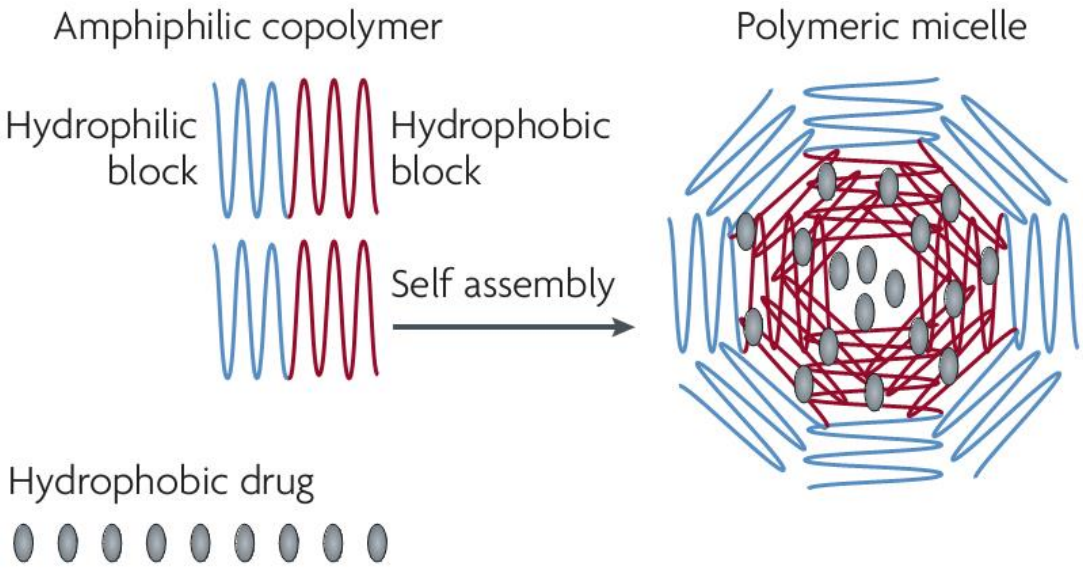

Figure 10 – Polymeric micelle structure composed with block co-polymers that self-assemble in water solutions (Adapted from [68]).

3.1. Hydrophobic polymers used for the production of self-assembled DDS micelles for cancer therapy

Poly (lactic acid) (PLA) and poly (D,L-lactide-co-glycolide) (PLGA) have been extensively used for the manufacture of DDS [112]. These synthetic polymers are highly biocompatible and biodegradable, since their hydrolysis yields degradation products (lactic acid or glycolic acid) that are inserted in natural metabolic pathways. Particularly, L-Lactic acid integrates the citric acid cycle [103], or is converted to glucose, in the Cori cycle [113, 114]. Moreover, since these degradation products are formed at a slow rate, they do not affect normal cell metabolism [103, 114]. These polymers have been largely tested in animals and are currently used for bone implants, sutures and other applications in humans, such as cancer therapy, as previously mentioned (Genexol-PM®) [101, 113, 115].

Lactic acid (LA) is the monomeric unit of the PLA polymer backbone [114]. This monomer can be formed by bacterial sugar conversion, which makes the LA an inexpensive raw material to obtain [114]. PLA can be produced by direct condensation or ring opening polymerization (ROP) of L-lactide, under specific conditions, yielding very homogeneous polymeric chains with low size and low polydispersity index (PDI) [116, 117]. As a hydrophobic polymer, PLA presents good hydrophobic drug encapsulation capacity, up to 10% of its weight. PCL is more

hydrophobic than PLA and promotes a slightly better encapsulation of hydrophobic drugs [118], but its rather slow biodegradation is a factor that can impair its biological applicability [119].

3.2. Hydrophilic polymers used for the production of self-assembled DDS micelles for cancer therapy

PEG is a widely investigated synthetic polymer approved by the FDA and by the European Medicines Agency (EMA) for nanocarriers production to be used for drug delivery applications due to its unique and versatile physicochemical characteristics [93, 120]. In fact, PEG is so versatile that it can be chemically synthesized with a plethora of pendant groups (e.g. -OH, -NH2, -COOH, -SH, -Maleimide, -NHS esters, among others) that unlock the possibility to graft PEG chains to virtually any other polymers including PLA and PLGA [121]. Moreover, the relative low cost of PEG polymers and their capacity to endow DDS with stealth ability in serum, as discussed henceforth, account for its ever growing use [93, 122]. PEG is also biocompatible, being generally considered to have low toxicity in comparison with cationic Liposomal formulations. Presently, PEG is used as an excipient in several intravenous medicines such as Ativan®, or in daily products such as toothpaste [123]. In fact, the World Health Organization as set as limit a daily dose of 10 mg/Kg for administration via oral route, although only for PEGs with a molecular weight (Mw) up to 10 kDa [123].

The latter parameter is crucial since PEG Mw and PDI plays an important role in envisioned biomedical applications [93]. The molar mass of PEG used in pharmaceutical and biomedical applications commonly ranges from 400Da to 50kDa [93]. Longer PEG chains have been conjugated to low-Mw drugs and other small molecules, like small interfering RNA (siRNA) and oligonucleotides, slowing down their clearance [93]. PEGs with 1 kDa to 5 kDa are more suitable for DDS production [93, 101]. PEG chains with this length range are very flexible, and the polymer can acquire various conformations which is very important for evading interaction with blood components such as opsonins [93]. PEG chains create a water barrier on nanoparticle surface that prevents opsonins adhesion [67]. Less opsonin coating results in lower immunological response and elimination by MPS is therefore reduced [93]. This protective character is only possible due to the steric hindrance effects that PEG promotes, functioning as an actual shield for protein or cell adsorption to DDS [124]. PEG also reduces enzymatic degradation and has the ability to shield the polymer from cationic charges that could contribute for erythrocyte lysis [93]. Regarding the PDI parameter, the polymer should have a PDI lower than 1.1 to ensure homogeneity in biological responses [125]. Due to these valuable characteristics PEG-based micelles have been widely used in self-assembled DDS formulations with core-shell structures, since the PEG moiety is highly hydrophilic [126].

PEG-PLA nanoparticles are widely used to deliver hydrophobic drugs due to their self-assembly capacity, high stability, relatively small size (20 to 200 nm), safe administration in humans and high drug loading capacity [93, 127]. The hydrophobic interaction between drugs and the hydrophobic moiety of the amphiphilic co-polymer governs the encapsulation stage [128]. A PEG-PLA micelle loaded with Paclitaxel (Genexol-PM) is currently approved in South Korea, for cancer therapy [129]. Moreover, PEG-PLA nanocarriers are also under stage II clinical trial, in United Stated of America (USA) for Doxorubicin delivery [15, 68]. Since this drug is considered to be more suitable for breast cancer therapy than standard Cremophor EL, a castor oil pegylated nanoparticle with encapsulate paclitaxel [130]. The high dose required for intravenous injection of Cremophor EL (26 mL per injection for treatment of an average weight patient) elicits side effects [104]. Besides, Genexol-PM proved in clinical trials with breast cancer patients, to have better therapeutic efficiency, since it presented a higher maximum tolerated dose (MTD), and improved pharmacokinetic profile, delaying the time of disease progression in 9 months [130].

Synthesis of block co-polymer PEG-PLA can be performed by ROP between PEG, which acts as macro initiator of the reaction and L-lactide [131]. Commonly tin(II), zinc and aluminium salts, such as stannous octoate ($Sn(Oct)_2$), are used to catalyze the ROP reaction, as shown in Figure 11 [132, 133]. The length of polymer can then be controlled by changing the weight ratio between the initiator and L-lactide monomer [126].

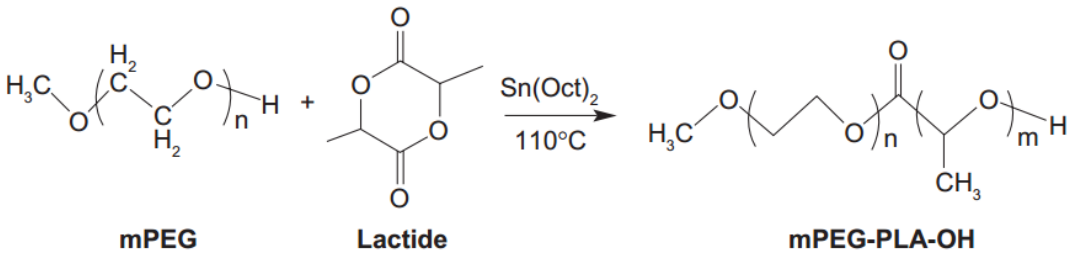

Figure 11 - Mechanism of polymerization of L-lactide. mPEG acts as macroinitiator and $Sn(Oct)_2$ act as a catalyst (Adapted from [131]).

The amphiphilic character of PEG-PLA allows its self-assembly in water [134]. Various methods can be used to assemble PEG-PLA micelles, such as: i.) direct dissolution in water, ii.) film rehydration, that consists in using an organic volatile solvent followed by evaporation-solubilisation cycles [135] and iii.) sonication [118], with this method yielding the highest encapsulation efficiency of hydrophobic drugs [118].

Aims

The global aim of this thesis was to develop a new approach for breast cancer therapy through the synthesis of micellar nanovehicles capable of co-delivery of two drugs to breast cancer cells. The specific aims of this research include the:

- Synthesis and characterization of amphiphilic block co-polymers capable of self-assembling into nanosized micelles;
- Characterization of the physicochemical properties of the self-assembled micelles;
- Evaluation of multi-drug loading efficiency by produced micelles and investigation of their release profile;
- Assessment of micelle uptake by breast cancer cells;
- Study of the anti-tumoral potential of free drug pharmaceutical formulations;
- Evaluation of the anti-tumoral and synergic effect through micellar vehicle delivery.

Chapter 2

Materials and Methods

2. Materials and Methods

All methods performed in this thesis are according to the directives set forth by the International Standards Organization (ISO) in the following standard guidelines: i.) ISO/Technical Report (TR) 13014-2013 - Nanotechnologies guidance on physicochemical characterization of engineered nanoscale materials for toxicological assessment; and ii.) ISO 10993-5:2009 - Biological evaluation of medical devices - Part 5: Tests for *in vitro* cytotoxicity.

2.1. Materials

Metoxy Poly(ethylene glycol) (mPEG) 2000 was obtained from Nanocs (New York, USA). Acetone, Acetonitrile (HPLC-grade), Dichloromethane, Dulbecco's Modified Eagle's Medium (DMEM), Methanol (MetOH) (High Performance Liquid Chromatography (HPLC)-grade), Resazurin, Rhodamine B Isothiocyanate (RITC), Toluene, were acquired from VWR Internacional (Carnaxide, Portugal). Antibiotic–Antimycotic (penicillin and streptomycin), Cacodylate, Cellulose dialysis membrane, Collagen type I, Fetal bovine serum (FBS), Glutaraldehyde, Paraformaldehyde, Phosphoric acid, and Triton X-100 were obtained from Sigma–Aldrich (Sintra, Portugal). MCF-7 (ATCC® HTB-22) mammary gland adenocarcinoma cell line was obtained from ATCC (Middlesex, United Kingdom) and primary normal human dermal fibroblasts (hFIB) from Promocell (Heidelberg, Germany). Rompun (Xylazine) was purchased from Bayer Health Care (Carnaxide, Portugal) and Imalgene (Ketamine) was obtained from Merial Laboratories, (Lyon, France). Stannous Octoate was purchased from (Cymit Quimica, Barcelona, Spain). All the glassware used in polymer synthesis was borosilicate 3.3 supplied by Afora SA (Spain). PF-02341066 (Crizotinib) and PF-4540124 (Sildenafil) were purchased from Tocris Bioscience (Nortpoint, United Kingdom). CellEvent™ Caspase-3/7® and Hoechst 33342® where obtained from Invitrogen (Carlsbad, USA). L-Lactide monomer and the Pyrene fluorescent probe were acquired from TCI (Tokyo Chemical Industry, Co., LTD., Japan). 3-(4,5-dimethylthiazol-2-yl)-5-(3-carboxymethoxyphenyl)-2-(4-sulfophenyl)-2H-tetrazolium) (MTS) was obtained from Promega (Madison, WI, USA). Phalloidin CruzFluor® 647 was obtained from Santa Cruz Biotechnology (Santa Cruz Biotechnology, Santa Cruz, Canada). All the used salts were of analytical grade and used without further purification.

2.2. Methods

2.2.1. Synthesis of mPEG-PLA

The polymerization process of PEG-PLA co-polymers was performed as described previously in the literature [131]. Initially, a 1:305 molar ratio of mPEG:L-LA were weighted into a reaction flask that was previously dried.

Prior to all reactions the system was purged with N_2 and sealed. Afterwards, 44.0 x 10^5 mL of toluene/mol of PEG where injected in the reaction flask. The system was then heated to 100°C and 0.1% of $Sn(Oct)_2$ was added. The reaction proceeded at 120°C to start the ROP. In order to obtain different block co-polymers the reactions were performed during three different time frames: i.) 4h; ii.) 8h and iii.) 30h. From this point onwards the nomenclature used to describe the co-polymers synthesized in function of ROP polymerization time is as follows: i.) PL4, ii.) PL8 and iii.) PL30, for the 4, 8 and 30h, respectively. After the above mentioned time the reaction was evaporated in a Buchi Rotavapor (R-250 Postfach Flawil, Switzerland) until the organic solvent was completely evaporated. The co-polymer film that was formed after evaporation was then dissolved and recovered by selective precipitation in excess MetOH.

The precipitation stage was allowed to proceed until a white precipitate was formed. The block co-polymers were afterwards dialyzed against mili-Q water (double deionised and filtered water) during 5 days to remove water soluble contaminants. The recovered product was finally freeze-dried in a Scanvac freez-drier (Scanvac CoolSafe™, ScanLaf A/S, Denmark). The purified powder was stored at 4°C until further use.

2.2.2. Nuclear Magnetic Resonance

The molecular characterization of the different synthesized co-polymers was performed through proton (1H) Nuclear Magnetic Resonance (NMR) spectroscopy, by using a Brüker Advance III 400 MHz spectrometer (Brüker Scientific Inc, USA). Prior to spectra acquisition polymer samples were dissolved in 1 mL of Deuterated Chloroform ($CDCl_3$). The samples were then carefully transferred to 5 mm NMR glass tubes. All the ^1H homonuclear spectra were acquired at a constant temperature of 298 K using a water pre-saturation pulse program (zgpr, Brüker Scientific Inc.). The data was recorded with a spectral width of 1 to 8.00 kHz. The recorded spectra where processed and integrated with the TOPSPIN 3.1 software (Brüker Scientific Inc), where a line broadening of 3 Hz was used. All data was also processed with an exponential window function in order to increase signal-to-noise ratio and eliminate possible acquisition artefacts. NMR peak integration was used to calculate the number average molecular weight (Mn) of the PLA chain, the molecular weight (Mw) of synthesized co-polymers, and the degree of polymerization of PLA as described by the following formulas:

$$M_{nPLA} = 72\left(\frac{M_{nPEG}}{44}\right)\left(\frac{EO}{LA}\right)$$ [136],

where EO is the Mw of ethylene oxide (PEG monomer)

$$DP_{PLA} = \left(\frac{M_{nPEG}}{44}\right)\left(\frac{EO}{LA}\right)$$ [136],

where LA is the Mw of Lactide (PLA monomer).

For this calculation the mPEG characteristic peak (δ=3.6 ppm) and the PLA characteristic peak (δ=5.2 ppm), were used as references for both polymers as previously described by Li and co-workers [136]. A total of five integrations were performed for all samples.

2.2.3. Fourier Transform Infrared Spectroscopy

The polymerization of PEG-PLA block co-polymers was additionally confirmed by Fourier Transform Infrared Spectroscopy (FTIR). The FTIR interferograms were acquired in a Nicolet iS10 spectrometer (Thermo Scientific Inc., USA) by recording 128 scans with a spectral width ranging from 4000 cm^{-1} to 600 cm^{-1}, at a spectral resolution of 4 cm^{-1}. A baseline correction and atmospheric suppression was performed in all the acquired data in order to avoid possible interferences in the FTIR spectra. Posterior data analysis and peak peaking was executed in the OMNIC Spectra software (Thermo Scientific).

2.2.4. Gel Permeation Chromatography

Gel Permeation Chromatography (GPC) measurement was performed at 25°C, with a fast protein liquid chromatography (FPLC) instrument (Amersham Biosciences, Sweden), equipped with Sephacryl S-100 HR column and a conductance detector. The column was equilibrated with 3 volumes of 0.2M of NaCl solution, at a flow rate of 0.5 mL/min. For GPC analysis, 1 mL of each sample was injected in the column. Molecular weights of analysed samples were calibrated with polyethylene glycol standards (PEG 2000, 4000 and 8000). All solutions used were previously filtrated with 0.22 μm filters and sonicated for at least 15 minutes. Sigma Plot software (Jandel Corp., Corte Madera, Canada) was used to analyse the obtained chromatograms.

2.2.5. X-ray Powder Diffraction

The characteristic crystallinity of the synthesized polymers was evaluated by X-ray Powder Diffraction (XRD) analysis. For these analysis freeze-dried samples of the different block co-polymers were mounted in appropriated silica supports by using a spatula and compressing the material into double sided adhesive tape. The mounted samples were then acquired in a Rigaku Geigger Flex D-max III/c diffractometer (Rigaku Americas Corporation, USA), equipped with a copper ray tube operated at voltage of 30 kV and current of 20 mA. XRD data was recorded over a range of 5 to 90°, with continuous scans at a rate of 1°C/min. The XRD diffractograms were compared to an international materials database, provided in the JADE 6 data processing software. Percentage of crystallinity of synthesized polymers can be calculated by the following formula:

$$\%\ \text{Cristallinity} = \frac{(\text{total area of cristalline peaks})}{(\text{total area of allpeaks})} \times 100 \quad [137]$$

2.2.6. Differential Scanning Calorimetry

Thermal analysis of the different block co-polymers synthesized was performed in a DSC-204 Phoenix (Netzsch Gerätebau, Germany) differential scanning calorimeter. For Differential Scanning Calorimetry (DSC) analysis approximately 3 mg of powder samples were deposited inside standard aluminium pans. The samples were then heated from room temperature (approximately 25°C) to 200°C, at a rate of 5°C/min, as previously described in the literature [138]. Protective gas (argon) was kept at a constant rate of 65 mL/min and was used to remove possible artefacts and maximize heat transfer. Calculation of the heat enthalpy (ΔH) and melting temperature (Tm) for each block co-polymer was performed through peak integration in the Proteus® software (Netzsch).

2.2.7. Micelle self-assembly - Film Hydration Method

PEG-PLA micelles were formulated via the film-hydration method, as described in the literature [139]. For micelle self-assembly, PEG-PLA block co-polymers dissolved in 1 mL of an equivolumetric mixture of dichloromethane/MetOH were placed in a round-bottom flask. 2.22×10^{-8} mol of Crizotinib/mg of polymer of a previously prepared solution were then added and gently mixed. The mixture was then evaporated on a Rotary evaporator (Rotavap® R-215, Büchi, Switzerland) to form a thin film. The polymer-drug film was then hydrated with 1 mL mili-Q water and sonicated for 30 min, in a Brandson 5510 bath sonicator (Branson Ultrasonic Corp., CT, USA). The obtained single drug micelles where pelleted at 30000 g during 30 min. The micelle pellets were then resuspended in mili-Q water until further use. To promote the self-assemble of the dual drug micelles, performed similar

procedure was used. For this purpose $2.11x10^{-8}$ mol of Sildenafil/mg of polymer and $2.22x10^{-8}$ mol of Crizotinib/mg of polymer were co-dissolved with PEG-PLA polymer as above mentioned. This methodology was carried out for the three different polymers (PL4, PL8 and PL30). Additionally, blank micelles, i.e., with no addition of drug, were also prepared as described before.

2.2.8. Determination of the Critical Micellar Concentration

The CMC of the different PEG-PLA co-polymers was determined by fluorescence spectroscopy. Pyrene was used as a model fluorescent probe as previously described by Laek and co-workers, 2013 [140]. To determine the CMC different polymer concentrations ranging from 0.001 to 2000 μg/mL were used to encapsulate pyrene (0.6 μM). Because of its hydrophobicity, pyrene tends to move to micelles core, and because it shows a shift on emitted fluorescence, when inside the micelles, micelle stability can be evaluated. The shift in pyrene fluorescence was measured in a Spectramax Gemini XS spectrofluorometer (Molecular Devices LLC, USA). To record the differences in pyrene fluorescence an excitation wavelength of $\lambda_{ex} \approx 333$ nm and $\lambda_{ex} \approx 335$ nm and an emission wavelength of $\lambda_{em} \approx 390$ nm were used, as previously described. The obtained data is presented as the ratio of the fluorescence intensity of the pyrene excitation peaks ($I\lambda_{ex} \approx 335$ / $I\lambda_{ex} \approx 333$) as a function of co-copolymer concentration.

2.2.9. Haemolysis Assay

In order to assess the blood compatibility of carriers, the synthesized micelles were incubated with rat erythrocytes. All the procedures used to manipulate animals were in agreement with European regulatory guidelines for care and use of laboratory animals (Directive 2010/63/UE). In addition, the experiments were performed in specialized in house facilities certified by the Portuguese Veterinary Department for animal research (ISO 9001 certification).

Initially for blood collection female Wistar rats were euthanized by terminal anaesthesia. Blood samples were then collected by cardiac puncture. The whole blood was immediately transferred to EDTA containing tubes. For the haemolysis experiments, 2mL of whole blood were pelleted for red blood cell (RBC) isolation. The supernatant containing platelets and plasma was then discarded and the RBC's pellet resuspended in 2 mL of Phosphate Buffer Saline (PBS) and rinsed twice as before mentioned to remove residual contaminants. Afterwards, the purified RBC's where incubated with a range of concentrations of PL4, PL8 and PL30 micelles (50 and 500 μg/mL), for 1 h, at 37 °C. PBS and Triton-X100 incubated RBC's were used as negative and positive controls, respectively. After the incubation period, the RBC's where pelleted and the supernatants recovered for further quantification. The

determination of free haemoglobin was performed by ultraviolet-visible (UV-vis) analysis at λ=540 nm in a Shimadzu–1700, UV-vis spectrophotometer (Shimadzu Inc., Japan).
Additionally, the integrity of the RBC's was also characterized by Scanning Electron Microscopy (SEM). For this analysis RBC's incubated with polymers were pelleted after the incubation period. The cells were then fixed by gentle resuspension with 0.1 M of sodium cacodilate for 10 min, at 4°C, and pelleted as before. This stage was followed by an additional fixation with 2.5 % (w/v) glutaraldehyde, for 1h, at room temperature (RT) with subsequent centrifugation. After fixation, pelleted RBC´s were dehydrated by sequential resuspension-centrigufation steps in which cells were progressively immersed in ethanol solutions of growing concentration (50 to 100 % (v/v)). The final dehydrated pellet was resuspended and dispersed in a cover glass (ø = 15 mm) for posterior SEM analysis as below described in section 2.2.11 (Page 52).

2.2.10. Encapsulation Efficiency and Release Profile samples analysis.

Encapsulation efficiency was quantified using an Agilent 1200 Ultra Performance Liquid Chromatography (UPLC). Separation was obtained using an Agilent ZORBAX Eclipse C18 Rapid Resolution column (Agilent Technologies, CA, USA). Resulting supernatant of centrifuged micelles was injected in UPLC to perform analysis. The balloon where nanoparticles where assembled was rinsed with MetOH to solubilize any rest of drug and was also analyzed. The total quantified, non-encapsulated drug was subtracted to initial drug concentration, to calculate the percentage of encapsulation efficiency as described below.

$$\text{Encapsulation Efficiency (\%)} = \frac{[\text{Drug}]_{\text{inicial}} - \left([\text{Drug}]_{\text{supernatant}} + [\text{Drug}]_{\text{flask}}\right)}{[\text{Drug}]_{\text{inicial}}} \times 100$$

The method for dual drug quantification was optimized following previously reported Sildenafil method [141]. Mobile phase used for separation and quantification of Crizotinib and Sildenafil were composed of Na_2HPO_4 and 0.01% Triethylamine (TEA) (v/v) at a concentration of 0.015M. pH was set to at 7.4 and temperature to 30°C. Sample analysis was performed at constant flow of 1mL/min. All mobile phases were prepared with MilliQ water to a final volume of 1 or 2 L, filtered through a 0.2 µm pore nylon membrane and degassed before use. Chemstation software was used to perform analysis of the obtained chromatograms. Integration of area under curve of the two analytes, as well as internal standart, were performed and ratio analyte/internal standard was calculated to eliminate mobile phase or equipment related fluctuations.

2.2.11. Morphological Characterization of PEG-PLA micelles

Self-assembled micelles morphological properties were visualized by SEM. Micelle suspensions were stained with the electron dense phosphotungstic acid (PTA) anionic stain (0.1 % w/v) for 5 min. Afterwards the stained micelles were dispersed in a cover glass (ø = 15 mm). All samples were dried overnight at 40°C, in an oven to remove residual water. The micelles were then mounted on aluminium stubs and sputter coated with gold by using an Emitech K550 sputter coater (Emitech Ltd, UK). The nano sized carriers where then observed on a Hitachi S-2700 (Hitachi, Tokyo, Japan) electron microscope configured with optimal detection settings, namely 20kV of accelerating voltage, using different acquisition modes and magnifications.

2.2.12. Characterization of PEG-PLA Micelle Size and Zeta Potential

Following the self-assembly of the drug loaded micelles their size and zeta potential (surface charge) was determined by dynamic light scattering (DLS). Prior to analysis the micelles were resuspended in 900 µL of mili-Q water, sonicated and analyzed immediately. Sample analysis was performed at 25 °C by using a disposable folded capillary cell. All sample measurements were performed in a Zetasizer Nano Zs instrument (Malvern Instruments, Worcestershire, UK) equipped with a He-Ne 633 nm laser, at a detection angle of 173°. This detection mode was used to minimize possible artefacts due to backscattering of the light. Micelle size was then determined by Cumulants/Correlogram analysis and by the Stokes-Einstein equation for colloidal dispersions.

$$\mathrm{D} = \frac{\mathrm{K_B T}}{6\pi\eta \mathrm{r}}$$

Zeta potential was computed by using the Smoluchowski model (f[Ka] =1.50) included in the Zetasizer software (v 6.32).

$$U_E = \frac{2\varepsilon\zeta f(ka)}{3\eta}$$

2.2.13. Release profile of encapsulated drugs

Drug release was performed using multiple samples of PL8 micelles resuspended in PBS 1% at a concentration of 0.1 mg/mL. Various samples were used to collect data at different time

points (1h, 2h, 3h, 1 to 8 days) and were incubated at 37°C with gentle agitation. After completing the time of incubation, each sample was centrifuged at 30 000 g for 30 min before UPLC analysis. Supernatant was analyzed using the methodology described above in 1.2.5.

2.2.14. Cell susceptibility with blank micelles

To evaluate micelle cytotoxicity, MCF-7 cells were initially seeded at a density of 8 x 10^3 cells/well in a 96-well flat bottom culture plates, containing DMEM-F12 supplemented with 10% FBS. Adherent cells were grown at 37 °C, in an incubator with a humidified atmosphere, containing 5 % CO_2. The following day, culture medium was refreshed and cells were incubated with different concentrations of PL8 blank micelles, to a final concentration ranging between 5 and 2000 µg/mL. Cell cytotoxicity was monitored by using the Resazurin assay. This method uses a highly sensitive and non-toxic reagent (Resazurin) that is reduced to a fluorescent substrate (Resofurin) by intracellular mitochondrial enzymes such as flavin mononucleotide dehydrogenase and nicotinamide adenine dehydrogenase [142]. Briefly, to perform this evaluation the culture medium was replaced at pre-determined periods after polymer incubation (24 and 48h), and the cells were incubated with 10 % (v/v) of Resazurin (1 mg/mL) during 4 h, at 37° C and 5 % CO_2 in the dark. The resofurin present in the culture medium was then transferred into black clear bottom 96-well plates for analysis. Fluorescence measurements were then performed in a plate reader spectrofluorometer (Spectramax Gemini XS, Molecular Devices LLC, USA) at an excitation/emission wavelength of λ_{ex} = 560 and λ_{em} = 590 nm respectively. Ethanol treated cells were used as positive controls (K+) and non-incubated cells were used as negative controls (K-).

2.2.15. Flow Cytometry

Characterization of micelle uptake was performed by flow cytometry. For uptake experiments, 6 well culture plates were seeded with 2 x 105 cells in DMEM-10 % FBS and grown for 24h. To evaluate micelle uptake, PL8 micelles were prepared by self-assembly in order to encapsulate RITC (10 µM) that was used as model hydrophobic fluorescent probe. Micelles were then resuspended in culture medium without antibiotics before their incubation. The particles were allowed to interact with MCF-7 cells for 2 and 4h and removed afterwards by extensive rinsing with PBS. The cells were then recovered by trypsinization (0.18 % trypsin – 5 mM EDTA), pelleted and resuspended in 500 µL of PBS for flow cytometry analysis. All the experiments were performed on a BD FACSCalibur flow cytometer equipped with 488 nm and 633 nm lasers. Data collection was performed using CellQuestTM Pro software where the fluorescent signals of 8 x 103 events present in the gated region of interest (ROI) were recorded with the FL-2 (585/42) band pass filter. Flow cytometry data

was analyzed in FlowJo software (Treestar, Inc., CA, USA) and is presented as mean fluorescence intensity (MFI).

2.2.16. Micelle uptake by Breast Cancer cells

Micelle uptake capacity and intracellular distribution in MCF-7 malignant cells was studied by confocal laser scanning microscopy (CLSM). Prior to CLSM experiments RITC was encapsulated in the micellar carriers as reported in section 2.2.7 (Page 49), using the film hydration method. For the visualization of micelle uptake 20 x 10^3 MCF-7 cells were seeded in µ-Slide 8 well Ibidi imaging plates pre-coated with fibronectin or collagen (Ibidi GmbH, Germany). On the following day, the cells were incubated with PL8 micelles during 4 h. After incubation, cells were fixed with 4% paraformaldehyde (PFA) (15 min, RT) and washed with PBS. MCF-7 cells were prepared for imunocytochemistry analysis by permeabilization with 1% Triton X-100 for (10 min, RT). Permeabilized cells were then blocked with a blocking solution (10 % FBS, 0.1 % Tween-20, in PBS) in order to avoid antibody binding to unspecific protein epitopes. After blocking the cells were extensively rinsed with PBS and incubated with the anti-F-actin Phalloidin CruzFluor® 647 conjugate antibody for 1h, at RT, in a humidified chamber. MCF-7 cells were then washed with PBS for 5 to 10 times to remove excess antibody and then labelled with the Hoechst 33342® (2 µM) nuclear probe, for 15 min at RT. After labelling cells were extensively rinsed with PBS. Imaging experiments were performed in a Zeiss LSM 710 confocal microscope (Carl Zeiss SMT Inc., USA), equipped with a Plan Apofluar 40x/1.4 Oil Differential Interference Contrast (DIC) objective. Image acquisition was performed in Z-stack mode where consecutive Z-stacks with a slice thickness of 0.23 µm were acquired. 3D reconstruction and image analysis was performed in Zeiss Zen 2010.

2.2.17. IC50 determination and Synergic effect evaluation

To evaluate IC50 of MCF-7 cells relatively to Crizotinib, MCF-7 cells were initially seeded at a density of 8 x 10^3 cells/well in a 96-well flat bottom culture plates, containing DMEM-F12 supplemented with 10% FBS. Adherent cells were grown in the same conditions described in 2.2.14 section (Page 53). The following day, culture medium was replaced and cells were incubated with crescent concentrations of Crizotinib ranging from 0.33 µM to 334 µM.

To evaluate synergic effect of both drugs (Crizotinib and Sildenafil), MCF-7 cells were initially seeded at a density of 8 x 10^3 cells/well in a 96-well flat bottom culture plates, containing DMEM-F12 supplemented with 10% FBS. Adherent cells were grown at the same conditions described in 2.2.14 section (Page 53). The following day, culture medium was changed and cells were incubated 48 h with Crizotinib (108.67 µM), Sildenafil (79.33 µM) and the (Crizotinib + Sildenafil) at the same concentrations that were used for each single drug.

Ethanol treated cells were used as positive controls (K+) and cells without incubation of micelles were used as negative controls (K-).

2.2.18. Drug Loaded Nanoparticle Incubation

The anti-tumoral activity of the different micelles was determined by the MTS assay to evaluate cell viability. Initially, 8 x 10^3 MCF-7 cells were seeded in 96 well plates, 24 h before the experiment in DMEM-F12 – 10% FBS. In the following day, the culture medium was replaced and the cells were incubated with PL8C and PL8CS micelles, at a final drug concentration of 55.25 μM of Crizotinib and 40.33 μM of Sildenafil. Cell viability was determined at various time periods (24 and 48 h) by incubating MCF-7 cells with the MTS reagent. The formazan product absorbance was measured at 492nm. Ethanol treated cells were used as positive controls (K+) and cells without be incubated with micelles were used as negative controls (K-).

2.2.19. Apoptosis assay

Apoptosis effect of PL8CS micelles on MCF-7 malignant cells was studied by CLSM. Prior to CLSM experiments, 20 x 10^3 MCF-7 cells were seeded in μ-Slide 8 well Ibidi imaging plates (Ibidi GmbH, Germany). After 24 h in culture, cells were incubated with PL8CS micelles during 12 h using the same final concentration of Crizotinib and Sildenafil described in section 2.2.18 (Page 55). After micelle incubation, cells were incubated with 7.5 μM of CellEvent™ Caspase-3/7 detection reagent during 30 min. Afterwards they were fixed with 4% paraformaldehyde (15 min, RT), washed with PBS and finally visualized in CLSM as described in 2.2.16 (Page 54).

2.2.20. Statistical Analysis

One-way analysis of variance (ANOVA) with the post-hoc Newman-Keuls test was used to compare the results obtained for the different groups used in the various assays. A p value below 0.05 ($p < 0.05$) was considered statistically significant. Additional p values ($p<0.01$ and $p<0.001$) were used to ascertain higher degrees of significance. The analysis of all data was performed in the GraphPad Prism v.5.0 software (Trial version, GraphPad Software, CA, USA).

Chapter 3

Results and Discussion

3. Results and Discussion

3.1. Synthesis of PEG-PLA block co-polymers

Block co-polymers represent a novel class of polymers with invaluable properties that are essential for the formulation of micellar DDS for cancer therapy [143]. Nanomicelles comprised of block co-polymers have the capacity to self-assemble in aqueous dispersions, forming very stable core-shell structures [144]. PEG-PLA block co-polymers are particularly interesting colloidal carriers due to their high loading capacity and controlled drug release [145]. Therefore, PEG-PLA co-polymers were chemically synthesized with the aim to promote the encapsulation of multiple drugs in self-assembled micelles. To improve drug encapsulation, the hydrophobic compartment of the nanocarrier must possess sufficient space to accommodate several hydrophobic drugs. However, it should be underscored that the polymer chain length also affects micelle size, a parameter that could compromise the envisioned therapeutic applications. Therefore, the block co-polymers were intentionally synthesized with an application-focused design, in order to tailor certain polymer features that could improve drug delivery and release.

The synthesis of various PEG-PLA co-polymers was promoted through the establishment of a living ROP reaction in which the monomer of L-Lactide was used as a template for PLA synthesis. The method of polymerization occurs via a COI mechanism where the L-Lactide ring is opened and two lactic acid molecules are added on the hydroxyl (–OH) terminal group of a macroinitiator, as shown in Figure 12. In this particular block co-polymer the macroinitiator used was mPEG. The monomethoxy-terminal of mPEG provides a perfect inert group, leaving only the –OH terminal to react with the living monomers. The ROP and consequent bulk polymerization of L-Lactide was initiated by the catalyst $Sn(Oct)_2$. This catalyst promotes ROP through the COI mechanism and provides an improved ROP in terms of the reaction rate and the polymerization yield. In fact it has been previously reported that $Sn(Oct)_2$ leads to the conversion of more than 90% of L-Lactide monomers [146]. Moreover, by using this approach the racemization of L-Lactide during ROP is largely reduced, with literature reports indicating that polymer racemization is generally less than 1%, in optimal conditions. Racemization of the polymer chain reduces its stereochemical purity, a limiting factor that ultimately influences the physichochemical properties of the synthesized polymer and should be addressed during the synthesis of PEG-PLA block co-polymers for therapeutic applications. Interestingly, a part from reducing racemization, the use of $Sn(Oct)_2$ provides further advantages in the synthesis of block co-polymers for drug delivery, since higher or lower Mw polymer chains can be obtained according to the envisioned applications only by modulating the the concentration of catalyst in ROP [146].

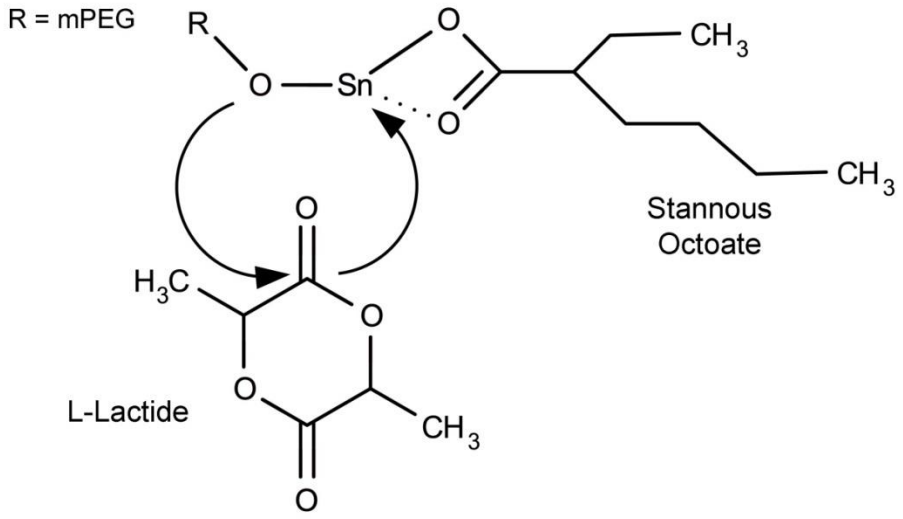

Figure 12 – COI mechanism of ROP of L-LA polymerization using mPEG as macroinitiator and $Sn(Oct)_2$ as catalyst. (Adapted from [147]).

Taking the former into account, the ROP reaction was performed with a L-Lactide-PEG monomer-to-macroinitiator mass ratio of 2:1, since it has been previously described that this is the optimal ratio of polymerization to synthesize PEG-PLA co-polymers with suitable Mw for therapeutic applications [148]. The ROP of PEG-PLA co-polymers were performed at various time points (4, 8 and 30 h) in order to modulate the length of the hydrophobic polymer chain. This strategy allows the existence of different block co-polymer batches with various physicochemical characteristics, bringing forth the opportunity to evaluate the most suitable synthesis for the envisioned therapeutic application. After establishing this initial experimental setup all the ROP reactions proceeded under inert and water-free conditions, as described in Section 2.2.1 (Page 46). The latter parameter is critical for ROP, since the presence of H_2O molecules in a Sn/-OH system leads to the conversion of Sn into stannous hydroxide derivatives that are less reactive [149]. This fact limits the rate of ROP and thus affects the final Mw of the PLA polymer chain.

The block co-polymer synthesis performed at different time frames yielded hydrophobic polymer chains with variable Mw's. This time-dependent manipulation of the PLA polymer length is only possible due to the existence excess L-Lactide in all the reactions performed. L-Lactide polymerization is temperature dependent [150]. A temperature of 120˚C was reported to be the optimal temperature of polymerization, resulting in longer PLA chains [151]. After ROP, the co-polymers were recovered by a three-step precipitation with MetOH. This recovery process was employed since PLA is highly insoluble in MetOH, and thus a selective precipitation of the PEG-PLA blocks is achieved. This procedure has been previously described as one of the most effective forms for PEG-PLA co-polymer recovery [152]. However, throughout the recovery process it was discovered that by using MetOH, the recovery yield was further improved. Due to this approach a faster precipitation process

occurred for longer PLA chains, a finding that is in accordance to what was expected, since MetOH lowers the solubility limit of PLA chains. It is also important to underscore that during this recovery process non-reacted mPEG polymer chains are also removed, since mPEG is highly soluble in MetOH. Nevertheless, an additional purification of the block co-polymers synthesized was performed through dialysis-freeze drying cycles, in order to remove traces of contaminants and obtain fully purified polymers. All the synthesized PEG-PLA polymers were then analyzed by NMR.

3.2. NMR analysis of PEG-PLA block co-polymers

NMR analysis was performed to evaluate the success of the ROP process since it is a highly sensitive technique that allows to evaluate the effectiveness of synthesis and purification stages. This in-line analysis unlocked the opportunity to control the synthesis process and to manipulate all the parameters accordingly to the intended final application.

The ^{1}H NMR spectra obtained for the different PEG-PLA block co-polymers are shown in Figure 14. In comparison with the NMR spectra of mPEG and L-Lactide (Figure 13) it can be observed that the spectra of the ROP synthesized polymers presents the characteristic proton peaks of mPEG, suggesting that the synthesis process does not alter the native structure of the hydrophilic block (Figures 13 and 14). To further characterize the synthesized co-polymers a full assignment of the proton peaks obtained in the NMR spectra was also performed. All the proton assignments were performed accordingly to the chemical shifts previously reported in the literature [136, 147].

As shown in figure 14, the proton peaks appearing at δ=5.2ppm and δ=1.5 ppm were assigned to the methyne (R_1-CH=R_2) and methyl (-CH3) protons of the PLA monomers, respectively [136, 147]. The mPEG monomers are characterized to have a peak at approximately δ≈3.7 ppm, that is assigned to methylene (=CH_2) protons [136, 147]. Moreover, the peak present at δ=3.4 ppm is correlated with the methyl (-CH_3) protons at the end of the mPEG polymer chain [136, 147]. The $CDCl_3$ characteristic peak (δ=7.3 ppm) was also seen in all spectra. It is also important to underline that no additional peaks were obtained, an important finding that illustrates the purity of the block co-polymers after synthesis. Interestingly, the ^{1}H spectra shows that the proton peaks at δ=5.2ppm and δ=1.5ppm were increased for longer polymerization periods. The EO/LA ratio was calculated through the integration of peaks as previously reported [136]. mPEG methylene protons peak δ=3.7 ppm and δ=5.2 ppm peak of PLA were integrated. Due to the constant length of mPEG in the different polymerization times, this correlation is possible, and so block-co polymer Mn can be calculated.

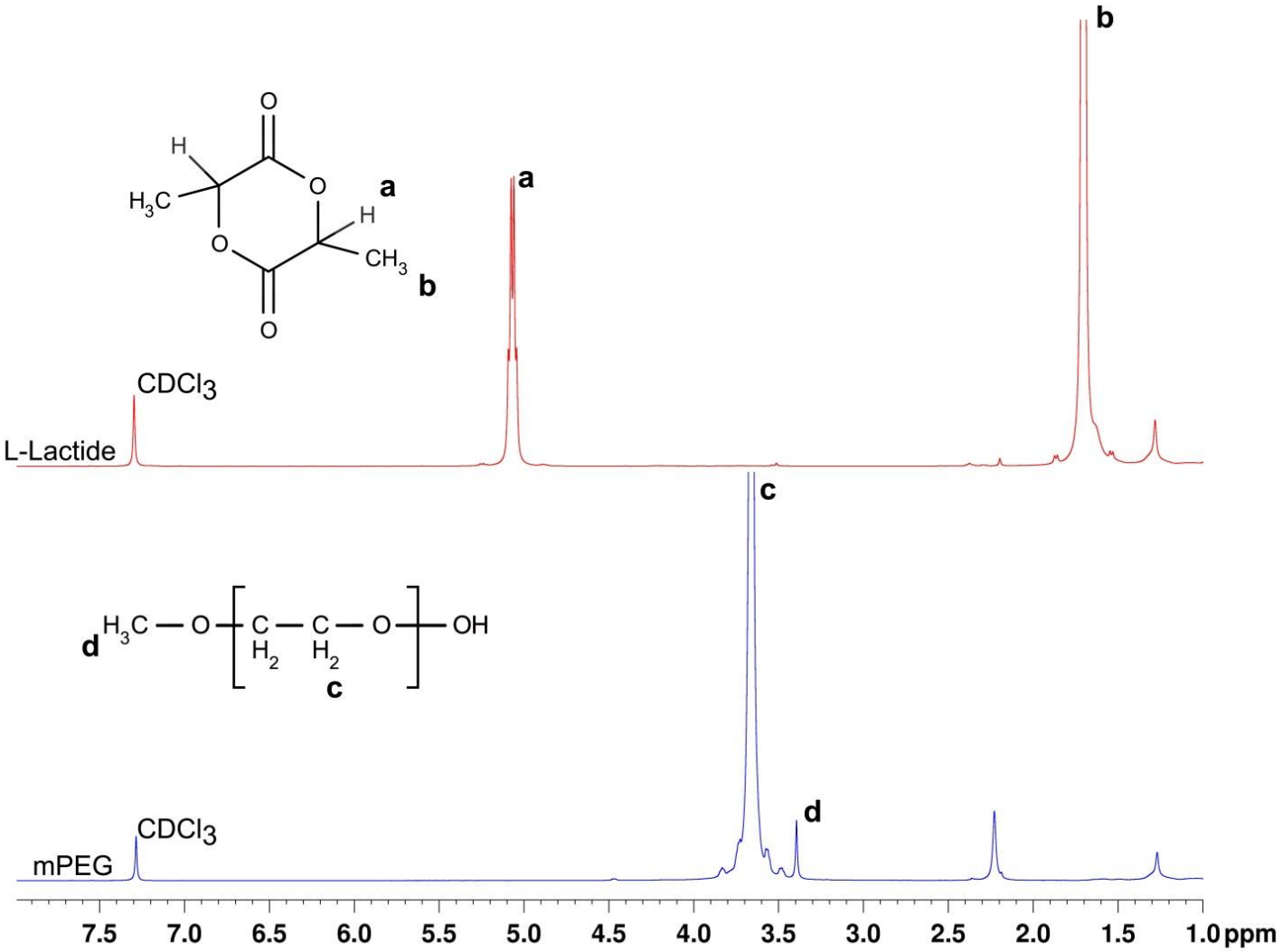

Figure 13 – NMR of the synthesized mPEG and L-Lactide raw materials used in the polymerization process.

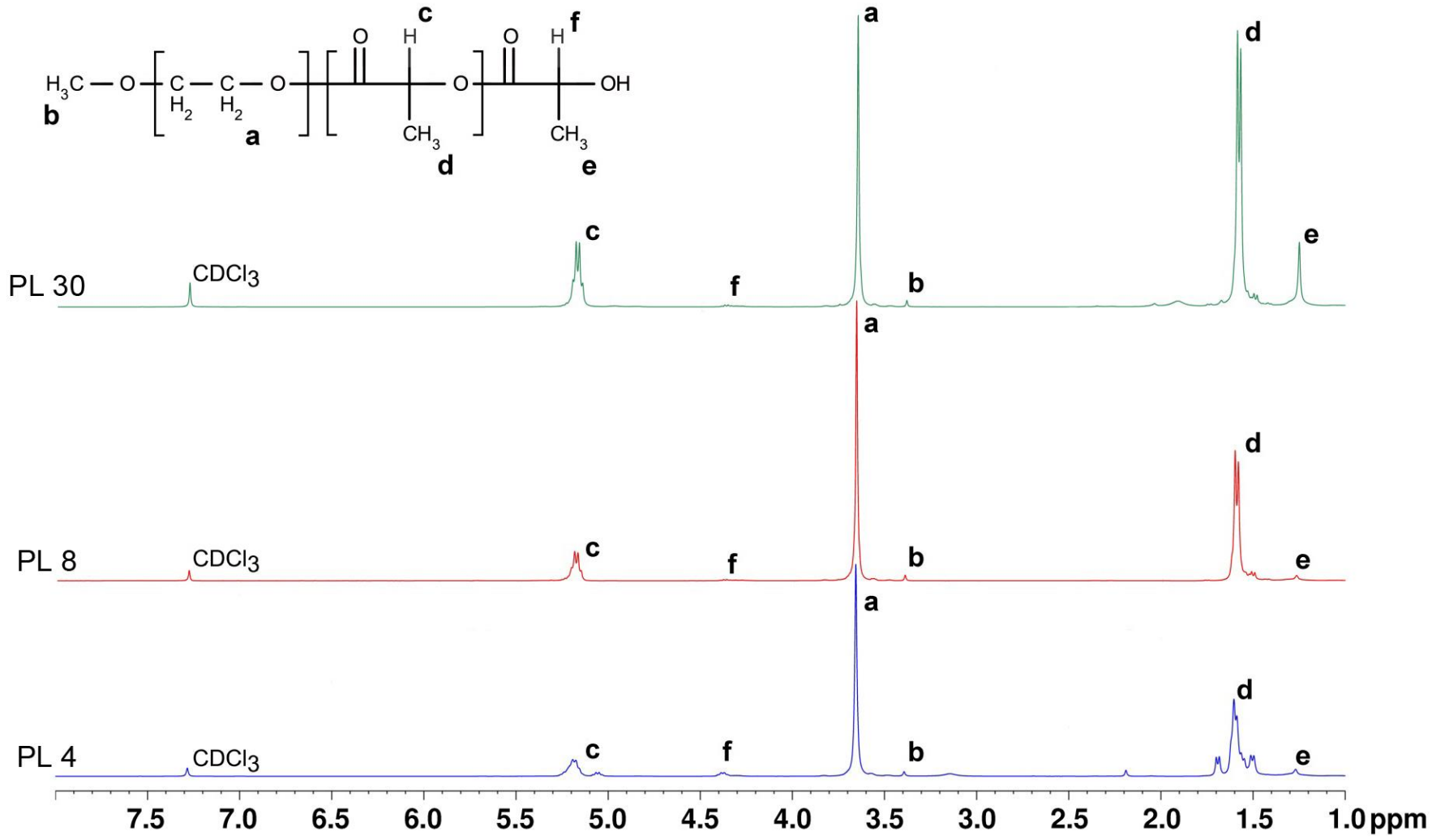

Figure 14 - NMR of the synthesized PEG-PLA block co-polymers with different polymerization times, (PL4, PL8 and PL30).

In fact as displayed in Table 2 the PLA different average weights can be obtained through NMR analysis. This is a valuable information that is crucial for the characterization of the synthesis process, since it allows the determination of the length of the hydrophobic chain and its correlation with the ROP polymerization time used.

Table 2 - Degree of polymerization, Mn of PLA and mPEG-PLA calculated by proton peak integration. *n*=5 integrations of each characteristic peak where performed.

Time of Polymerization (h)	Degree of Polymerization	PLA (Mn)	EO/LA (n=5)					Mean PEG-PLA Mn (PEG Mn=2000)
4	203.05	738	4.47	4.46	4.43	4.36	4.39	2738±7.64
8	160.46	932	3.53	3.50	3.50	3.51	3.53	2932±4.06
30	83.14	1898	1.76	1.72	1.74	1.72	1.72	3898±15.88

Interestingly, as the results in Table 2 demonstrate, the increase of polymerization time was proportional to an increase in the PLA chain length. The polymerization of 4h led to the synthesis of the smallest hydrophobic blocks (Mn ≈738). On the contrary, extending the ROP for 30 h resulted in the largest PLA obtained herein (Mn ≈1898). These findings are in accordance to the results previously reported in the literature, that for longer times of polymerization results in longer PLA chains [151], and emphasize the feasibility of this straightforward approach in the optimization of the length of the hydrophobic block.

3.3. FTIR analysis of PEG-PLA co-polymers

In addition, FTIR analysis was also performed to characterize the L-Lactide polymerization (Figure 15). The FTIR data obtained for mPEG shows a characteristic C-O-C stretching band at 1085 cm^{-1}. The strong band observed at 1755 cm^{-1} a (green color) is assigned to the carbonyl ester (C=O) of PLA [153]. The bands obtained at 2880 and 2946 cm^{-1} are assigned to the C-H stretching vibration of ($-CH_3$) (yellow color) and -CH- (red color) groups of PLA, respectively [153]. The characteristic bands obtained for PL4, PL8 and PL30 are the similar to those of PEG-PLA co-polymers, already described in literature [153], further corroborating the success of the synthesis process.

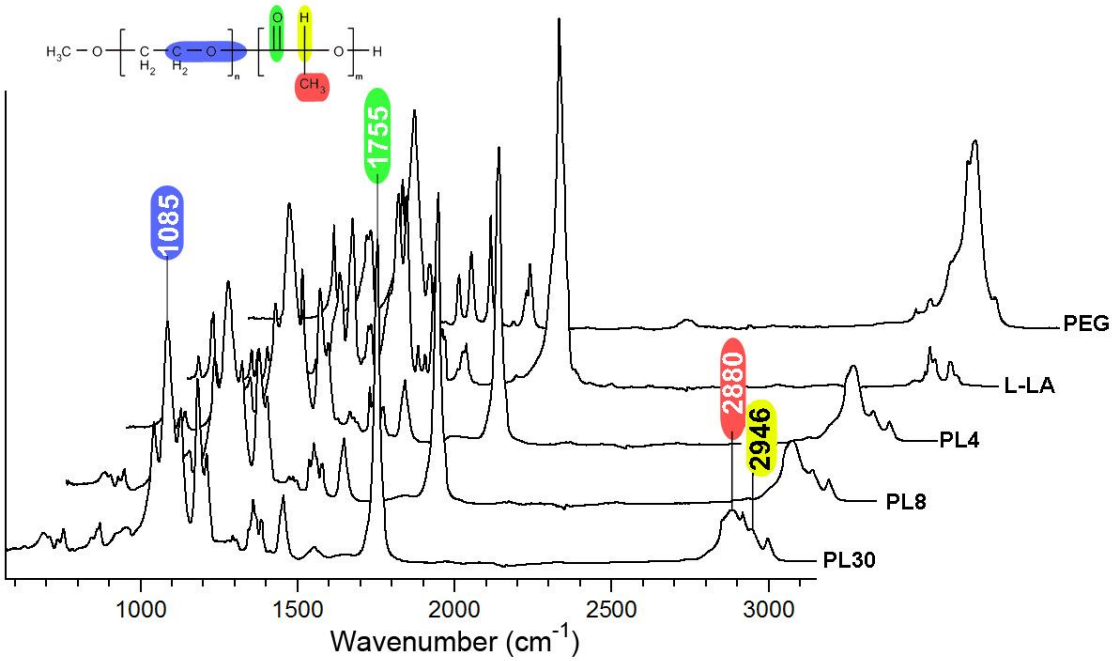

Figure 15 – FTIR spectra of the native materials (L-Lactide and PEG) and of the synthesized block co-polymers (PL4, PL8 and PL30). mPEG and L-LA spectra were used as controls.

3.4. GPC analysis of block co-polymer

Gel permeation chromatography was performed to further characterize the molecular weight of the various PEG-PLA co-polymers.

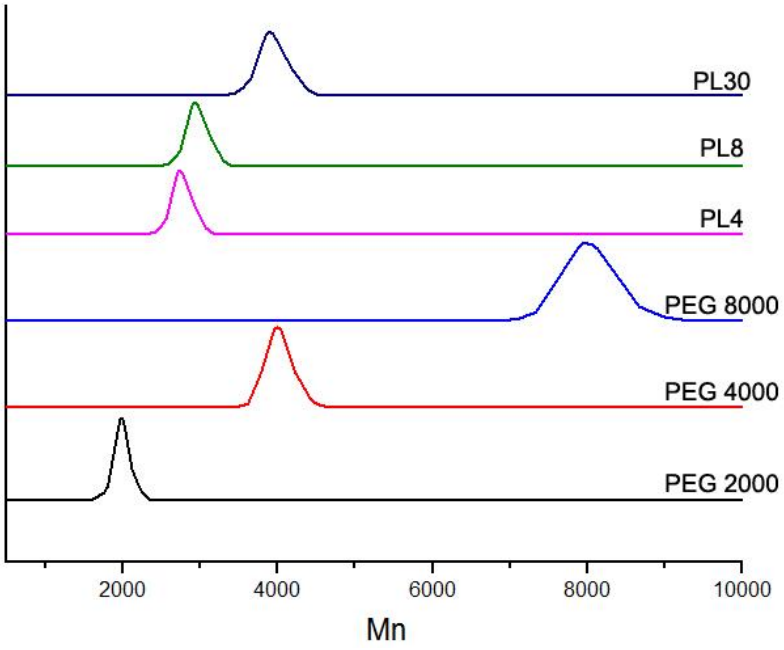

Figure 16 – Chromatograms of PEG standards (PEG 2000, PEG 4000 and PEG 8000) and of the synthesized materials (PL4, PL8 and PL30).

The GPC analysis provides important insights into the molecular weight distribution of the PEG-PLA co-polymers synthetized. As the chromatograms in Figure 16 demonstrate the PL4, PL8 and PL30 co-polymers present Gaussian distribution profiles instead of highly broad peaks. This result indicates that the PL polymers have relatively low polidispersity, an important characteristic for therapeutic applications, envisioned since this parameter ultimately influences batch-to-batch reproducibility of polymer-based pharmaceutical formulations [93]. Moreover, it should be emphasized that PL chromatograms present well resolved peaks since the average molecular weight of the different samples is higher than 10%, which is above the resolution limit of GPC [154]. It is also important to mention the experimental conditions of the chromatographic run, since a salt solution (0.2M NaCl) was used as both equilibration and eluent. This fact led to an increase in the mean residence time of larger polymers and a decrease for smaller ones. Generally, in GPC the separation is based on the radius of gyration of the analytes, with larger analytes having a lower mean residence time than smaller ones, with the latter being those that are retained in the gel for longer periods of time [155]. The obtained results demonstrate that after running the three PEG standards, the retention times of the polymers where inverted, i.e., PEG 2000 had a lower retention time than PEG 4000 and 8000. Eluent used (0.2 M NaCl) have high conductivity. After retention of polymer inside the column it passes through the conductance detector, overall eluent conductivity thus decreases, and the signal is registered in a chromatographic detector. In accordance with the previous results, the loading of PL4, Pl8 and PL30 into the column led to the the same pattern of elution, i.e., longer polymers have been retained more than shorter polymers (Figure 16). This can be explained by the establishment of some non-specific interactions between the polymer samples and the Sephacryl S-100 HR column matrix which is composed of allyl dextran and N,N'-methylene bisacrylamide. It is postulated that NaCl salt concentration has a large influence in the radius of gyration of the mPEG polymer or co-polymer chains as recently described by Heeb and co-workers, 2009 and this might contribute for the observed results [156].

3.5. XRD analysis of PEG-PLA co-polymers

The XRD characterization of the co-polymers reveals that the crystalline structure of mPEG was maintained after synthesis. This is evidenced by the appearance of the characteristic diffraction peaks at 19.1° and 23.3°. These peaks are obtained in the diffractograms of all co-polymer samples (PL4, PL8 and PL30). Interestingly, a new crystallization peak, derived from the PLA chain, was found at 16.6°. New occurrence peak means that PLA chain is long enough to crystalize [136]. L-LA crystallization peak does not appear in synthesized materials spectra, which suggests a good purity at the end of the purification steps. Moreover, as previously described by Nampoothiri and co-workers, the high crystallinity of PLA interferes with controlled degradation, reducing biocompatibility [157].

Characteristic peak of PLA crystallinity (16.6°) was used to perform the calculation of % of crystallinity. The obtained results show an increase of crystallinity for longer PLA chains as described in Table 3.

Table 3 - Calculated percentage of crystallinity of PL4, PL8 and PL30.

	PL4	PL8	PL30
Crystallinity (%)	14.52 ± 0.90	16.33 ± 0.16	19.05 ± 0.19

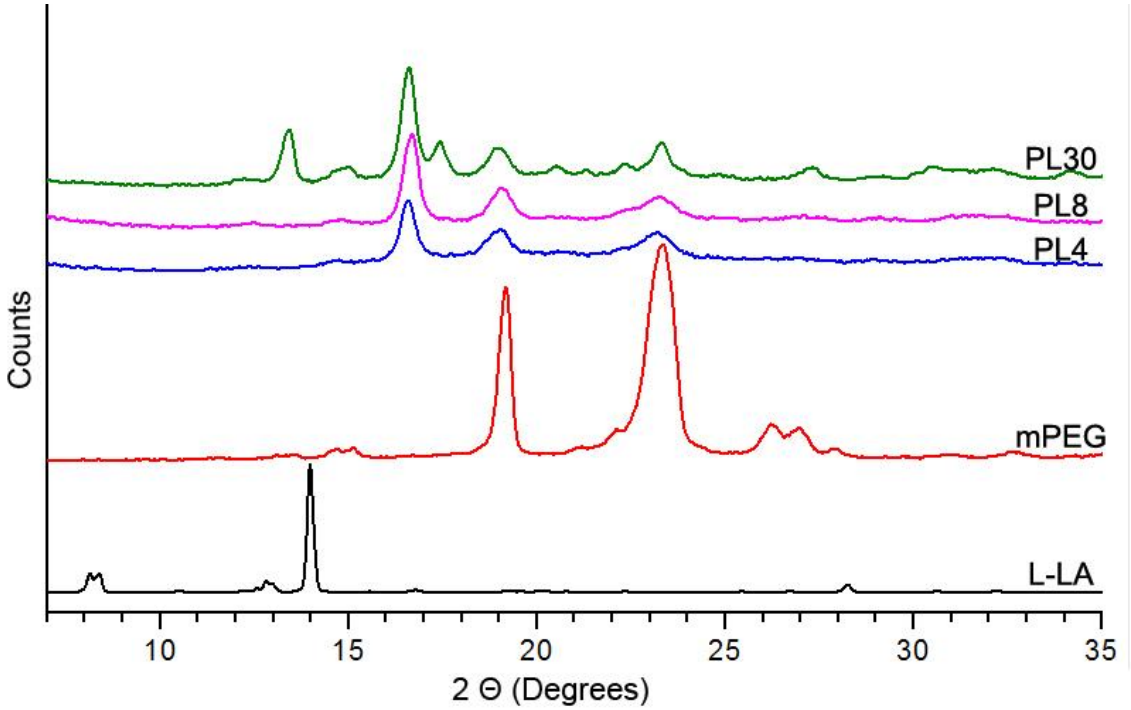

Figure 17 - X-ray diffraction spectra of native materials (L-Lactide and mPEG) and of the synthesized block co-polymers (PL4, PL8 and PL30).

3.6. DSC characterization

Differential scanning calorimetry was performed to evaluate the thermal properties of novel PEG-PLA materials and correlate them with their native precursors. PLA is described to suffer degradation with temperature [158]. Degradation can occur through depolymerization, transesterification or oxidative processes [158]. Moreover, unreacted L-Lactide monomer and/or residues of catalyst can increase the degradability of PLA [158].

Modification of mPEG polymer chains with the inclusion of PLA, changed the melting temperature (Tm) and the enthalpy (ΔH) of melting temperature transition in comparison with the original materials. As described by Li and co-workers the PEG melting temperature decreases (approximately 10ºC) when PLA is added to its backbone [136]. This decrease is

indicative of the attachment of the PLA chain to the PEG macroinitiator. It is also important to mention that mPEG characteristic Tm and ΔH decrease as the PLA chain is longer, a fact that can be explained by the reduction in the mobility of PEG chains due to PLA polymerization in its backbone [136]. By analyzing the thermograms (Figure 18) and their peak integrations it can be observed that the Tm of PEG in the PL samples decreases by approximately 10% (Table 4). These results are corroborated by the above mentioned findings. Moreover, in respect to PLA thermal characteristics, it is interesting to denote that an increase in the PLA degree of polymerization is proportional to its melting temperature, i.e., the longer the PLA chain gets, the greater Tm and ΔH will be. These findings were also obtained by Li and co-workers, 2007 [136].

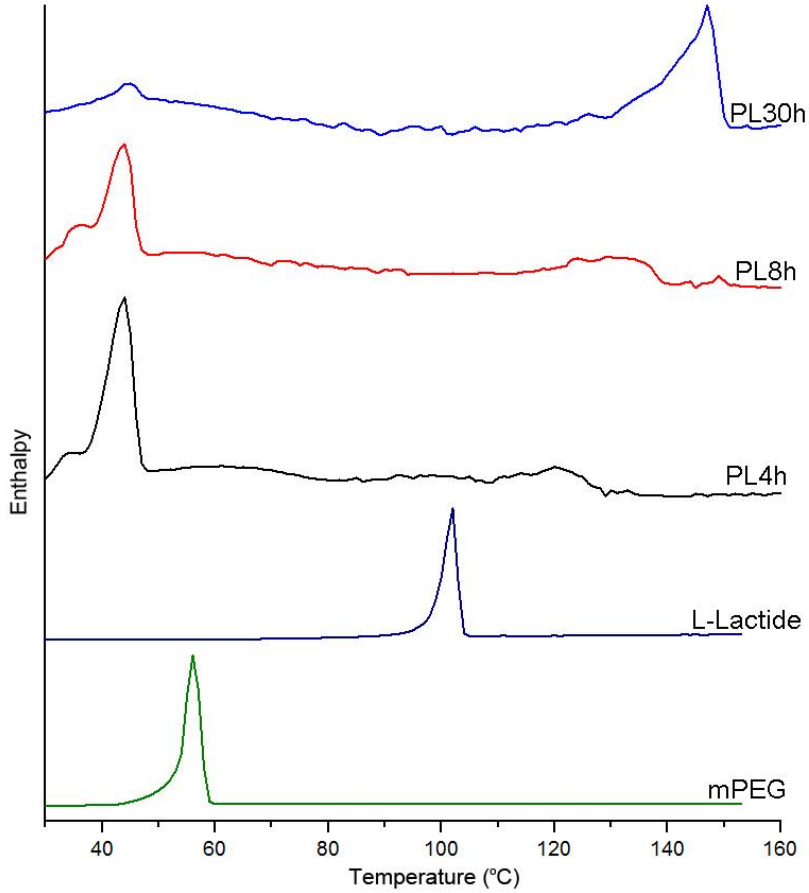

Figure 18 – DSC analysis of mPEG, L-Lactide, PL4, PL8 and PL30.

Table 4 - DSC data analysis of L-LA, mPEG, PL4, PL8 and PL30. (NA - non-applicable).

Polymer	Tm PEG (°C)	ΔH PEG (J/g)	Tm PLA (°C)	ΔH PLA (J/g)
L-LA	N/A	N/A	99.03	9.33
mPEG	53.25	64.21	N/A	N/A
PL 4	43.80	27.79	120	26.03
PL 8	43.65	22.71	129.26	29.30
PL 30	44.69	11.68	147.15	34.42

3.7. CMC Determination

Following polymer synthesis and physicochemical characterization, the ability of PEG-PLA block co-polymers to form micelles with core-shell structures was evaluated. For this purpose the CMC of the various synthesized polymers was determined. CMC, is defined as the minimum concentration necessary for an amphiphilic material to be able to form nanomicelles by self-assembly, in aqueous environments [159]. CMC is also a measure of micelle stability in solution [159]. It is generally accepted that a lower CMC, leads to the formation of more stable self-assembled micelles, in aqueous dispersions [159]. It is important to emphasize that as a potential DDS, PEG-PLA micelles must be stable at a low concentration for being administered for instance in the blood stream and maintain their structure, thus keeping its drug payload inside the core [159]. By using pyrene as hydrophobic fluorescent probe, it was possible to determine the CMC for the three synthesized co-polymers. Actually, this methodology if very valuable since by simply measuring fluorescence emission after a double excitation (335 and 333 nm) as described previously, in section 2.2.8 (Page 50), it was possible to obtain a steep shift in the I_{335}/I_{333} fluorescence intensity ratio when the polymer concentration was high enough to allow polymers to self-assemble into micelles. The interception of the two trend lines presented in Figure 19 represents the CMC of the different polymers. The obtained CMC results demonstrate that the increase in the hydrophobic chain length from PL4 to PL30 markedly decreases the CMC value, suggesting that the critical concentration is dependent on the PLA chain length (Figure 19). This is in agreement with the definition of self-assembled micelles, since the higher the hydrophobic chain the lower is the polymer concentration needed for micelle formation [160]. The CMC's obtained in this study are comparable to those reported in the literature. However a special emphasis should be given to the PL30 CMC (7.8×10^{-4} mg/mL) that is 10-fold lower than the average CMC's reported for PEG-PLA micelles [122].

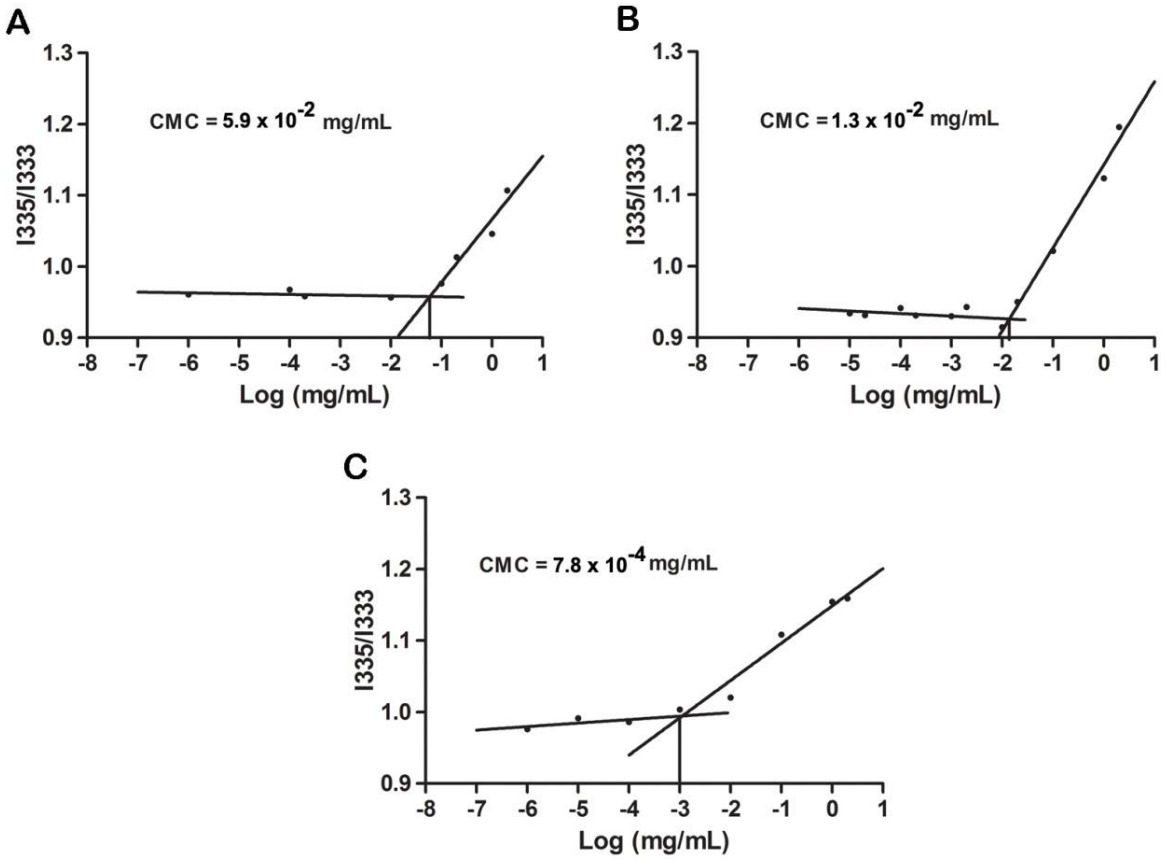

Figure 19 – CMC determination for (A) PL4, (B) PL8 and (C) PL30 micelles self-assembly.

These important findings indicate that the PEG-PLA co-polymers synthesized have the ability to form very stable micellar carriers due to their amphiphilic character, having suitable characteristics for loading the hydrophobic anti-tumoral drugs [161].

3.8. Haemocompatibility Assay

Based on the concept that the formulated micelles will be applied in cancer therapy through their administration via systemic injection, it is crucial to characterize the blood haemocompatibility of the carriers. For this purpose, the synthesized materials where incubated with freshly drawn rat whole blood to ascertain if there is any interference in the envisioned intravenous injection of PEG-PLA micelles. As shown in Figure 20, all samples incubated with PEG-PLA amphiphilic polymers present supernatants similar to those of negative control (PBS). In contrast the supernatant of the positive control is clearly red colored, indicating the release of hemoglobin by the lysed Red blood cells (RBCs). Moreover, as the SEM micrographs demonstrate, the integrity of the RBCs morphology is maintained even after incubation with the amphiphilic polymers. To further provide a quantitative

analysis the percentage of hemolysis was determined. The results obtained suggest that all the materials present excellent RBC viability, up to 500 µg/mL (Figure 20). This achievement allows to state that the different synthesized PEG-PLA's are DDS have the suitable properties for being used in subsequent *in vivo* studies.

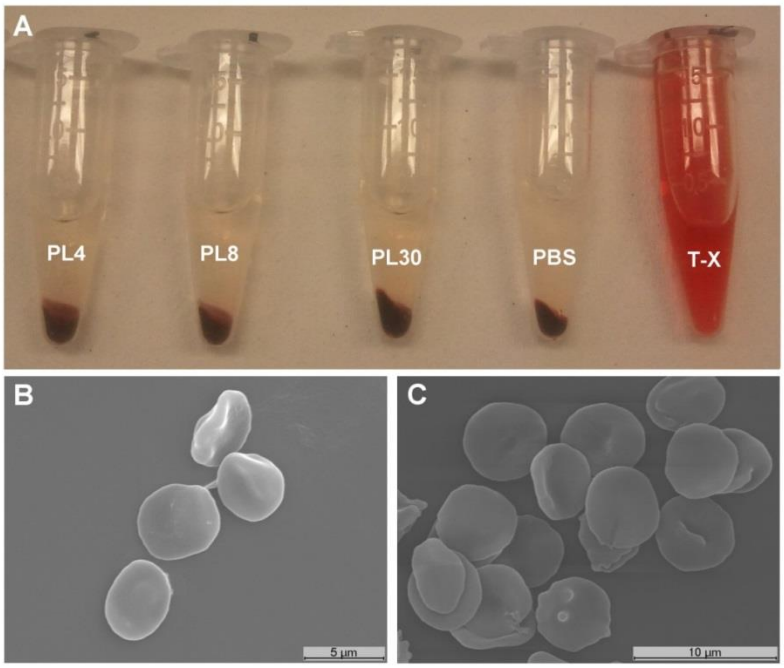

Figure 20 - Supernatants resulting from the haemolysis assay (A). On the bottom of the image two representative SEM images of RBC previously incubated with nanoparticles: (B) PL8 and (C) PL30.

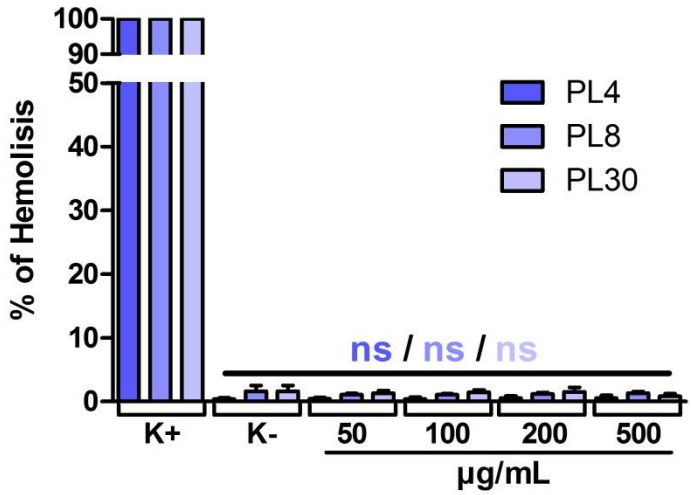

Figure 21 - Quantification of free heme groups (indicator of haemolysis) after incubation with synthesized micelles (PL4, PL8 and PL30). K+ (positive control) represents Triton X-100 treated RBC, K- represents RBCs incubated with PBS. n=3; *p < 0.05; **p < 0.01; ***p < 0.001; ns=non-significant.

All the results of quantification where equals to, or smaller than the negative control (PBS), therefore no significant difference was observed (Figure 21). These results are within the % of

haemolysis set forth by the ISO 13014-2013, which determines that values for hemolysis lower than 5% are in the interval of security, further revealing an excellent compatibility of synthesized materials with RBCs. Furthermore, it is important to state that values were normalized by the maximum percentage of hemolysis (performed by Triton-X 100).

3.9. Analysis of Single and Multiple Drug Loading into Micellar Carriers

Subsequent to the CMC determination, the different co-polymers were used to formulate micellar carriers for the encapsulation of the anti-tumoral drugs, Crizotinib and Sildenafil, either performing just Crizotinib-loading, or throught the simultaneous encapsulation of both drugs in micelles. As previously described in Chapter 2, all drug-loaded micelles were formulated by the film hydration-sonication method [139]. It is described in the literature that this provides enhanced loading in comparison with others, such as solvent evaporation method or dialysis method [118]. UPLC was then used to determine the amount of drug encapsulated. This technique provides a unique sensitivity, since its detection limits are in a concentration range of ng/mL. For establishing a viable approach two different methodologies were optimized to quantify the presence of Crizotinib and Sildenafil, either alone, or simultaneously, in various solvents: i.) MetOH, ii.) Water and iii.) PBS. Since no previous methodology was established to simultaneously quantify Crizotinib and Sildenafil, the initial method used was adapted from the one previously used by Quintero and co-workers, that reports the quantification of Sildenafil and metabolites in blood plasma [162]. In the preliminary studies, several combinations of the mobile phases were used, in order to discover the most suitable solvent system to separate Sildenafil, Crizotinib and the internal standard used, Protriptiline.

During the optimization process, different pH values, ranging between 6 and 7.4, were tested. In addition, the gradient of acetonitrile/ammonium acetate ($NH_4C_2H_3O_2$), as well as the run temperature and the mobile phase flow rate were also manipulated during this stage. However, problems in detection of Sildenafil and Crizotinib were found when the samples were injected in PBS, probably due to the excess of salt in both samples and the mobile phase (Figure 22). Therefore, another Sildenafil separation method, with a new mobile phase di-sodium hydrogen phosphate (Na_2HPO_4), was adapted from [141] (. Once again the gradient of acetonitrile and column temperature where adjusted to investigate the optimal separation conditions for the three compounds. An increase in the acetonitrile fraction of the mobile phase promoted faster chromatographic runs. Actually after the final optimization stage with the second mobile phase, the running time was reduced from 10 minutes (first mobile phase tested ($NH_4C_2H_3O_2$)) to 7 minutes (Na_2HPO_4). These findings can be explained by a decreased exposure of the C18 column groups when acetonitrile flows through. With this approach Sildenafil was easily separated, however, to resolve the Crizotinib and Protriptiline peaks, the

mobile phase gradients and the run temperature had to be optimized, as described in the materials and methods section 2.2.10 (Page 51). A selective separation of the three compounds was then obtained as shown in Figure 22 B.

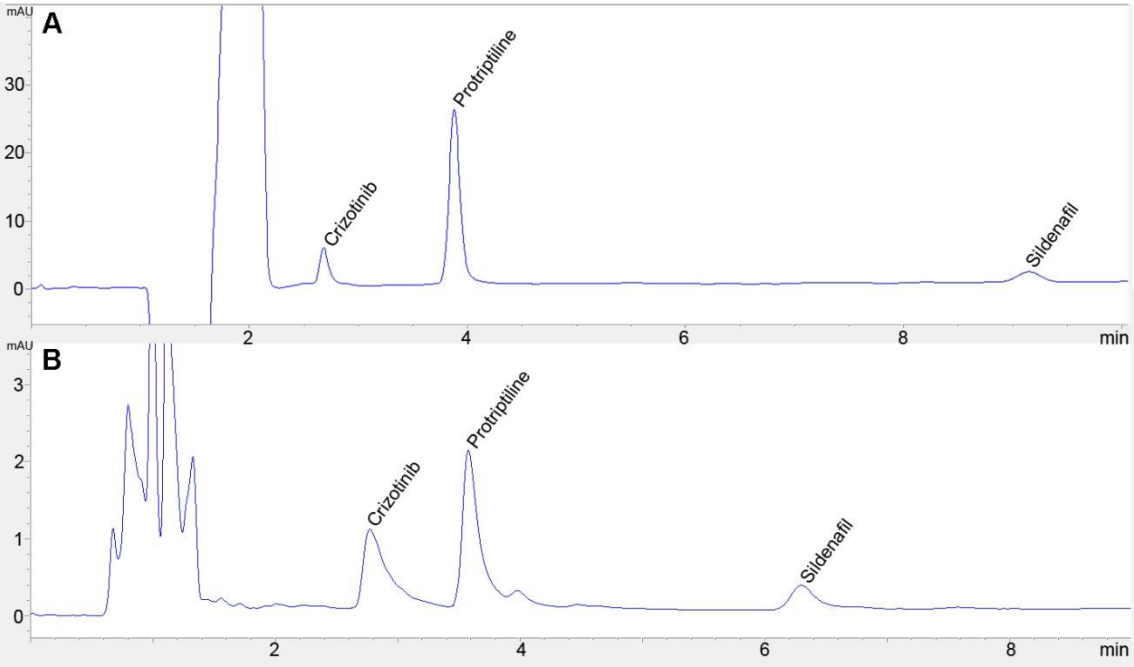

Figure 22 – Representative chromatograms of the separation of Crizotinib and Sildenafil analytes and the Internal Standard (Protriptiline) with two different mobile phases: $CH_3CO_2NH_4$ (A) and Na_2HPO_4 (B).

After optimization process, the method was completely validated according to FDA [163], as can be seen in Table 5, 6, 7 and 8 on Appendix section (Page 98).

After method validation, the amount of drug encapsulated was determined by measuring the drug concentration present in the supernatant. As the results in Figure 23 show, the encapsulation efficiency of Crizotinib was above 65% in all PEG-PLA micelles (Crizotinib alone, Crizotinib+Sildenafil).

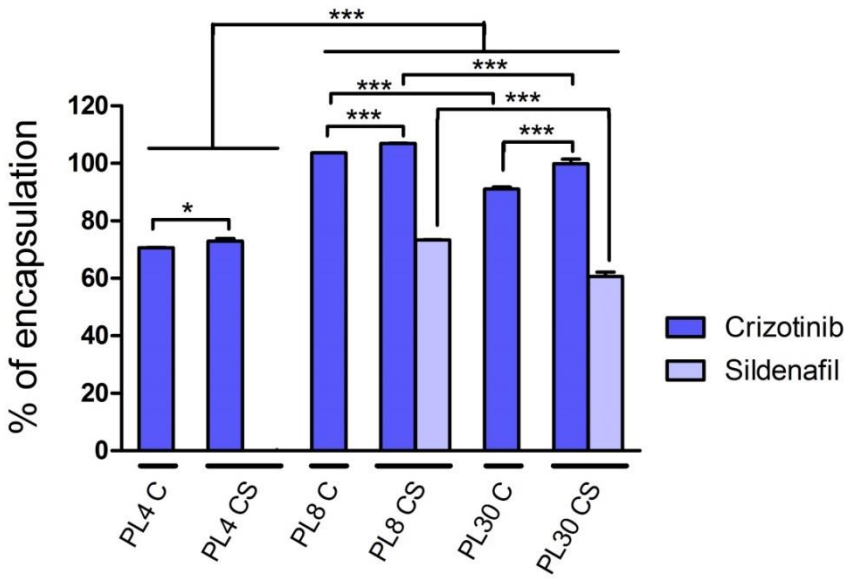

Figure 23 – Encapsulation efficiency of Crizotinib and Crizotinib/Sildenafil combination in PL4, PL8 and PL30 nanoparticles. *n*=5; *p < 0.05; **p < 0.01; ***p < 0.001; ns=non-significant. Data is presented as mean ± s.d.

The encapsulation efficiency of Crizotinib alone is particularly high for the PL8 micelle formulations, achieving 100% of the initial Crizotinib amount. This important finding highlights the unique drug loading capacity of these particular micelles. Further analysis reveals that Crizotinib is encapsulated to a slightly higher extent in PL8 micelles than in PL30 micelles, however, no significant differences were found. In addition, in comparison with the PL4 micelles, the other formulations with increased PLA chain lengths presented better encapsulation efficiency (Figure 23). This fact is likely correlated with the hydrophobic characteristics of Crizotinib and suggests that encapsulation efficiency varies according to the hydrophobic chain lengths. Sildenafil was encapsulated with an efficiency of 73% in PL8 formulation and 61% in the PL30 micelles, which is related to the slightly less hydrophobic character of this drug. In fact, the encapsulation of Sildenafil by PL4 micelles is approximately 0%. This fact can be explained due to shorter PLA chains that promote lower hydrophobic interactions with drug molecules, hence originating lower encapsulation efficiency. Besides, PL4 micelles have the lowest single and dual drug encapsulation in comparison with all other formulations, due to this fact, from this point onwards PL8 and PL30 have been chosen for the subsequent studies. This can be explained by the large amount of hydrophobic chains in the inner micelle core that occupies the free space required for molecule entrapment.

3.10. Morphological Characterization of Nano-sized PEG-PLA micelles

SEM images were acquired in order to evaluate the morphological characteristics of PEG-PLA micelles. As show in the electron microscopy images of Figure 24, all the micelles presented spherical-like morphologies. These results are corroborated by different studies in the literature, that describe the formulation of PEG-PLA spherical micelles [147, 164, 165]. Nanoparticle morphology is crucial to maximize cellular uptake. Spherical shape is thought to maximize cellular uptake, as previously described by Albanese *et* al [75]. Spherical form contributes for a better hydrodynamic behavior in the blood stream [75].

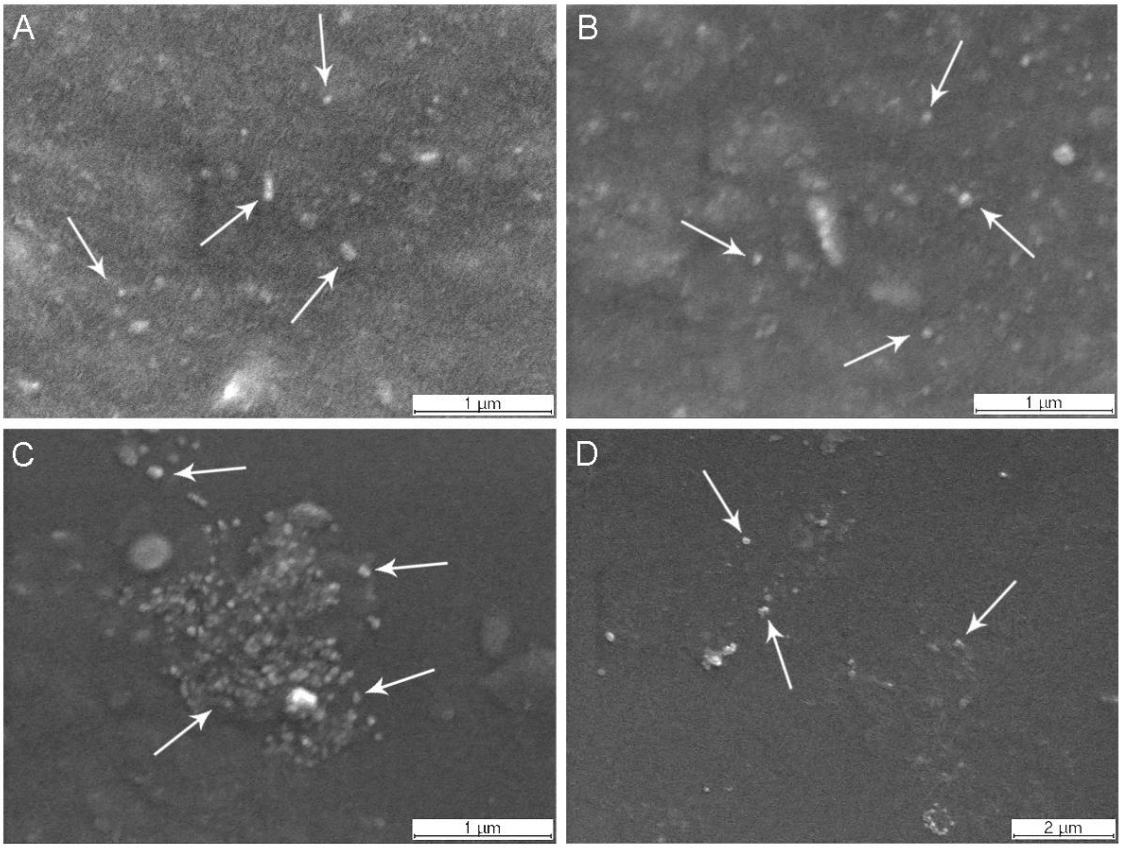

Figure 24 - SEM micrographs of: PL8 micelles with ecapsulated Crizotinib (A) and Crizotinib+Sildenafil (B) respectively; and PL30 micelles with loaded Crizotinib (C) and Crizotinib+Sildenafil (D) respectively. White arrows indicate micellar carriers.

3.11. Micelle physicochemical characterization – Size and Surface Charge

Micelle size is a critical characteristic since it ultimately determines nanocarriers accumulation in tumor tissues through the EPR effect. The size characterization results show that PL30 formulations are able to form nano-sized micelles with narrower size range (98 to 101 nm) than that of PL8 formulations (126 to 132 nm) (figure 25). This difference in micelle size is observed in both Crizotinib and Crizotinib+Sildenafil-loaded micelles. Because these two co-polymers only differ in the PLA chain length, the difference in size can be explained by the fact that PL30 has less drug encapsulation efficiency, with less core space being occupied [166]. The drug-loaded micelles formulated with a single or dual drugs present slightly lower size than those reported in the literature for these DDS [167, 168]. Nanoparticle size plays a critical role in biodistribution and blood clearance [169]. It is described that nanoparticles with less than 200 nm have a longer blood circulation time than that of larger sized particles [169]. Furthermore, nanoparticles larger than 250 nm are described to be extensively accumulate in organs such as the spleen, liver and lungs [169]. Therefore, it is very important to produce micellar carriers with suitable size ranges in order to avoid these issues. PDI, of the produced micelles is under 0.25, which shows good properties for biomedical application, since low PDI of nanoparticle is required for good biological response [170]. Regarding the zeta potential, the results show that PL8 formulations present a more negative surface charge than the PL30-based formulations. This finding is observed in single drug and dual drug-loaded micelles (Figure 25). The lower negativity of PL30 nanoparticles is due to better capping of carboxyl acid groups of PLA by PEG chain. Because of the lower mobility of PEG, when attached to longer PLA chains [171]. These results are in accordance with those reported in the literature for PEG-PLA micelles that commonly possess zeta potential values in the range of +10 to -10 mV [167, 168].

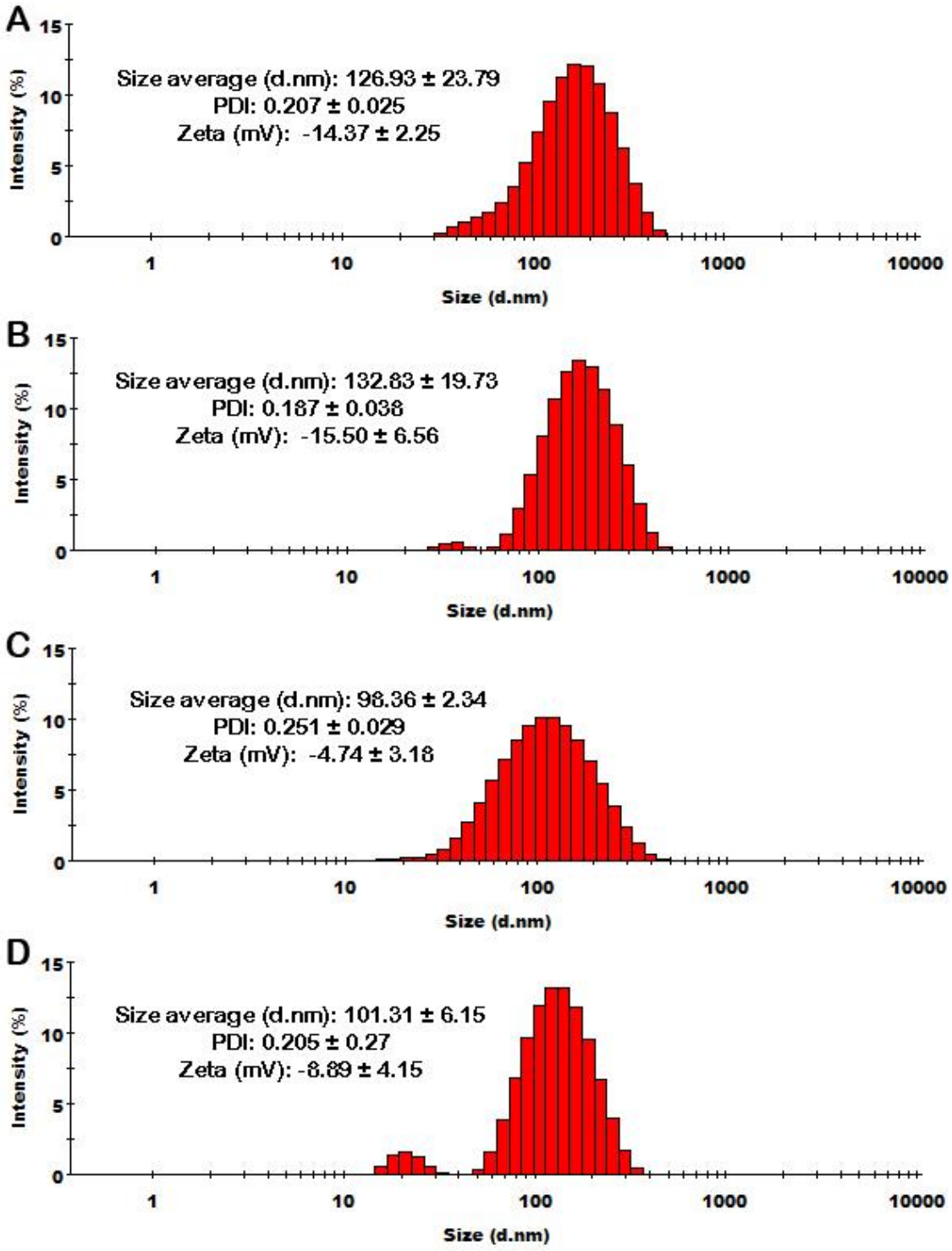

Figure 25 - Size, PDI and zeta potential of PL micelles loaded with drugs. (A and B) PL8 loaded with Crizotinib and loaded with Crizotinib+Sildenafil, respectively; (C and D) PL30 nanoparticles loaded with Crizotinib and with Crizotinib+Sildenafil, respectively. n=3. Data is presented as mean ± s.d.

The more negative zeta potential values obtained for PL8 provide an important advantage in respect to non-specific interactions with blood components, especially erythrocytes [172]. Another important aspect involved in cell-nanoparticle interaction is the surface charge of nanoparticles. Positively charged nanoparticles are quickly involved by serum proteins, which

impairs their function, since they are eliminated by mononuclear phagocytic system in spleen and liver [75]. This is a critical finding for the envisioned application of this DDS, since its administration route will be primarily by systemic injection. Overall, the formulated PEG-PLA micelles had relatively low size and zeta potential variations, regardless whether they are used for encapsulation of one or two drugs simultaneously.

Due to higher loading efficiency and more negative zeta potential, PL8 formulations gather the optimal DDS characteristics for therapeutic applications, and were then chosen from this point onwards to perform all the *in vitro* studies.

3.12. Evaluation of Drug Release Profile

It is important that a micelle can retain the drug in its inner core during relatively long periods of time, in order to provide its controlled release. In addition, increasing the period among which drug is released it is important to reduce de number of administrations, whilst always assuring that the drug concentrations are within the therapeutic window. After an intravenous injection it is highly important to ensure that the greatest possible amount of drug reaches its final destination, i.e., tumor cells. This characteristic is ensured by a slow release profile [173]. The release profile of nanoparticles was quantified as described above using UPLC technology. Regarding the release profile obtained, several aspects have contribute for the behavior of drugs encapsulated in micellar carriers [174]. Drug solubility, desorption of surface bound drugs, DDS degradation, drug diffusion, or the combination of all of these characteristics determines the release profile of an encapsulated drug [174]. PEG-PLA micelles are described to hold encapsulated hydrophobic drugs with high efficacy [175]. Based on the better encapsulation efficiency of PL8 formulation, as well as greater negative zeta potential, the following studies were performed with PL8 formulation only. The micelles produced herein were able to sustain 80% of its payload of Crizotinib, resulting on a release of only 20% during 8 days of study (Figure 26). On the contrary, sildenafil appears to have a burst release profile, which is slightly explained by its increased water solubility in comparison with than of Crizotinib. As Sildenafil is more soluble in water (medium used for micelle self-assembly), its interaction with the hydrophobic chains of the polymer will be lower. Due to poor hydrophobic interaction with PLA hydrophobic chain, encapsulated sildenafil might be weakly interacting with PEG chains, which in turn promotes its faster release [176].

In the literature, it is reported that some micelles can sustain 80% of the drug in their core for long periods, up to 4 days [147, 177]. The results obtained here revealed that these DDS have similar release profile to that previously reported for PEG-PLA micelles in the literature [178]. However, these micelles were loaded with other drugs, since Crizotinib and Sildenafil approach were never tested. A combination of different release profiles can explain this simultaneous release. Wu and co-workers [177] encapsulated Doxorubicin (a potent

chemotherapy drug) and obtained a comparable release profile in respect to that of Crizotinib alone. Moreover as described by Yoo and co-workers a burst release was also obtained for PEG-PLA micelles [179]. The difference observed between Crizotinib and Sildenafil in the release profile can be related to hydrophobic drug interactions with the hydrophobic PLA polymer chain.

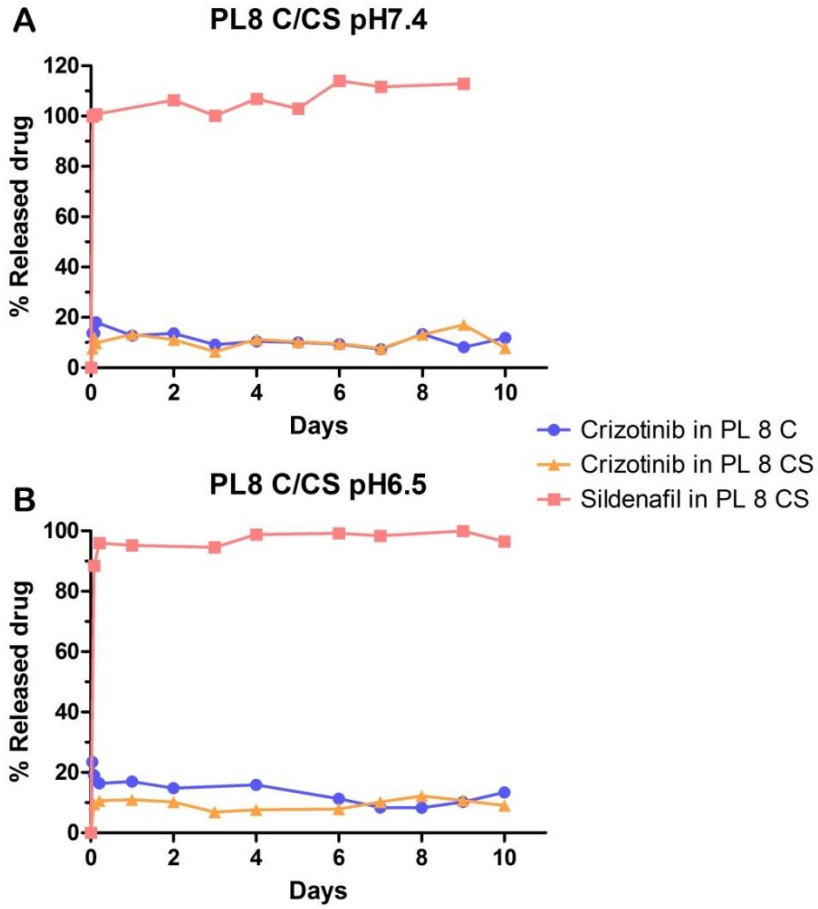

Figure 26 - Release profile of PL8 formulations at physiologic pH (pH = 7.4) (A) and at the characteristic acidic tumor pH (pH = 6.5) (B). PL8C/CS represents Crizotinib and Sildenafil loaded PL8 micelles.

3.13. PEG-PLA co-polymers biocompatibility

PEG-PLA is described as a highly biocompatible block co-polymer [180]. Nevertheless, to further characterize the synthesized materials, cytotoxic profile was characterized by using breast carcinoma cells (MCF-7) and human fibroblasts (Fib-H) [181].

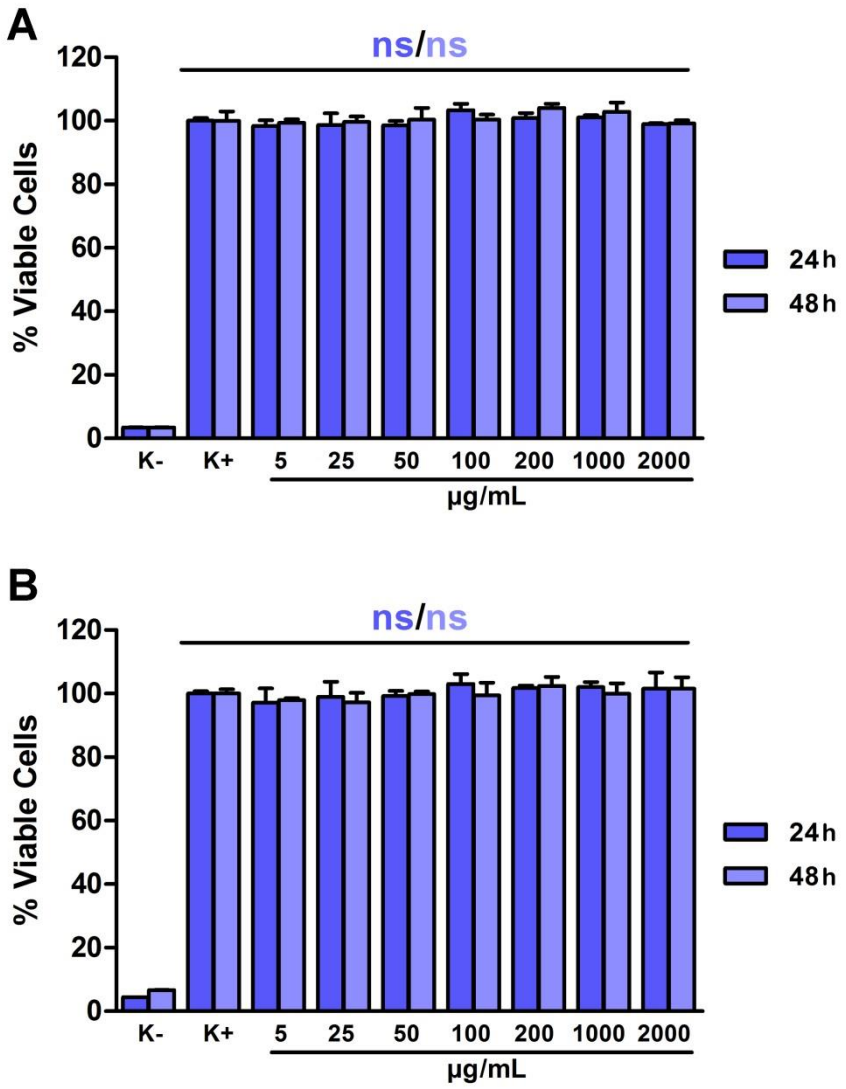

Figure 27 – Characterization of PL8 micelles cytotoxicity using: MCF-7 cells (A) and Fib-H (B). *n*=5; *p < 0.05; **p < 0.01; ***p < 0.001; ns=non-significant. Data is presented as mean ± s.d.

The results presented in Figure 27 show that cells present viability values above 95%, which is a similar cellular viability to that of K-. Both cell types maintained their viability in the presence of blank micelles up to concentrations of 2000 µg/mL. For MCF-7 cells the viability remains near 100% after their incubation with the same concentrations of polymers previously tested.

3.14. Characterization of Micelle Cellular Uptake

3.14.1. Flow Cytometry analysis

In order to address micelle cell uptake in MCF-7 breast cancer cells the carriers were loaded with RITC in their hydrophobic core using the same loading method that was previously used for loading drugs. Micelle uptake was evaluated at both 2 and 4 h after micelle incubation. During the different incubation times no relevant difference in the percentage of cells containing micelles was obtained, 99.82% (2h) and 98.02% (4h) (Figure 28). These results suggest that after 2h of incubation almost all the MCF-7 cells had internalized the PEG-PLA micelles, indicating the suitability of the delivery systems to be applied in cancer therapy. Moreover, further analysis of flow cytometry data reveals that the Mean Fluorescent Intensity (MFI) was increased from 92.2, at 2 h of incubation to 128.9, at 4 h of incubation. These results suggest that MCF-7, have internalized more micelles than the cells incubated with micelles only for 2h, providing therefore important insights for the future administration schedule of these DDS's.

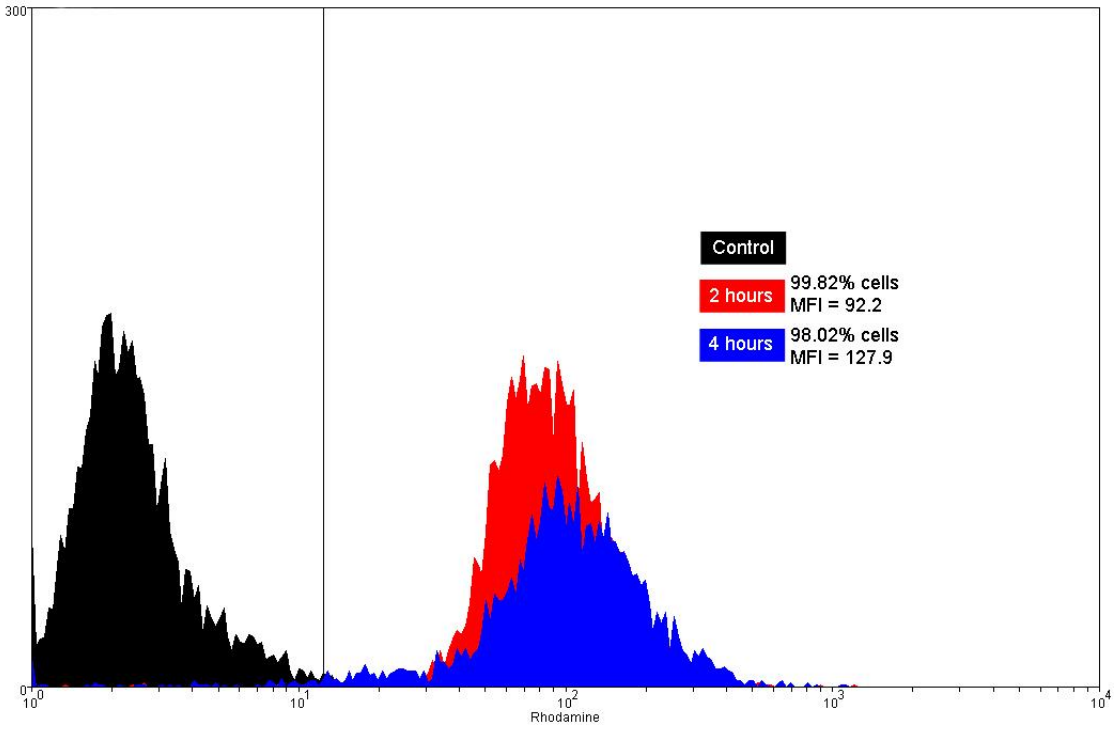

Figure 28 – Overlaid cytometry histograms of MCF-7 cells incubated during 2 and 4 h with RITC-micelles. Black color represents auto fluorescence of MCF-7 cells, red represents fluorescence of MCF-7 incubated during 2 hours with RITC-micelles and blue shows incubation with the same RITC-micelles during 4 hours.

To further confirm cell internalization of PEG-PLA micelles in MCF-7 cells, RITC-Micelles where incubated with MCF-7 cells and then analyzed by CLSM. In Figure 29 the white arrows show the RITC-micelles internalized in MCF-7 cells, being extensively localized the cell

cytoplasm. This is a very relevant finding since when the micelles start to release the drugs these will be available in their site of action. In fact this increase in drug bioavailability improves the therapeutic effect.

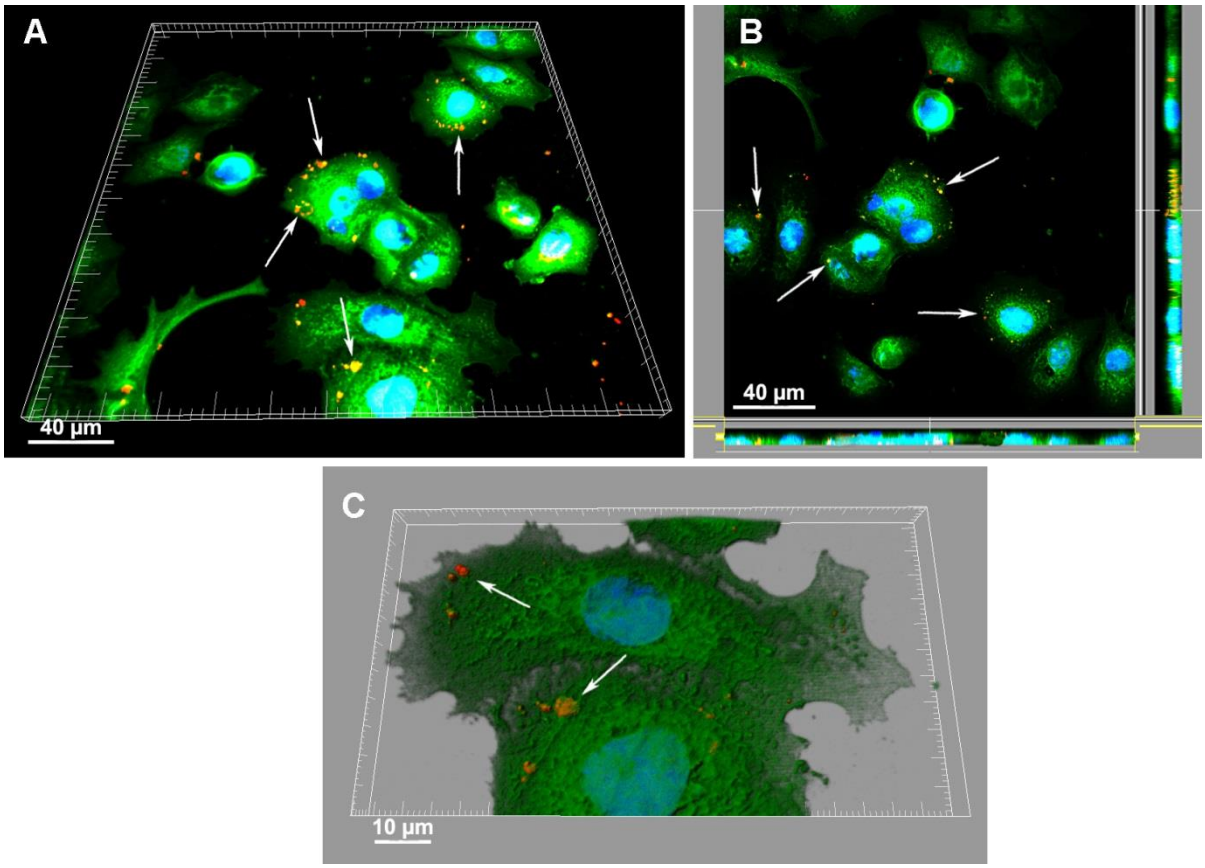

Figure 29 - CLSM images of MCF-7 cell with internalized PEG-PLA micelles encapsulating RITC. White arrows indicate micellar carriers. (A) 3D reconstruction of micelle cellular uptake; (B) Orthogonal slices of MCF-7 internalized micelles; (C) High resolution 3D surface rendering of micelle uptake. Green channel: Phalloidin-labelled F-actine; Blue channel: Hoechst 33342®; Red channel: RITC-loaded micelles. Yellow color is the result of co-localization of RITC (red) and phalloidin-F-actin (green). White arrows indicate some of the labeled micelles internalized in MCF-7 Cells.

3.14.2. Determination of the Inhibitory concentration of free Crizotinib in Breast Cancer Cells

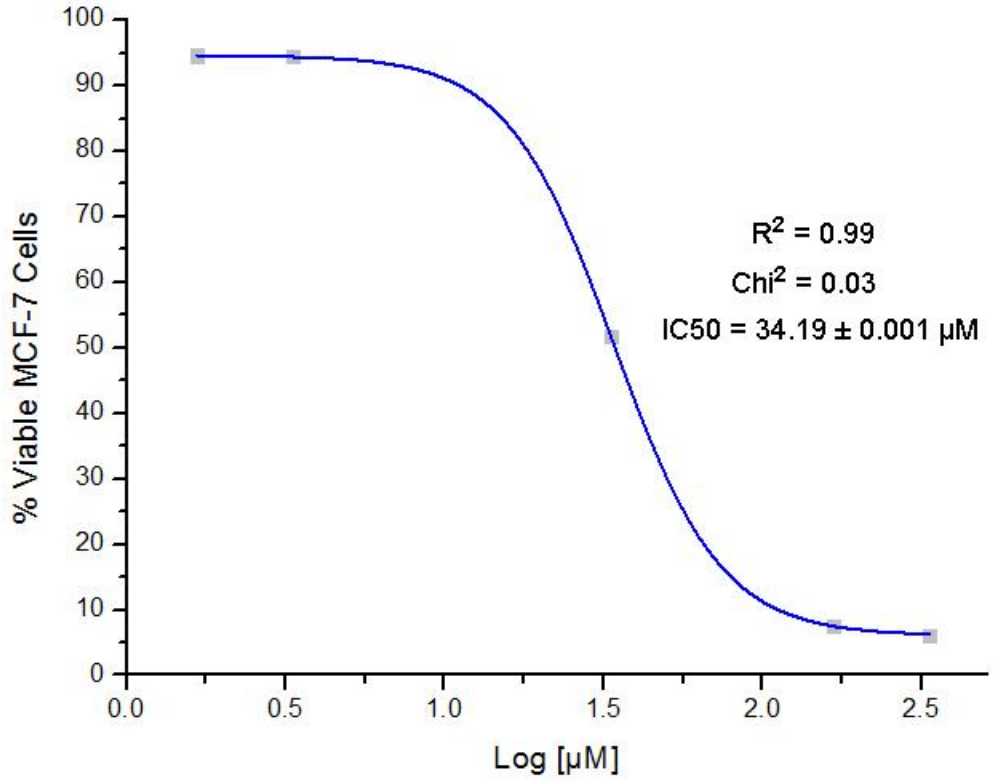

Figure 30 - IC 50 determination of Crizotinib anti-tumoral activity in MCF-7 breast cancer cells. Blue curve represents the mathematical fitting performed for IC50 calculation. n=5; Chi2=Chi-Squared; R2=R-Squared.

After the characterization of the biocompatibility it is important to address the actual anti-tumoral activity of Crizotinib before further studies are performed. Therefore the IC 50 of Crizotinib was determined (Figure 30). The IC50 of a drug is the minimum concentration that is able to kill half of the tumor cell population. Due to possible variations in *in vitro* cell line models during cell passages, it is critical to assess the experimental IC50. Experimental IC50 calculated trough fitting (34.19 ± 0.001 µM) is almost 10-fold higher than that reported in the literature 3.34 ± 0.52 µM [33]. This fact can be explained by the possible acquisition of a resistant phenotype from behalf of the MCF-7 breast cancer cells while in culture for long periods. Should be noted that R^2 and Chi^2 values obtained in this IC50 curve fit provide a high confidence in the obtained results.

3.15. Evaluation of the anti-tumoral effect of combinational drugs

3.15.1. Free Crizotinib and Sildenafil

In order to primarily address one of the main objectives of this thesis workplan, the anti-tumoral effect of free Crizotinib in MCF-7 cancer cells was evaluated. Moreover, the synergistic application of free Crizotinib with free Sildenafil was also investigated, since it was initially postulated that this novel combinatorial approach could further improve any anti-tumoral effect of Crizotinib. Therefore, to prove these concepts, several assays were performed with an experimental design based on the use of single or multiple free drugs.

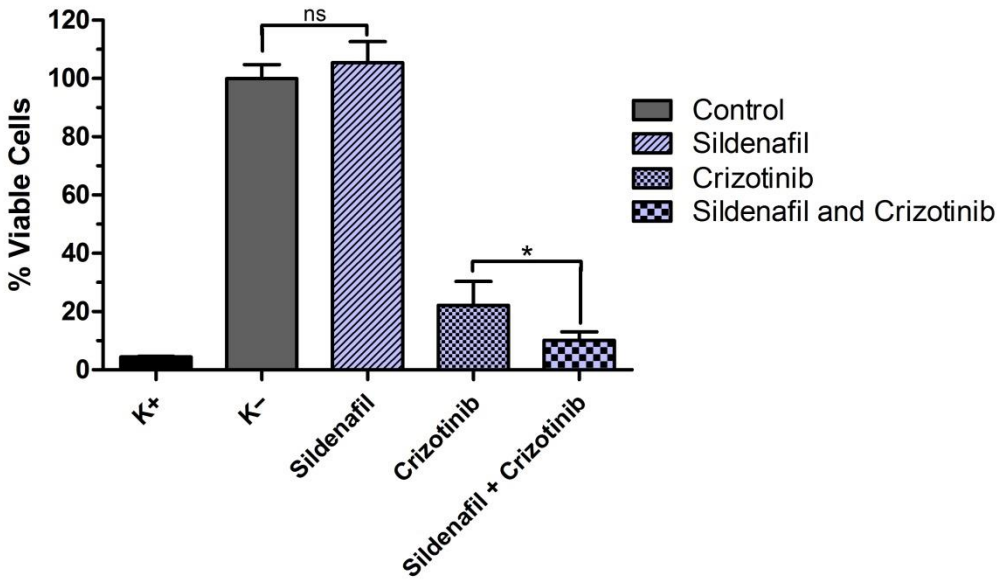

Figure 31 – Evaluation of anti-tumoral activity of Crizotinib (alone) and Sildenafil (alone) and when Sildenafil was compbined with Crizotinib after 48 h incubation. n=5; *p < 0.05; **p < 0.01; ***p < 0.001; ns=non-significant. Data is presented as mean ± s.d.

As demonstrated by Figure 31, after 48 h, only Sildenafil incubation does not elicit an anti-tumoral effect. Actually, the MCF-7 cells incubated with Sildenafil alone, present a higher rate of proliferation than non-incubated cells. On the other hand, the anti-tumoral effect of Crizotinib was markedly pronounced with only 22% of MCF-7 remaining viable after their incubation with this drug. The simultaneous incubation of cells with Crizotinib and Sildenafil resulted in a steep decrease in cellular viability (only 10% of cells remained viable), when compared with the incubation of Crizotinib alone. Based on this achievement, it is possible to state with 99.5% of assurance, that there is a significatively improved anti-tumoral effect, and hence, corroborates the synergic effect obtained when these two drugs are administered into breast cancer cells. This synergy effect is likely due to occur because of the inhibitory

effect of Sildenafil on ABC transporters, which are one of the efflux pumps that transport drugs from the cytoplasm to the extracellular medium [59].

3.15.2. Single and Multiple Drug-loaded Micelles

After establishing that there is an actual synergic effect associated with the use Crizotinib and Sildenafil, the PL8 micellar formulations containing both drugs were then incubated with MCF-7 breast cancer cells. These experiments were performed with half of the dose of Crizotinib and Sildenafil, that was previously used for free drugs, either alone or in combination. When drugs were delivered by micellar carriers to MCF-7 cells, a marked decrease in cell proliferation was observed for both single and dual drug formulations (Figure 32). Particularly, even after only 24h the PL8C micelles decreased breast cancer cells viability to 37% (Figure 32). More importantly, the administration of dual-loaded micelles reduced cell viability to 25% with 24h incubation, revealing that combinational therapy of Crizotinib and Sildenafil remains significantly different when delivery through PL8 micelles. After 48 hours, the differences in cell viability in the single and dual micelle formulations were still observed. At this stage, single-loaded PL8C micelles (Crizotinib alone) promoted a decrease in MCF-7 cell viability levels up to 14%. Nonetheless, in the dual-loaded PL8CS micelles cell viability levels decreased to about 4%, a significant difference that undeniably illustrates once more the therapeutic potential of this co-delivery approach. These results are in agreement with the therapeutic effect that Chen and co-workers reported in 2012 [55], when they manipulated the activity of Pg-p (ABC1) and ABCC10/MRP7 proteins of MCF-7 cells, as an approach that led to an enhanced anti-tumoral effect of chemotherapy drugs [55]

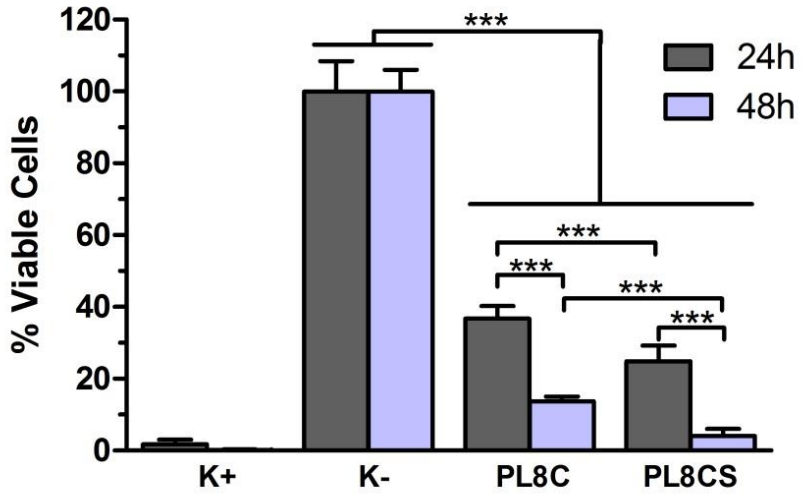

Figure 32 – Evaluation of the anti-tumoral activity of Crizotinib, Sildenafil and synergic effect between both when delivery through PEG-PLA micelles. n=5; *p < 0.05; **p < 0.01; ***p < 0.001; ns=non-significant. Data is presented as mean ± s.d.

In addition, the results of these experiments also indicate that the synthesized PEG-PLA micelles are an excellent drug delivery platform since it should be underlined that MCF-7 cell viability was outstandingly reduced with only half of the Crizotinib and Sildenfil concentration used in the assays with free drug, when these were delivered by the micellar carriers. This fact is correlated with the excellent micelle cell uptake, demonstrated by CLSM and flow cytometry which accounts for the increase in drug bioavailability within cell cytoplasm and for the consequent improvement in the therapeutic effect. Interestingly, the remarkable decrease in cancer cell viability also indicates that the spatiotemporal release profile of the drugs is suitable enough to maintain drug concentration levels within the therapeutic window.

3.16. Breast cancer cell apoptosis

As an attempt to shed light on the biological events triggered by the use of Crizotinib in combination with Sildenafil in MCF-7 cancer cells, a fluorescence-based apoptosis assay using the CellEvent™ Caspase-3/7 detection reagent was performed. As shown in Figure 33, the incubation of dual-loaded PL8CS micelles for 24h induced caspase-3 and caspase-7 activation, since a bright fluorescence yellow signal is acquired in CLSM images. This signal is provided by a substrate that once cleaved by active caspase-3/7 emits fluorescence. This evidences the role of Crizotinib in promoting cell death trough apoptosis. Cell death by apoptosis promoted by Crizotinib action via caspase-3/7 activation was already reported by Zhou in 2007 [49], emphasizing that this is a valuable approach to promote breast cancer cell death.

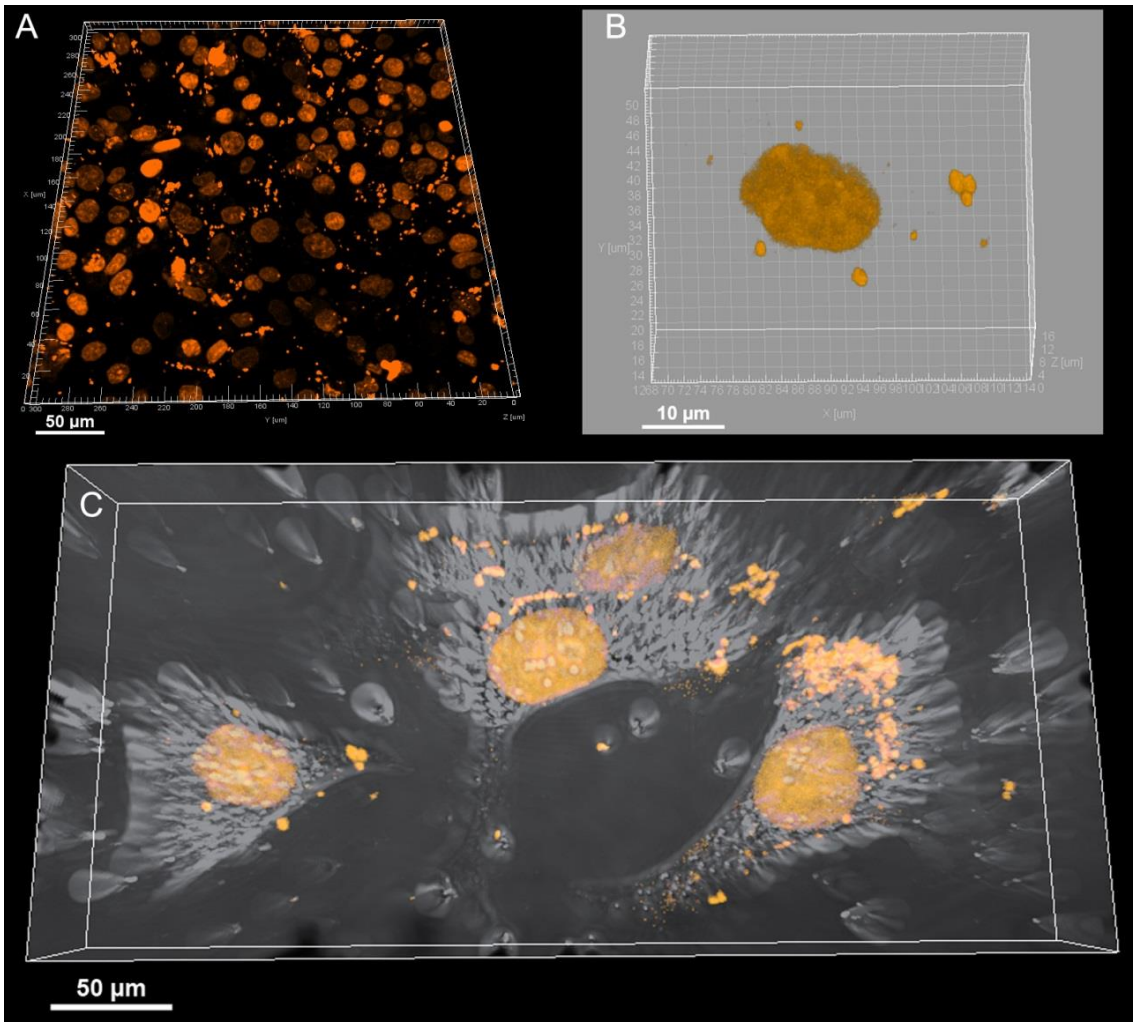

Figure 33 - CLSM images of apoptotic MCF-7 cells that were incubated 24 h with PL8CS micelles. (A) 3D reconstruction of MCF-7 cell nucleous; (B) High resolution reconstruction of apoptotic cell nucleous; (C) Merged 3D image of MCF-7 cells. Yellow channel represents caspase-3 activated MCF-7 cells, derived from CellEventTM Caspase-3/7 detection probe.

Conclusion and Future Perspectives

Cancer therapy is a fast growing research field that gathers the efforts from both the scientific and medical communities towards the development of an ultimate cure that can eradicate cancer cells and improve patient life-style. However, despite the outstanding achievements made to date, cancer cells maintain their capacity to tackle the majority of anti-tumoral drugs and survive. Nevertheless, the future of cancer therapeutics must rely on the combination of therapeutic approaches that can target particular hallmarks of cancer.

The straightforward research described in this thesis elucidates the applicability of Crizotinib and Sildenafil against breast cancer, when delivered through highly efficient micellar carriers, like those synthesized herein. The results obtained showed the biocompatibility and haemocompatibility, of the synthesized materials, providing important insights for their potential use in biomedical applications. In fact, it should be emphasized that the materials used for micelle self-assembly are approved by FDA and EMEA. These self-assembly characteristics of the block co-polymers synthesized in aqueous environments originated highly stable micelles as evidenced by the low CMC values obtained.

Furthermore, the optimized method allowed the production of self-assembled micelles with optimum size and zeta potential for being applied as DDSs. Both drugs used in this study were encapsulated with high efficiency on the synthesized micelles. The carriers have also demonstrated to have a long term sustained release with good efficacy at both physiological and tumor acidic pH. Moreover, produced micelles demonstrated to have an excellent uptake by breast cancer cells at very short time frames. The synergic effect between Sildenafil and Crizotinib was observed when free drugs where incubated with MCF-7 cells. This evidence shows the improvement of the anti-tumoral effect of Crizotinib when used in combination with Sildenafil. This effect is even more evident when both drugs where delivered using the produced micelles. The anti-tumoral effect of these two drugs was much higher when both drugs were simultaneously used in DDS Furthermore, the concentration required to produce same therapeutic effect of free drugs was reduced to half when drugs were loaded in micelles.

In the future the produced micelles can be modified with specific targeting moieties at their surface to enhance uptake and target specificity to malignant cells *in vivo*. Moreover, this novel co-delivery approach can be extended to novel combinatorial experiments that use more than two drugs. Moreover, *in vivo* studies can also be performed on suitable mice models of breast cancer in order to further demonstrate the applicability of these systems in a clinical context.

In summary, the results obtained in this work open a whole new window of opportunities in what concerns the combinatorial discovery of drug conjugations with synergistic and potent anti-tumoral capacity.

References

1. Hanahan, D. and R.A. Weinberg, *Hallmarks of cancer: the next generation.* Cell, 2011. **144**(5): p. 646-674.
2. Brabletz, T., et al., *Migrating cancer stem cells - an integrated concept of malignant tumour progression.* Nature Reviews Cancer, 2005. **5**(9): p. 744-749.
3. MacMahon, B., P. Cole, and J. Brown, *Etiology of human breast cancer: a review.* Journal of the National Cancer Institute, 1973. **50**(1): p. 21-42.
4. Lambe, M., et al., *Transient increase in the risk of breast cancer after giving birth.* New England Journal of Medicine, 1994. **331**(1): p. 5-9.
5. Garraway, L.A. and E.S. Lander, *Lessons from the cancer genome.* Cell, 2013. **153**(1): p. 17-37.
6. Richard, V. and M.R. Pillai, *The stem cell code in oral epithelial tumorigenesis:'The cancer stem cell shift hypothesis'.* Biochimica et Biophysica Acta (BBA)-Reviews on Cancer, 2010. **1806**(2): p. 146-162.
7. Moul, J.W., *Angiogenesis, p53, bcl-2 and Ki-67 in the progression of prostate cancer after radical prostatectomy.* European urology, 2012. **35**(5-6): p. 399-407.
8. Greider, C.W., *Telomere length regulation.* Annual review of biochemistry, 1996. **65**(1): p. 337-365.
9. Blasco, M.A., *Telomeres and human disease: ageing, cancer and beyond.* Nature Reviews Genetics, 2005. **6**(8): p. 611-622.
10. Ferrara, N., *Vascular endothelial growth factor.* Arterioscler Thromb Vasc Biol, 2009. **29**(6): p. 789-791.
11. Mac Gabhann, F. and A.S. Popel, *Systems biology of vascular endothelial growth factors.* Microcirculation, 2008. **15**(8): p. 715-738.
12. Niu, G., et al., *Constitutive Stat3 activity up-regulates VEGF expression and tumor angiogenesis.* Oncogene, 2002. **21**(13): p. 2000-2008.
13. Xie, Q., et al., *Recombinant Snake Venom Cystatin Inhibits Tumor Angiogenesis in vitro and in vivo Associated with Downregulation of VEGF-A165, Flt-1 and bFGF.* Anti-cancer agents in medicinal chemistry, 2012. **13**(4): p. 663-671.
14. Nagy, J.A., et al., *Heterogeneity of the tumor vasculature.* Semin Thromb Hemost, 2010. **36**(3): p. 321-331.
15. Wang, A.Z., R. Langer, and O.C. Farokhzad, *Nanoparticle delivery of cancer drugs.* Annu Rev Med, 2012. **63**: p. 185-198.
16. Berx, G. and F. van Roy, *Involvement of members of the cadherin superfamily in cancer.* Cold Spring Harbor Perspectives in Biology, 2009. **1**(6): p. a003129.
17. Jemal, A., et al., *Global cancer statistics.* CA: A Cancer Journal for Clinicians, 2011. **61**(2): p. 69-90.
18. Forouzanfar, M.H., et al., *Breast and cervical cancer in 187 countries between 1980 and 2010: a systematic analysis.* The Lancet, 2011. **378**(9801): p. 1461-1484.
19. Ferlay, J., et al., *Cancer incidence and mortality patterns in Europe: Estimates for 40 countries in 2012.* Eur J Cancer, 2013. **49**(6): p. 1374-1403.
20. Liu, R., et al., *Prevention of nodal metastases in breast cancer following the lymphatic migration of paclitaxel-loaded expansile nanoparticles.* Biomaterials, 2013. **34**(7): p. 1810-1819.
21. Banerji, S., et al., *Sequence analysis of mutations and translocations across breast cancer subtypes.* Nature, 2012. **486**(7403): p. 405-409.

22. Rakha, E.A., J.S. Reis-Filho, and I.O. Ellis, *Basal-like breast cancer: a critical review.* Journal of Clinical Oncology, 2008. **26**(15): p. 2568-2581.
23. Sørlie, T., et al., *Repeated observation of breast tumor subtypes in independent gene expression data sets.* Proceedings of the National Academy of Sciences, 2003. **100**(14): p. 8418-8423.
24. Bauer, K.R., et al., *Descriptive analysis of estrogen receptor (ER)-negative, progesterone receptor (PR)-negative, and HER2-negative invasive breast cancer, the so-called triple-negative phenotype: a population-based study from the California cancer Registry.* Cancer, 2007. **109**(9): p. 1721-1728.
25. Smith, I.C., et al., *Neoadjuvant chemotherapy in breast cancer: significantly enhanced response with docetaxel.* Journal of Clinical Oncology, 2002. **20**(6): p. 1456-1466.
26. Chen, J., et al., *Drug concentrations in axillary lymph nodes after lymphatic chemotherapy on patients with breast cancer.* Breast Cancer Research, 2004. **6**(4): p. 474-477.
27. Shi, Z., et al., *Roles of sildenafil in enhancing drug sensitivity in cancer.* Cancer Research, 2011. **71**(11): p. 3735-3738.
28. Gillet, J.P. and M.M. Gottesman, *Mechanisms of multidrug resistance in cancer.* Methods in Molecular Biology, 2010. **596**: p. 47-76.
29. Gottesman, M.M., *Mechanisms of cancer drug resistance.* Annual Review of Medicine, 2002. **53**(1): p. 615-627.
30. Gottesman, M.M., T. Fojo, and S.E. Bates, *Multidrug resistance in cancer: role of ATP–dependent transporters.* Nature Reviews Cancer, 2002. **2**(1): p. 48-58.
31. Davis, M.E., *Nanoparticle therapeutics: an emerging treatment modality for cancer.* Nature Reviews Drug Discovery, 2008. **7**(9): p. 771-782.
32. Heldin, C.-H., et al., *High interstitial fluid pressure—an obstacle in cancer therapy.* Nature Reviews Cancer, 2004. **4**(10): p. 806-813.
33. Zhou, W.J., et al., *Crizotinib (PF-02341066) reverses multidrug resistance in cancer cells by inhibiting the function of P-glycoprotein.* British Journal of Pharmacology, 2012. **166**(5): p. 1669-1683.
34. Di, X., et al., *Influence of the phosphodiesterase-5 inhibitor, sildenafil, on sensitivity to chemotherapy in breast tumor cells.* Breast Cancer Research and Treatment, 2010. **124**(2): p. 349-360.
35. Robey, R.W., et al., *ABCG2: determining its relevance in clinical drug resistance.* Cancer and Metastasis Reviews, 2007. **26**(1): p. 39-57.
36. Schuetz, E.G., W.T. Beck, and J.D. Schuetz, *Modulators and substrates of P-glycoprotein and cytochrome P4503A coordinately up-regulate these proteins in human colon carcinoma cells.* Molecular pharmacology, 1996. **49**(2): p. 311-318.
37. Abdul, B. and R. Hassan, *Main Critical Side Effects Associated with Chemotherapy Used in Cancer Treatment.* Pharmaceutica Analytica Acta, 2012. **3**(5): p. 1000e113.
38. Parveen, S., R. Misra, and S.K. Sahoo, *Nanoparticles: a boon to drug delivery, therapeutics, diagnostics and imaging.* Nanomedicine, 2012. **8**(2): p. 147-66.
39. Powles, T.J., *Extended adjuvant tamoxifen for breast cancer—a new era?* The Lancet, 2013. **381**(9869): p. 782-783.
40. Yezhelyev, M., et al., *Emerging use of nanoparticles in diagnosis and treatment of breast cancer.* The Lancet Oncology, 2006. **7**(8): p. 657-667.

41. Shenoy, D.B. and M.M. Amiji, *Poly(ethylene oxide)-modified poly(epsilon-caprolactone) nanoparticles for targeted delivery of tamoxifen in breast cancer.* International Journal of Pharmaceutics, 2005. **293**(1-2): p. 261-270.
42. Vogel, C.L., et al., *Efficacy and Safety of Trastuzumab as a Single Agent in First-Line Treatment of HER2-Overexpressing Metastatic Breast Cancer.* Journal of Clinical Oncology, 2002. **20**(3): p. 719-726.
43. Mi, Y., J. Zhao, and S.-S. Feng, *Targeted co-delivery of docetaxel, cisplatin and herceptin by Vitamin E TPGS-cisplatin prodrug nanoparticles for multimodality treatment of cancer.* Journal of Controlled Release, 2013. **169**(3): p. 185-192.
44. Das, A., et al., *Sildenafil increases chemotherapeutic efficacy of doxorubicin in prostate cancer and ameliorates cardiac dysfunction.* Proceedings of the National Academy of Sciences, 2010. **107**(42): p. 18202-18207.
45. Shi, J., et al., *Nanotechnology in drug delivery and tissue engineering: from discovery to applications.* Nano letters, 2010. **10**(9): p. 3223-3230.
46. Kuang, Y.-H., et al., *Lapatinib and erlotinib are potent reversal agents for MRP7 (ABCC10)-mediated multidrug resistance.* Biochemical pharmacology, 2010. **79**(2): p. 154-161.
47. Shaw, A.T., U. Yasothan, and P. Kirkpatrick, *Crizotinib.* Nat Rev Drug Discov, 2011. **10**(12): p. 897-898.
48. Zhou, W.j., et al., *Crizotinib (PF-02341066) reverses multidrug resistance in cancer cells by inhibiting the function of P-glycoprotein.* British Journal of Pharmacology, 2012. **166**(5): p. 1669-1683.
49. Zou, H.Y., et al., *An Orally Available Small-Molecule Inhibitor of c-Met, PF-2341066, Exhibits Cytoreductive Antitumor Efficacy through Antiproliferative and Antiangiogenic Mechanisms.* Cancer Research, 2007. **67**(9): p. 4408-4417.
50. Cui, J.J., et al., *Structure based drug design of crizotinib (PF-02341066), a potent and selective dual inhibitor of mesenchymal-epithelial transition factor (c-MET) kinase and anaplastic lymphoma kinase (ALK).* Journal of Medicinal Chemistry, 2011. **54**(18): p. 6342-6363.
51. Birchmeier, C., et al., *Met, metastasis, motility and more.* Nature reviews Molecular cell biology, 2003. **4**(12): p. 915-925.
52. Lengyel, E., et al., *C-Met overexpression in node-positive breast cancer identifies patients with poor clinical outcome independent of Her2/neu.* International journal of cancer, 2005. **113**(4): p. 678-682.
53. Gschwind, A., O.M. Fischer, and A. Ullrich, *The discovery of receptor tyrosine kinases: targets for cancer therapy.* Nature Reviews Cancer, 2004. **4**(5): p. 361-370.
54. Casaluce, F., et al., *Emerging mitotic inhibitors for non-small cell carcinoma.* Expert Opinion on Emerging Drugs, 2013. **18**(1): p. 97-107.
55. Chen, J.J., et al., *PDE5 inhibitors, sildenafil and vardenafil, reverse multidrug resistance by inhibiting the efflux function of multidrug resistance protein 7 (ATP-binding Cassette C10) transporter.* Cancer Science, 2012. **103**(8): p. 1531-1537.
56. Das, A., et al., *Sildenafil increases chemotherapeutic efficacy of doxorubicin in prostate cancer and ameliorates cardiac dysfunction.* Proceedings of the National Academy of Sciences, 2010. **107**(42): p. 18202-18207.
57. Hamilton, T.K., et al., *Potential therapeutic applications of phosphodiesterase inhibition in prostate cancer.* World Journal of Urology, 2013. **31**(2): p. 325-330.

58. Das, A., L. Xi, and R.C. Kukreja, *Phosphodiesterase-5 inhibitor sildenafil preconditions adult cardiac myocytes against necrosis and apoptosis Essential role of nitric oxide signaling.* Journal of Biological Chemistry, 2005. **280**(13): p. 12944-12955.
59. Shi, Z., et al., *Sildenafil reverses ABCB1- and ABCG2-mediated chemotherapeutic drug resistance.* Cancer Research, 2011. **71**(8): p. 3029-3041.
60. Pusztai, L., et al., *Phase I and II study of exisulind in combination with capecitabine in patients with metastatic breast cancer.* Journal of Clinical Oncology, 2003. **21**(18): p. 3454-61.
61. Das, A., et al., *Protein kinase C plays an essential role in sildenafil-induced cardioprotection in rabbits.* American Journal of Physiology-Heart and Circulatory Physiology, 2004. **286**(4): p. 1455-1460.
62. Das, A., L. Xi, and R.C. Kukreja, *Protein kinase G-dependent cardioprotective mechanism of phosphodiesterase-5 inhibition involves phosphorylation of ERK and GSK3β.* Journal of Biological Chemistry, 2008. **283**(43): p. 29572-29585.
63. Muro, S., *Challenges in design and characterization of ligand-targeted drug delivery systems.* Journal of Controlled Release, 2012. **164**(2): p. 125-137.
64. Park, J., et al., *Combination delivery of TGF-β inhibitor and IL-2 by nanoscale liposomal polymeric gels enhances tumour immunotherapy.* Nature Materials, 2012. **11**(10): p. 895-905.
65. Kolhe, S. and K. Parikh, *Application of nanotechnology in cancer: a review.* International Journal of Bioinformatics Research and Applications, 2012. **8**(1): p. 112-125.
66. Singh, S., A. Sharma, and G.P. Robertson, *Realizing the Clinical Potential of Cancer Nanotechnology by Minimizing Toxicologic and Targeted Delivery Concerns.* Cancer Res, 2012. **72**(22): p. 5663-5668.
67. Letchford, K. and H. Burt, *A review of the formation and classification of amphiphilic block copolymer nanoparticulate structures: micelles, nanospheres, nanocapsules and polymersomes.* European Journal of Pharmaceutics and Biopharmaceutics, 2007. **65**(3): p. 259-269.
68. Davis, M.E., Z.G. Chen, and D.M. Shin, *Nanoparticle therapeutics: an emerging treatment modality for cancer.* Nature Reviews Drug Discovery, 2008. **7**(9): p. 771-782.
69. Petros, R.A. and J.M. DeSimone, *Strategies in the design of nanoparticles for therapeutic applications.* Nature Reviews Drug Discovery, 2010. **9**(8): p. 615-627.
70. Herd, H., et al., *Nanoparticle Geometry and Surface Orientation Influences Mode of Cellular Uptake.* ACS nano, 2013. **7**(3): p. 1961–1973.
71. Bangham, A.D. and R.W. Horne, *Negative staining of phospholipids and their structural modification by surface-active agents as observed in the electron microscope.* Journal of Molecular Biology, 1964. **8**(5): p. 660-668.
72. Saha, R.N., et al., *Nanoparticulate drug delivery systems for cancer chemotherapy.* Molecular Membrane Biology, 2010. **27**(7): p. 215-231.
73. Schluep, T., et al., *Pharmacokinetics and biodistribution of the camptothecin-polymer conjugate IT-101 in rats and tumor-bearing mice.* Cancer Chemother Pharmacol, 2006. **57**(5): p. 654-662.
74. M. Rabanel, J., et al., *Drug-Loaded Nanocarriers: Passive Targeting and Crossing of Biological Barriers.* Current Medicinal Chemistry, 2012. **19**(19): p. 3070-3102.

75. Albanese, A., P.S. Tang, and W.C. Chan, *The effect of nanoparticle size, shape, and surface chemistry on biological systems.* Annual review of biomedical engineering, 2012. **14**: p. 1-16.
76. Owens III, D.E. and N.A. Peppas, *Opsonization, biodistribution, and pharmacokinetics of polymeric nanoparticles.* Int J Pharm, 2006. **307**(1): p. 93-102.
77. Peer, D., et al., *Nanocarriers as an emerging platform for cancer therapy.* Nature nanotechnology, 2007. **2**(12): p. 751-760.
78. Danhier, F., O. Feron, and V. Préat, *To exploit the tumor microenvironment: Passive and active tumor targeting of nanocarriers for anti-cancer drug delivery.* Journal of Controlled Release, 2010. **148**(2): p. 135-146.
79. Haley, B. and E. Frenkel. *Nanoparticles for drug delivery in cancer treatment*. in *Urologic Oncology: Seminars and original investigations*. 2008. Elsevier.
80. Brannon-Peppas, L. and J.O. Blanchette, *Nanoparticle and targeted systems for cancer therapy.* Advanced Drug Delivery Reviews, 2004. **56**(11): p. 1649-1659.
81. Stylianopoulos, T., *EPR-effect: utilizing size-dependent nanoparticle delivery to solid tumors.* Therapeutic delivery, 2013. **4**(4): p. 421-423.
82. Fang, J., H. Nakamura, and H. Maeda, *The EPR effect: Unique features of tumor blood vessels for drug delivery, factors involved, and limitations and augmentation of the effect.* Advanced Drug Delivery Reviews, 2011. **63**(3): p. 136-151.
83. Taurin, S. and K. Greish, *Enhanced Vascular Permeability in Solid Tumors: A Promise for Anticancer Nanomedicine*, in *Tight Junctions in Cancer Metastasis*2013, Springer. p. 81-118.
84. Nomura, T., et al., *Effect of particle size and charge on the disposition of lipid carriers after intratumoral injection into tissue-isolated tumors.* Pharmaceutical research, 1998. **15**(1): p. 128-132.
85. Heine, M., et al., *High interstitial fluid pressure is associated with low tumour penetration of diagnostic monoclonal antibodies applied for molecular imaging purposes.* PloS one, 2012. **7**(5): p. e36258.
86. Kong, G., R.D. Braun, and M.W. Dewhirst, *Characterization of the effect of hyperthermia on nanoparticle extravasation from tumor vasculature.* Cancer Research, 2001. **61**(7): p. 3027-3032.
87. Chauhan, V.P., et al., *Normalization of tumour blood vessels improves the delivery of nanomedicines in a size-dependent manner.* Nature nanotechnology, 2012. **7**(6): p. 383-388.
88. Xu, Z.P., et al., *Inorganic nanoparticles as carriers for efficient cellular delivery.* Chemical Engineering Science, 2006. **61**(3): p. 1027-1040.
89. Sahoo, S.K. and V. Labhasetwar, *Nanotech approaches to drug delivery and imaging.* Drug discovery today, 2003. **8**(24): p. 1112-1120.
90. López-Dávila, V., A.M. Seifalian, and M. Loizidou, *Organic nanocarriers for cancer drug delivery.* Current Opinion in Pharmacology, 2012. **12**(4): p. 414-419.
91. Zhang, L., et al., *self-assembled lipid− polymer hybrid nanoparticles: a robust drug delivery platform.* ACS nano, 2008. **2**(8): p. 1696-1702.
92. Rösler, A., G.W. Vandermeulen, and H.-A. Klok, *Advanced drug delivery devices via self-assembly of amphiphilic block copolymers.* Advanced drug delivery reviews, 2012.
93. Knop, K., et al., *Poly(ethylene glycol) in drug delivery: pros and cons as well as potential alternatives.* Angew Chem Int Ed Engl, 2010. **49**(36): p. 6288-6308.

94. Torchilin, V.P., *Recent advances with liposomes as pharmaceutical carriers.* Nature Reviews Drug Discovery, 2005. **4**(2): p. 145-160.
95. Pang, X., et al., *Novel Amphiphilic Multiarm, Starlike Coil–Rod Diblock Copolymers via a Combination of Click Chemistry with Living Polymerization.* Macromolecules, 2011. **44**(18): p. 7176-7183.
96. Cosco, D., et al., *Gemcitabine and tamoxifen-loaded liposomes as multidrug carriers for the treatment of breast cancer diseases.* International Journal of Pharmaceutics, 2012. **422**(1): p. 229-237.
97. Lila, A.S.A., et al., *Multiple administration of PEG-coated liposomal oxaliplatin enhances its therapeutic efficacy: a possible mechanism and the potential for clinical application.* International Journal of Pharmaceutics, 2012. **438**(1): p. 176-183.
98. Watanabe, K., M. Kaneko, and Y. Maitani, *Functional coating of liposomes using a folate–polymer conjugate to target folate receptors.* International Journal of Nanomedicine, 2012. **7**: p. 3679-3688.
99. Colbern, G.T., et al., *Significant increase in antitumor potency of doxorubicin Hc1 by its encapsulation in pegylated liposomes.* Journal of Liposome Research, 1999. **9**(4): p. 523-538.
100. Barenholz, Y.C., *Doxil®—The first fda-approved nano-drug: Lessons learned.* Journal of Controlled Release, 2012. **160**(2): p. 117–134.
101. Sutton, D., et al., *Functionalized micellar systems for cancer targeted drug delivery.* Pharmaceutical Research, 2007. **24**(6): p. 1029-1046.
102. Soppimath, K.S., et al., *Biodegradable polymeric nanoparticles as drug delivery devices.* Journal of controlled release, 2001. **70**(1): p. 1-20.
103. Panyam, J. and V. Labhasetwar, *Biodegradable nanoparticles for drug and gene delivery to cells and tissue.* Advanced Drug Delivery Reviews, 2012. **64**: p. 61-71.
104. Soga, O., et al., *Thermosensitive and biodegradable polymeric micelles for paclitaxel delivery.* Journal of Controlled Release, 2005. **103**(2): p. 341-353.
105. Hu, Q., et al., *F3 peptide-functionalized PEG-PLA nanoparticles co-administrated with tLyp-1 peptide for anti-glioma drug delivery.* Biomaterials, 2012. **34**(4): p. 1135–1145.
106. Basile, L., R. Pignatello, and C. Passirani, *Active targeting strategies for anticancer drug nanocarriers.* Current Drug Delivery, 2012. **9**(3): p. 255-268.
107. Allen, C., D. Maysinger, and A. Eisenberg, *Nano-engineering block copolymer aggregates for drug delivery.* Colloids and Surfaces B: Biointerfaces, 1999. **16**(1–4): p. 3-27.
108. Kataoka, K., A. Harada, and Y. Nagasaki, *Block copolymer micelles for drug delivery: Design, characterization and biological significance.* Advanced drug delivery reviews, 2012.
109. Cheng, R., et al., *Biodegradable poly (ε-caprolactone)-g-poly (2-hydroxyethyl methacrylate) graft copolymer micelles as superior nano-carriers for "smart" doxorubicin release.* Journal of Materials Chemistry, 2012. **22**(23): p. 11730-11738.
110. Tsai, H.C., et al., *Graft and diblock copolymer multifunctional micelles for cancer chemotherapy and imaging.* Biomaterials, 2010. **31**(8): p. 2293-301.
111. Zhang, Y., et al., *The eradication of breast cancer and cancer stem cells using octreotide modified paclitaxel active targeting micelles and salinomycin passive targeting micelles.* Biomaterials, 2012. **33**(2): p. 679-691.

112. Jain, R.A., *The manufacturing techniques of various drug loaded biodegradable poly(lactide-co-glycolide) (PLGA) devices.* Biomaterials, 2000. **21**(23): p. 2475-2490.
113. Lasprilla, A.J., et al., *Poly-lactic acid synthesis for application in biomedical devices - a review.* Biotechnology Advances, 2012. **30**(1): p. 321-328.
114. Rasal, R.M., A.V. Janorkar, and D.E. Hirt, *Poly(lactic acid) modifications.* Progress in Polymer Science, 2010. **35**(3): p. 338-356.
115. Hanafusa, S., et al., *Biodegradable plate fixation of rabbit femoral shaft osteotomies: a comparative study.* Clinical orthopaedics and related research, 1995. **315**: p. 262-271.
116. Wischke, C. and S.P. Schwendeman, *Principles of encapsulating hydrophobic drugs in PLA/PLGA microparticles.* International Journal of Pharmaceutics, 2008. **364**(2): p. 298-327.
117. Inkinen, S., et al., *From Lactic Acid to Poly(lactic acid) (PLA): Characterization and Analysis of PLA and Its Precursors.* Biomacromolecules, 2011. **12**(3): p. 523-532.
118. Pungkham, H., et al. *PEG-b-PCL and PEG-b-PLA polymeric micelles as nanocarrieres for lamellarin N delivery*. in *Engineering in Medicine and Biology Society, EMBC, 2011 Annual International Conference of the IEEE*. 2011. IEEE.
119. Hu, Y., et al., *Preparation and drug release behaviors of nimodipine-loaded poly(caprolactone)–poly(ethylene oxide)–polylactide amphiphilic copolymer nanoparticles.* Biomaterials, 2003. **24**(13): p. 2395-2404.
120. Jain, K.K., *Ethical and Regulatory Aspects of Nanomedicine*, in *The Handbook of Nanomedicine*2012, Springer. p. 477-492.
121. Öcal, H., et al., *5-Fluorouracil-loaded PLA/PLGA PEG-PPG-PEG polymeric nanoparticles: formulation, in vitro characterization and cell culture studies.* Drug development and industrial pharmacy, 2013. **13**(1): p. 1-8.
122. He, G., et al., *ABA and BAB type triblock copolymers of PEG and PLA: a comparative study of drug release properties and "stealth" particle characteristics.* Int J Pharm, 2007. **334**(1): p. 48-55.
123. Webster, R., et al., *PEG and PEG conjugates toxicity: towards an understanding of the toxicity of PEG and its relevance to PEGylated biologicals*, in *PEGylated Protein Drugs: Basic Science and Clinical Applications*, F. Veronese, Editor 2009, Birkhäuser Basel. p. 127-146.
124. Cruz, L.J., et al., *The influence of PEG chain length and targeting moiety on antibody-mediated delivery of nanoparticle vaccines to human dendritic cells.* Biomaterials, 2011. **32**(28): p. 6791-6803.
125. Ishida, T. and H. Kiwada, *Accelerated blood clearance (ABC) phenomenon upon repeated injection of PEGylated liposomes.* International Journal of Pharmaceutics, 2008. **354**(1-2): p. 56-62.
126. Xiao, R.Z., et al., *Recent advances in PEG-PLA block copolymer nanoparticles.* International Journal of Nanomedicine, 2010. **5**: p. 1057-65.
127. Riley, T., et al., *Physicochemical evaluation of nanoparticles assembled from poly (lactic acid)-poly (ethylene glycol)(PLA-PEG) block copolymers as drug delivery vehicles.* Langmuir, 2001. **17**(11): p. 3168-3174.
128. Shin, H.C., et al., *A 3-in-1 polymeric micelle nanocontainer for poorly water-soluble drugs.* Molecular Pharmaceutics, 2011. **8**(4): p. 1257-1265.

129. Prabhakar, U., et al., *Challenges and Key Considerations of the Enhanced Permeability and Retention Effect for Nanomedicine Drug Delivery in Oncology.* Cancer Res, 2013. **73**(8): p. 2412-2417.
130. Lee, K.S., et al., *Multicenter phase II trial of Genexol-PM, a Cremophor-free, polymeric micelle formulation of paclitaxel, in patients with metastatic breast cancer.* Breast Cancer Research and Treatment, 2008. **108**(2): p. 241-250.
131. Zhang, X., et al., *Synthesis and characterization of the paclitaxel/MPEG-PLA block copolymer conjugate.* Biomaterials, 2005. **26**(14): p. 2121-2128.
132. Wu, Q., et al., *Synthesis and micellization of a new amphiphilic star-shaped poly(D,L-lactide)/polyphosphoester block copolymer.* Reactive and Functional Polymers, 2012. **72**(6): p. 372-377.
133. D'Addio, S.M., et al., *Effects of block copolymer properties on nanocarrier protection from in vivo clearance.* Journal of Controlled Release, 2012. **162**(1): p. 208-217.
134. He, G., et al., *ABA and BAB type triblock copolymers of PEG and PLA: a comparative study of drug release properties and "stealth" particle characteristics.* International Journal of Pharmaceutics, 2007. **334**(1-2): p. 48-55.
135. Zhan, C., et al., *Cyclic RGD conjugated poly(ethylene glycol)-co-poly(lactic acid) micelle enhances paclitaxel anti-glioblastoma effect.* Journal of Controlled Release, 2010. **143**(1): p. 136-142.
136. Li, F., et al., *Synthesis and Gelation Properties of PEG−PLA−PEG Triblock Copolymers Obtained by Coupling Monohydroxylated PEG−PLA with Adipoyl Chloride.* Langmuir, 2007. **23**(5): p. 2778-2783.
137. Goikhman, A.S., et al., *X-ray diffraction determination of the degree of crystallinity of cellulose using a computer.* Fibre Chemistry, 1992. **24**(1): p. 80-85.
138. Hsi-Huang, M., et al., *Synthesis and Characterization of Block Copolymers of ε-Caprolactone and DL-Lactide Initiated by Ethylene Glycol or Poly(ethylene glycol).* Macromolecular Chemistry and Physics, 2003. **204**(16): p. 1994-2001.
139. Gaucher, G., et al., *Block copolymer micelles: preparation, characterization and application in drug delivery.* Journal of controlled release, 2005. **109**(1): p. 169-188.
140. Layek, B. and J. Singh, *Amino Acid Grafted Chitosan for High Performance Gene Delivery: Comparison of Amino Acid Hydrophobicity on Vector and Polyplex Characteristics.* Biomacromolecules, 2013. **14**(2): p. 485-494.
141. Pistos, C., et al., *Off-line HPLC method combined to LC-MS for the determination of sildenafil and its active metabolite in post-mortem human blood according to confirmation criteria.* Forensic Science International, 2008. **178**(2-3): p. 192-198.
142. Czekanska, E.M., *Assessment of cell proliferation with resazurin-based fluorescent dye*, in *Mammalian Cell Viability*2011, Springer. p. 27-32.
143. Kataoka, K., A. Harada, and Y. Nagasaki, *Block copolymer micelles for drug delivery: design, characterization and biological significance.* Advanced drug delivery reviews, 2001. **47**(1): p. 113-131.
144. Cheng, R., et al., *Dual and multi-stimuli responsive polymeric nanoparticles for programmed site-specific drug delivery.* Biomaterials, 2013. **34**(14): p. 3647-3657.

145. Cui, H., et al., *PLA-PEG-PLA and Its Electroactive Tetraaniline Copolymer as Multi-interactive Injectable Hydrogels for Tissue Engineering.* Biomacromolecules, 2013. **14**(6): p. 1904–1912.
146. Du, Y.J., et al., *ABA type copolymers of lactide with poly (ethylene glycol). Kinetic, mechanistic, and model studies.* Macromolecules, 1995. **28**(7): p. 2124-2132.
147. Jie, P., et al., *Micelle-like nanoparticles of star-branched PEO–PLA copolymers as chemotherapeutic carrier.* Journal of controlled release, 2005. **110**(1): p. 20-33.
148. Shi, Y., et al., *Improvement of in vivo efficacy of recombinant human erythropoietin by encapsulation in PEG–PLA micelle.* International journal of nanomedicine, 2013. **8**: p. 1-11.
149. Mehta, R., et al., *Synthesis of poly (lactic acid): a review.* Journal of Macromolecular Science, Part C: Polymer Reviews, 2005. **45**(4): p. 325-349.
150. Harrane, A., M.E.A. Belaouedj, and M. Belbachir, *Cationic ring-opening polymerization of (d,l-lactide) using Maghnite-H+, a non-toxic catalyst.* Reactive and Functional Polymers, 2011. **71**(2): p. 126-130.
151. Katiyar, V. and H. Nanavati, *Ring-opening polymerization of L-lactide using N-heterocyclic molecules: mechanistic, kinetics and DFT studies.* Polymer Chemistry, 2010. **1**(9): p. 1491-1500.
152. Ando, H., et al., *Polyethylene Glycol-solvolyzed Poly-(L)-lactic Acids and Their Stereocomplexes with Poly-(D)-lactic Acid.* Polymer Degradation and Stability, 2013. **98**(5): p. 958–962.
153. Zhao, H., et al., *Preparation and Characterization of PEG/PLA Multiblock and Triblock Copolymer.* Bulletin of the Korean Chemical Society, 2012. **33**(5): p. 1638-1642.
154. Skoog, D.A., *Principles of Instrumental Analysis*, 2006, Thompson Brooks/Cole: Belmont, CA.
155. Popl, M., J. Fähnrich, and M. Stejskal, *Adsorption effect in GPC separation of polycyclic aromatic hydrocarbons.* Journal of Chromatographic Science, 1976. **14**(11): p. 537-540.
156. Heeb, R., et al., *Influence of Salt on the Aqueous Lubrication Properties of End-Grafted, Ethylene Glycol-Based Self-Assembled Monolayers.* ACS Applied Materials & Interfaces, 2009. **1**(5): p. 1105-1112.
157. Madhavan Nampoothiri, K., N.R. Nair, and R.P. John, *An overview of the recent developments in polylactide (PLA) research.* Bioresource Technology, 2010. **101**(22): p. 8493-8501.
158. Signori, F., M.-B. Coltelli, and S. Bronco, *Thermal degradation of poly(lactic acid) (PLA) and poly(butylene adipate-co-terephthalate) (PBAT) and their blends upon melt processing.* Polymer Degradation and Stability, 2009. **94**(1): p. 74-82.
159. Rösler, A., G.W. Vandermeulen, and H.-A. Klok, *Advanced drug delivery devices via self-assembly of amphiphilic block copolymers.* Advanced Drug Delivery Reviews, 2012. **53**(1): p. 95–108.
160. Theerasilp, M. and N. Nasongkla, *Comparative studies of poly (ε-caprolactone) and poly (D, L-lactide) as core materials of polymeric micelles.* Journal of microencapsulation, 2012. **30**(4): p. 390-397.
161. Forde, P.M. and C.M. Rudin, *Crizotinib in the treatment of non-small-cell lung cancer.* Expert Opinion on Pharmacotherapy, 2012. **13**(8): p. 1195-1201.

162. Quintero, A., et al., *Validation of an HPLC method for sildenafil citrate analysis in human plasma samples.* Pharmazie, 2009. **64**(12): p. 796-799.
163. Food, U., *Drug Administration. FDA Guidance for Industry: Bioanalytical Method Validation. US Department of Health and Human Services.* Food and Drug Administration, Center for Drug Evaluation and Research: Rockville, MD, 2001.
164. Dong, Y. and S.-S. Feng, *Methoxy poly (ethylene glycol)-poly (lactide)(MPEG-PLA) nanoparticles for controlled delivery of anticancer drugs.* Biomaterials, 2004. **25**(14): p. 2843-2849.
165. Zhang, H., et al., *High intensity focused ultrasound-responsive release behavior of PLA-b-PEG copolymer micelles.* Journal of controlled release, 2009. **139**(1): p. 31-39.
166. Kim, S.Y., et al., *Methoxy poly (ethylene glycol) and-caprolactone amphiphilic block copolymeric micelle containing indomethacin: II. Micelle formation and drug release behaviours.* Journal of controlled release, 1998. **51**(1): p. 13-22.
167. Gref, R., et al., *Development and characterization of CyA-loaded poly(lactic acid)–poly(ethylene glycol)PEG micro- and nanoparticles. Comparison with conventional PLA particulate carriers.* European Journal of Pharmaceutics and Biopharmaceutics, 2001. **51**(2): p. 111-118.
168. Vila, A., et al., *Transport of PLA-PEG particles across the nasal mucosa: effect of particle size and PEG coating density.* Journal of controlled release, 2004. **98**(2): p. 231-244.
169. Owens Iii, D.E. and N.A. Peppas, *Opsonization, biodistribution, and pharmacokinetics of polymeric nanoparticles.* International Journal of Pharmaceutics, 2006. **307**(1): p. 93-102.
170. Asadi, H., et al., *Preparation of biodegradable nanoparticles of tri-block PLA-PEG-PLA copolymer and determination of factors controlling the particle size using artificial neural network.* Journal of microencapsulation, 2011. **28**(5): p. 406-416.
171. Govender, T., et al., *Defining the drug incorporation properties of PLA–PEG nanoparticles.* International Journal of Pharmaceutics, 2000. **199**(1): p. 95-110.
172. Cho, W.-S., et al., *Zeta potential and solubility to toxic ions as mechanisms of lung inflammation caused by metal/metal oxide nanoparticles.* Toxicological Sciences, 2012. **126**(2): p. 469-477.
173. Taurin, S., et al., *Curcumin-derivative nanomicelles for the treatment of triple negative breast cancer.* Journal of drug targeting, 2013(0): p. 1-9.
174. Mohanraj, V. and Y. Chen, *Nanoparticles-a review.* Tropical Journal of Pharmaceutical Research, 2007. **5**(1): p. 561-573.
175. Blanco, E., et al., *β-Lapachone-containing PEG–PLA polymer micelles as novel nanotherapeutics against NQO1-overexpressing tumor cells.* Journal of controlled release, 2007. **122**(3): p. 365-374.
176. Magenheim, B., M. Levy, and S. Benita, *A new in vitro technique for the evaluation of drug release profile from colloidal carriers-ultrafiltration technique at low pressure.* International Journal of Pharmaceutics, 1993. **94**(1): p. 115-123.
177. Wu, X.L., et al., *Tumor-Targeting Peptide Conjugated pH-Responsive Micelles as a Potential Drug Carrier for Cancer Therapy.* Bioconjugate Chemistry, 2010. **21**(2): p. 208-213.

178. Ayano, E., et al., *Poly (N-isopropylacrylamide)–PLA and PLA blend nanoparticles for temperature-controllable drug release and intracellular uptake.* Colloids and Surfaces B: Biointerfaces, 2012. **99**: p. 67-73.
179. Yoo, H.S. and T.G. Park, *Biodegradable polymeric micelles composed of doxorubicin conjugated PLGA–PEG block copolymer*. Journal of controlled release, 2001. **70**(1–2): p. 63-70.
180. Hu, K., et al., *Lactoferrin-conjugated PEG-PLA nanoparticles with improved brain delivery: in vitro and in vivo evaluations.* Journal of controlled release, 2009. **134**(1): p. 55-61.
181. Gao, M.Q., et al., *Stromal fibroblasts from the interface zone of human breast carcinomas induce an epithelial-mesenchymal transition-like state in breast cancer cells in vitro.* Journal of Cell Science, 2010. **123**(Pt 20): p. 3507-3514.

Appendix

Table 5 – Calibration standards with injection on mobile phase, coefficient of variation (CV) and bias.

	Concentration (ug/mL)	*Measured Concentration (ug/mL)*	*CV (%)*	*BIAS (%)*
Sildenafil	1	0.84±0.13	16.06674	0.716
	2.5	2.41±0.23	9.690798	-8.981
	5	5.31±0.35	6.499651	-7.345
	10	10.70±0.69	6.458676	-10.722
	25	31.81±5.22	16.4119	3.957
	50	68.34±8.70	12.73484	10.212
	100	144.66±2.33	1.612328	2.945
Crizotinib	1	1.50±0.16	10.54124	4.060
	2.5	4.02±0.28	6.929635	-8.156
	5	8.76±0.65	7.446644	-6.421
	10	17.66±0.10	5.639156	-8.832
	25	50.07±7.37	14.71209	1.582
	50	107.77±13.29	12.33603	8.128
	100	217.89±31.58	14.494	2.792

Table 6 – Calibration standards with injection on PBS, coefficient of variation (CV) and bias.

	Concentration (ug/mL)	*Measured Concentration (ug/mL)*	*CV (%)*	*BIAS (%)*
Sildenafil	0.05	0.050±0.01	10.13897	5.940
	0.075	0.07±0.01	12.11502	-1.886
	0.1	0.10±0.01	3.834572	3.636
	0.25	0.22±0.01	2.835565	-12.539
	0.5	0.47±0.08	6.477353	-5.910
	1	0.97±0.20	8.672041	-3.794
	3	3.23±0.41	6.219391	6.714
Crizotinib	0.05	0.053±0.01	4.05882	5.296
	0.075	0.072±0.01	4.369462	-3.811
	0.1	0.096±0.01	7.696951	-4.499
	0.25	0.236±0.05	2.729624	-5.805
	0.5	0.479±0.09	11.68526	-5.378
	1	0.974±0.24	9.322478	-3.357
	3	3.169±0.58	7.653258	4.879

Table 7 – Calibration standards with injection on water, coefficient of variation (CV) and bias.

	Concentration (ug/mL)	*Measured Concentration (ug/mL)*	*CV (%)*	*BIAS (%)*
Sildenafil	3	2.99±0.07	2.332422	-0.220
	10	10.26±0.72	7.049127	2.109
	25	23.43±2.78	11.86824	-7.814
	50	50.72±2.25	4.426129	1.271
	100	102.44±10.50	10.24554	1.506
Crizotinib	3	3.07±0.12	3.920651	1.047
	10	9.69±1.02	10.48906	-0.512
	25	22.25±0.65	2.938635	-13.194
	50	52.39±3.92	7.48131	1.215
	100	105.24±13.53	12.85894	6.845

Table 8 – Linearity data of Sildenafil and Crizotinib (*n*=5). m – Slope, b – intercept, LLOQ – lower limit of quantification.

		Weighting factor	*Calibration Range (µg/mL)*	*Regression*		R^2	*LLOQ (µg/mL)*
				m	b		
MetOH Calibration	Sildenafil	$1/X^2$	1 - 100	-0.41 ±0.18	1.23 ±0.13	0.99 ±0.01	1
	Crizotinib	$1/X^2$	1 - 100	1.98 ±0.17	-0.56 ±0.27	0.99 ±0.01	1
PBS Calibration	Sildenafil	$1/X^2$	0.05 - 3	0.08 ±0.01	0.00 ±0.01	0.99 ±0.01	0.05
	Crizotinib	$1/X^2$	0.05 - 3	1.23 ±0.51	0.04 ±0.03	0.99 ±0.01	0.05
H_2O Calibration	Sildenafil	$1/X^2$	3 - 100	1.03 ±0.29	0.09 ±0.51	0.99 ±0.01	3
	Crizotinib	$1/X^2$	3 - 100	1.27 ±0.09	2.88 ±0.27	0.98 ±0.01	3